Development of a Lightweight and High Strength Underactuated Lower Limb Robot Exoskeleton for Gait Rehabilitation

Fahad Hussain

Enrolment ID: U3211600

Supervisor: Prof. Roland Goecke

Co-Supervisor: Assoc. Prof. Masoud Mohammadian

A thesis submitted for the degree of Doctor of Philosophy at the

University of Canberra.

October 2023

ABSTRACT

The field of robot-assisted physical rehabilitation and robotics technology for providing support to the elderly population is rapidly evolving. Lower limb robot aided rehabilitation and assistive technology have been a focus for the engineering community over the last three decades as several robotic lower limb exoskeletons have been proposed in the literature as well as some being commercially available. One of the most important aspects of developing exoskeletons is the selection of the appropriate material. Strength to weight ratio is the most important factor to be considered before selection of a manufacturing material. The material selection strongly influences the overall weight and performance of the exoskeleton robot. In addition to material selection the type of mechanism and the actuation strongly effect the overall weight of the lower limb robotic exoskeleton. Most of the lower limb exoskeleton provided in the literature use a parallel mechanism, are properly actuated and either use aluminium or steel as their manufacturing materials. All these factors significantly increase the weight of the lower limb robot exoskeleton and make the device heavy, bulky, and uncomfortable for the wearer. Furthermore, an increase in weight contributes to a decrease of energy efficiency, reduces the energy efficiency of the final product, and increase the running cost of the designed robot devices.

This thesis explores the wide-ranging potential of lower limb robot exoskeletons in the context of physical rehabilitation. Implementation and testing of a lightweight and high strength material without effecting the reliability was the main research objective of the present work. In this research, a linkage based under-actuated mechanism was used for the development of a lightweight design. Structural and mechanical load analysis of the mechanism was performed by using an advanced approach of finite element analysis. Three materials, namely structural steel, aluminium, and carbon reinforced fibre were compared as the manufacturing materials of the modelled mechanism. After that, a weight estimation was carried out for all three materials and the material which exhibits the best response under mechanical load analysis was selected. From the weight comparison, the carbon reinforced fibre provided the least weight for the digital twin of a lower limb exoskeleton. After material selection, the next step was the topology optimisation to further decrease the mass of the designed prototype without effecting the mechanical performance. The optimisation was carried out by using a multi-mode single objective genetic algorithm (GA) and a reduction of 30 % in the weight of the designed prototype was obtained. The selected material, which is carbon fibre, is a type of polymer material that is highly anisotropic, meaning it shows different

material behaviour in different orientations of applied force. The next stage of the research work was the material characterization of the manufacturing material, which was carried out both analytically and experimentally. For defining the optimal criteria for fiber orientation, Hashin's Failure Criteria is considered, and experimental work is performed to determine the most suitable fibre orientation. The material monotonic tensile properties were experimentally determined by experimental work and used to select a suitable orientation to manufacture a physical prototype model of the lower limb robot exoskeleton.

After that the manufacturing process was carried out which is divided into three main steps. The first step was the use of the suitable lightweight and high strength material, which was selected by weight comparison in the design stage. The second step was the use of a single actuator to actuate the whole mechanical system and the final step was the use fabrication method to get a strong and reliable structure. Shaping of the different exoskeleton parts was carried out by CNC milling and parts were assembled to build a robotic prototype. A DC motor was used to actuate the complete prototype, which includes hip, knee, and ankle joints. In the end, a reliability analysis was carried out by using a machine learning based approach. A machine learning framework was developed for time-dependent reliability analysis of the developed robot. A neural network algorithm was designed to estimate the time-dependent reliability of the joint displacement and the positions of the end-effector first.

From the above methodology, a lightweight and high strength lower limb robot exoskeleton was just not only conceptualized but a significant work was done to get a physical model starting from the material selection and concluding with the fabrication of a physical prototype. The reliability analysis gives an overview of the mechanism safety as a function of joint displacement. The designed prototype of carbon reinforced fibre was four times lighter in weight as compared to steel and three times lighter than aluminium, which is expected to give the wearer a comfortable wearing experience and improves the overall physical rehabilitation experience for the patients.

ACKNOWLEDGMENTS

I would like to express my sincere gratitude and appreciation to my supervisor Prof. Roland Goecke for his guidance, support, and encouragement throughout my doctoral program. His contagious enthusiasm for this project was the greatest motivation. I would also like to thank my co-supervisors Assoc. Prof. Masoud Mohammadian for his devotion to the project.

I would like to put on record my thanks to laboratory technicians Bill Shelly and Ehsan Amiri Tehranizedah for their help and inputs in the construction of prototype and specimen for material testing. The faculty technical manager Jason Weber also deserves my appreciation for timely purchase of instruments needed to perform the experimental work. University of Canberra needs to be acknowledged for providing me with Research Training Scholarship (RTP) to support my studies and stay in Canberra. Dr. Juan Pablo Escobedo-Diaz from University of New South Wales (UNSW) also deserves my special thanks for providing the lab facilities to perform the material testing at Australian defence force academy (ADFA) campus.

My sincere appreciation goes to my fellow PhD students Tanishka Goyal, Yinan Jin, and Akim Kapsalyamov for providing important inputs to my exoskeleton design and for sparing time for constructive discussions throughout my research.

Finally, I would like to express my gratitude to my loving parents for inspiring me to complete my PhD and they were always worried about my well-being. I could never have finished my thesis without the support of my brother Dr. Zahid Hussain. All along this has been a blissful journey which has bestowed the knowledge and has further kindled the quest for more knowledge.

List of Publications

The following journal publications have resulted from the research described in this thesis.

1. **Fahad Hussain**, Roland Goecke, and Masoud Mohammadian, "Exoskeleton robots for lower limb assistance: A review of materials, actuation, and manufacturing methods", *Proceedings of the Institution of Mechanical Engineers, Part H: Journal of Engineering in Medicine*, Vol. 235, Issue 12, Pages 1375-1385, 2021.
2. **Fahad Hussain**, Masoud Mohammadian, and Roland Goecke, "Topology and material optimization of an underactuated robot for gait rehabilitation", *Mechanics Based Design of Structures and Machines*, Pages 1-18, (In press), DOI: doi.org/10.1080/15397734.2023.2252492, 2023.
3. **Fahad Hussain**, Tanishka Goyal, Masoud Mohammadian, and Roland Goecke, "Material characterization and time-dependent reliability analysis of an underactuated lower-limb robot exoskeleton for gait rehabilitation", *Robotica, (submitted)*.
4. **Fahad Hussain**, Tanishka Goyal, Masoud Mohammadian, and Roland Goecke, "Optimizing Orientation for Optimal Strength of CRPF using Hasin's Criteria", *Structural and Multidisciplinary Optimization, (To be submitted)*.

Table of Contents

List of Figures

List of Tables

List of Acronyms, Abbreviations and Mathematical Notations

List of Acronyms, Abbreviations

Active Leg Exoskeleton	ALEX
Activities of daily living	ADL
Computer Aided Design	CAD
Computer Numerical Control	CNC
Evolutionary Algorithms	EA
Genetic Algorithms	GA
Global Conditioning Index	GCI
Hybrid Assistive Limb	HAL
Knee Ankle Foot Orthosis	KAFO
Lower Extremity Powered Exoskeleton	LOPES
Pelvic Assist Manipulator	PAM
Pneumatically Operated Gait Orthosis	POGO
Spinal Cord Injured	SCI
Trunk Recovery Scale	TRS
Additive Manufacturing	AM
Fused Deposition Modelling	FDM
Pneumatic Muscle Actuators	PMA
Series Elastic Actuators	SEA
Long Short-Term Memory network	LSTM
Degree of Freedom	DOF
Gait Cycle	GC
Drawing Exchange Format	DXF
Carbon Reinforced Fibre Polymer	CRFP

Berkeley Lower Extremity Exoskeleton	BLEEX
Monte Carlo Simulation	MCS
Feedforward Neural Network	FNN
Revolutions Per Minute	RPM
Limit State Function	LSF

Mathematical Notations

A_i	Cross-sectional area of exoskeleton links
A_i^*	Optimised cross sectional area of exoskeleton links
E_1	Motion accuracy of the hip joint
E_2	Motion accuracy of the knee joint
E_3	Motion accuracy of the ankle joint
K_i	The set of normalized lengths
M^*	Optimised mass of exoskeleton
N_f	Failure Samples Over the Decided Period
P_f	Probability of failure
$R_h(t)$	Reliability of hip joint
$R_a(t)$	Reliability of ankle joint
$R_k(t)$	Reliability of knee joint
W_f	Input Weights
$x_s(t)$	State variable
ρ_j	The density for the chosen material
τ_E	Torque at the knee Joint
L	Link lengths of the mechanism
Syc	Compressive yield strength
Syt	Tensile yield strength

A	Area of cross section of the tensile specimen
F	Force applied on the tensile specimen
M	Calculated mass of the exoskeleton
U	Displacements
f	Externally applied forces
$z(t)$	Stochastic process
σ	Applied stress
ϵ	Strain in tensile specimen

CHAPTER 1 INTRODUCTION

A robot is a re-programmable, multi-functional, mechanical manipulator designed to move materials, tools, or specialized devices as well as assist humans in performing variable programmed motions [1-3]. Robots are widely used in manufacturing industries, warehouses and in various other applications such as mining and deep-sea search and rescue [4-6]. Although robots are being used in major aspects of life, their use is still limited in close human proximity, such as in service and healthcare applications. This is mainly due to the design, interaction, and safety issues associated with the robot manipulators. As a matter of fact, there is a rise in elderly human population worldwide. To counter the escalating demand for health and aged care services, the field of assistive and rehabilitation robotics has been evolving constantly in recent years and there are promising advancements in this field of research [5, 7-9]. The present research is carried out in accordance with this new development in the field of assistive and rehabilitation robotics and aims to investigate structural design, manufacturing material, safety, and reliability of a wearable lower limb rehabilitation robot. This chapter gives an overview of certain research issues encountered while developing lower limb robotic exoskeleton for the rehabilitation and assistance of physically disabled and elderly people. The importance of lower limb rehabilitation and assistive robots will be discussed briefly followed by a brief description of the lower limb biomechanics to determine the design of a lower limb exoskeleton. Towards the end of this chapter, research motivations will be presented, followed by an outline of the thesis structure.

1.1 Rehabilitation and Robots

The term “Rehabilitation” is defined as a set of interventions designed to improve physical functioning and reduce physical disability in individuals with health issues [10]. The disability could be due to an accidental injury or due to a neurologic impairment, such as stroke, as well as due to ageing [11]. Conventionally, the recovery process to restore the range of motion and regain the strength of limbs involves rigorous and repetitive exercises. These exercises are carried out under the supervision of a qualified physiotherapist. Over time, these exercises improve motor function by enhancing neuroplasticity and neuro-recovery of affected limbs [12]. The conventional manual rehabilitation treatment includes cooperative and intensive efforts of physiotherapists and patients. The treatment process requires visits to rehabilitation clinics for longer periods, but beyond that the majority of patients is asked to perform the prescribed exercises at home for a speedy recovery [13]. It has been documented that the recovery process using conventional ways of manual rehabilitation treatment is slow [14].

Patients, therapists, and the rehabilitation process suffer from the drawbacks of conventional treatments. The main drawbacks from the patients' perspective are listed below:

1. Travelling difficulty: Travelling to rehabilitation clinics or medical centres is quite difficult for a patient with a disability. Special arrangements are needed for frequent visits, and the transport may worsen the injury.
2. Short clinical sessions: The clinical sessions offered to the patients are short and non-intensive, which hinder the speedy recovery of the patients suffering from disability.
3. Fatigue: Exercises that are prescribed are often tiring and cause muscle fatigue to the patients. As a result of this, patients are not able to achieve stipulated rehabilitation goals.

The problems faced by physiotherapists in the process of carrying out conventional manual rehabilitation treatments are given below:

1. Fatigue: Highly repetitive efforts performed by a therapist result in both physical and mental fatigue and the therapists have frequently reported back pain.
2. Inadequate output: The physical involvement of therapists in prolonged treatment sessions restricts them to attend to only a limited number of patients. Hence, an inadequate output is achieved in terms of the number of patients receiving rehabilitation treatment.
3. Decision inaccuracy: Often, the treatment and rehabilitation progress of patients is not well managed and documented. It is, therefore, common practice, that therapists advise further treatment based on their own perception, which may not be accurate and there is always a chance of human error.

Finally, the rehabilitation process is the last pillar of the conventional treatment, and it suffers from following drawbacks:

1. Inconsistency in treatment: In the conventional rehabilitation treatment, there is a lack of repetitive efforts from the patient's side. As a result, the provided motion and force trajectories result in an inconsistent treatment.
2. Therapeutic subjectivity: Mostly, therapists evaluate the recovery of the patients undergoing conventional rehabilitation based on their perception, which may lead to undesired subjective decisions during treatment.
3. Slow recovery process: Due to its monotonous and tiresome nature, there is a lack of active participation from patients resulting in slow recovery.

Over the last two decades, robot assisted physical rehabilitation gradually began making its way in the rehabilitation clinics around the globe as it can improve the treatment

procedure by aiding the therapists and patients in numerous ways [15]. Certain virtual reality-based effects can be added to the robot assisted rehabilitation to make exercises more interactive and motivating for the patients. It has been noted that the motivation results in active participation from patients, which effectively enhances the rehabilitation treatment [16]. Another advantage for the patients is the decrease in the number of clinical visits as these robots can provide more intensive physical rehabilitation. The use of these robots can save time, travel cost and efforts of the patients undergoing rehabilitation. By using robotic rehabilitation devices, the burden on physiotherapists can be reduced significantly [17]. The number of patients treated by the therapists can increase as their physical involvement in treatment decreases with the support of robotic devices [18].

It has been noted that the use of certain sensors mounted on these rehabilitation robots can help in the collection of useful treatment data, which can be further processed for additional information. Using this information, it is possible to provide the rehabilitation treatment more objectively. It is easy to establish remote connections with the patients treated by rehabilitation robots and receive information about patient's progress [19]. Based on this information, decisions can be made by therapists about further treatments. There is a high repeatability in robotic rehabilitation treatment, which is helpful in providing a consistent physical therapy to patients, which makes the treatment more effective as compared to the conventional manual therapy. The use of visual and haptic effects increases the patient's active participation, which may further speed up the recovery process [20]. Therefore, all three stakeholders – patients, therapists, and the rehabilitation process – can benefit from the development of robot rehabilitation devices.

There are many rehabilitation robots currently in use for both the upper and lower limbs rehabilitation. Out of these robots, the lower limbs robots are commonly used for gait rehabilitation. The main purpose of gait rehabilitation robots is to assist a patient recovering from injury or stroke so that the patient can perform Activities of Daily Living (ADL). There are several gait rehabilitation robots, which have been designed to support patients with neurologic injuries. The commonly used gait rehabilitation robots are LOKOMAT, MINDWALKER, and ALEX [21] .There are many ways by which these robots can be classified. The two most commonly used ways to classify them are according to treatment approaches and according to robot structures [22]. While looking at the structural aspects, the choice of suitable material is of primary importance as every structure is composed of a certain material.

1.2 Materials for Gait Robots

In the category of gait rehabilitation robots, the term exoskeleton is used for a wearable robotic system [23]. These robot exoskeletons are also used by elderly with weaker limbs and, hence, there is a continuous effort to make these robots as lightweight as possible. For elderly people, the exoskeleton must be as lightweight for their convenience to move with little effort. Therefore, the manufacturing material is the most important parameter for the development of a lightweight exoskeleton structure [24, 25]. Metallic alloys of steel and aluminium are the traditionally used material for robot exoskeletons. These metallic alloys have been used in various preliminary robotic gait rehabilitation exoskeleton devices, such as LOKOMAT and ALEX, which are made of steel [26]. Other gait rehabilitation robots, such as LOPES, and WPAL have either steel or aluminium made structures [27-29]. Titanium is another metal, which can replace steel or aluminium due to its better strength to weight ratio. A lower limb robotic exoskeleton made of titanium has been developed at South China University of Technology (SCUT) [30]. In recent years, there is a trend shift towards carbon composite materials and these polymer composites are gradually replacing traditional metals in many manufacturing industries including robotic exoskeletons [31].

After the selections of material, the suitable design for a robotic exoskeleton is an important parameter to obtain a lightweight and less bulky device. There are certain design challenges, manufacturing methods, and material optimisation challenges that must be addressed. These aspects are further elaborated below.

1.2.1 Design Challenges

The design of a robot exoskeleton is a complicated task. There are certain design criteria that should be achieved during the design process:

1) Bio-inspired design: A bio-inspired design is necessary, which means that the robot must align with the anatomy of human limbs, and it must maintain the kinematic compatibility during rehabilitation motion.
2) Weight consideration: Weight reduction is necessary while designing the various components of the robotic exoskeleton. This is important to reduce the applied torque requirements of the exoskeleton as well as to reduce the slippage between anatomical joints of patients and the exoskeleton joints. The choice of the suitable mechanism and actuator also play important roles in the reduction of the overall weight of the designed exoskeleton.

3) Design Optimisation: To achieve a compact, lightweight, and portable exoskeleton robot, it is necessary to optimise certain design parameters. Owing to the large number of optimisation objectives, currently used evolutionary algorithms (EA) are less effective [32]. Therefore, newer optimisation algorithms are needed, which are advanced versions of evolutionary algorithms (EA), such as Genetic algorithms (GA), that must be investigated and utilised.

While dealing with various optimisation parameters, material optimisation is the most important factor. Not much research work has been published on the optimisation of the manufacturing material for lower limb exoskeleton robot as most of the robot manufacturing companies keep that material as a trade secret [33].

1.2.2 Material Optimisation

The selection of the proper manufacturing material is an important parameter for the lower limb exoskeleton design. Based on material properties, a robot exoskeleton can either be built by a soft or a hard/stiff material or a combination of both [34]. Hard and stiff materials, such as steel and aluminium, are the traditional choice for robot exoskeletons as these materials provide excessive strength and manufacturing preciseness. Aluminium alloys and steel are widely used to create links between the exoskeleton joints. Generally, the design and performance requirements of robot exoskeletons demand to utilize strong, stiff, and lightweight material for the application of necessary torque to the joints. However, the material properties need to be optimised to find a suitable material that is not heavy and can easily support the body weight of the wearer as well as the exoskeleton joints can bear the torque applied by mechanical actuators [35]. In order to optimise various material parameters a Genetic Algorithm-based optimisation routine will be used in this research work to obtain the best possible material, which can fulfil the mechanical design requirements of the exoskeleton while keeping the cost at a minimum level.

After the material selection, the suitable manufacturing method is an important parameter to consider. The selection of an appropriate manufacturing method ensures that the robot exoskeleton has the required strength at the links as well as joints.

1.2.3 Manufacturing Methods

Manufacturing methods play a vital role in the development of robot exoskeletons. The mechanical properties and durability of the robot exoskeleton, as well as the comfort level for the wearer also ensured by the manufacturing methods as these methods can provide the required strength and functional capabilities to the robot exoskeletons. The manufacturing

methods are mostly selected after the material has been finalized for the design of robot exoskeleton as these methods vary depending upon the selected material. Different manufacturing methods are utilized for metals and non-metallic materials [36]. The commonly used robotic exoskeletons manufacturing methods are listed below:

1. Extrusion: Extrusion is a metal forming process in which a metal or work piece is forced to flow through a die to reduce its cross section or convert it into the desired shape. This process is extensively employed to form metal rods and tubes used as a part of robot exoskeleton structures. Some advanced rehabilitation robots, such as the ATALANTE and Chuk-Exo robot exoskeletons, have been manufactured by extrusion [37].
2. Metal casting: Metal casting is a modern process with ancient roots. In the metal casting process, metal shapes are formed by pouring molten metal into a mould cavity, where it is cooled and later extracted from the mould. This traditional technique is still in use to manufacture various components of the lower limb rehabilitation robot exoskeletons, such as Expos, LOPES, ICRO, and ALEXIII [38, 39].
3. Computer Numerical Control (CNC): CNC machining is the most advanced manufacturing technique for the manufacturing of robot exoskeleton. It is a computerized manufacturing process in which pre-programmed software and code controls the movement of production equipment. The ETH Knee perturbator has been manufactured by using CNC machining [40].
4. Additive manufacturing and 3D Printing: Additive manufacturing using 3D printing is another shaping technique, which is particularly useful to design the various robotic components [41]. This technique has been widely used in the manufacturing of various lower limb robotic exoskeleton, such as for a lower limb exoskeleton for gait rehabilitation. The various exoskeleton components have been manufactured by using 3D printing method [42]. A combination of both 3D printing along with the CNC cutting method has been used to manufacture a carbon fibre lower limb exoskeleton with pneumatic actuators designed for ankle rehabilitation [42] .

Every technique has some benefits and drawbacks. Moreover, there are various factors involved in the selection of the manufacturing methods, which will be discussed in detail in Chapter 2 of this thesis.

1.3 Research Motivation

To use the wearable robotic exoskeleton for gait rehabilitation treatments and for aiding elderly, certain design, and material aspects of such robot exoskeletons need to be researched.

The increase in the elderly population and the need of more advance rehabilitation techniques motivates the author to work on the topic of rehabilitation robot exoskeletons. The limited access to the material properties of the available lower limb exoskeleton devices was another factor. Furthermore, the bulkiness and reduced wearability of the existing metallic robotic exoskeletons was other factors, which provided motivation to do material optimisation in this research. The motivation was to decrease the mass and keep it to a minimum without effecting the strength of the exoskeleton device. Another motivation of this research work was to simplify the design of the robot exoskeleton through a reduced need of mechanical actuators, which will further reduce the weight as well as the energy consumption of the exoskeleton. At last, the reliability and longevity of the robot exoskeleton was an important factor as the users of these devices are mostly interested in that due to the high cost of these rehabilitation robots. To summarize, the main research motivation factors are decrease in weight, improve strength, decrease in cost, and increase in the reliability of the robotic exoskeleton for gait rehabilitation.

1.4 Thesis outline

This thesis is divided into the following chapters:

1. The first introduction chapter outlines the design challenges and the motivation for carrying out this research work.
2. The second chapter of the thesis includes the literature review, which outlines the major research studies carried out previously in the field of rehabilitation robots. The research gaps are identified from the review of these studies and research goals are set out in the form of research objectives.
3. The third chapter gives a detailed description of mechanism and conceptual design of a lower limb robot exoskeleton for gait rehabilitation.
4. The fourth chapter focuses on the analytical work and gives a detailed description of the finite element analysis and optimisation carried out. The optimisation includes topology and material optimisation to select the most suitable lightweight material and design for the lower limb exoskeleton.
5. The fifth chapter includes the experimental work for material testing and optimisation to get the most reliable structure of lower limb exoskeleton. The material properties are tested and optimized to obtain a lightweight structure, which can last longer without any failure.
6. Chapter 6 describes the various processes of fabrication and assembly of the lower limb exoskeleton.

7. Chapter 7 gives a detailed description of the reliability analysis of the developed system by using a machine learning based approach.
8. Finally, Chapter 8 presents the main research findings of this thesis along with the major contributions and an overview of the future work.

1.5 Chapter Summary

This chapter discussed the need to develop a novel robotic gait rehabilitation and assistance exoskeleton for automated rehabilitation treatment along with its benefits in the context of patients, therapists, and the rehabilitation process in general. The importance of manufacturing materials in weight reduction of the gait rehabilitation robots were also discussed. Design challenges of the wearable robot exoskeletons were also explained along with the various design criterion. The need of material and design optimisation was explained. The important aspects of manufacturing methods were briefly discussed. Various examples of the robot exoskeleton manufactured by using the different techniques were presented. In the end, the research motivations to design a lower limb robot exoskeleton were given.

CHAPTER 2 LITERATURE REVIEW

A comprehensive literature review is carried out in this chapter to identify the fundamental research problems involved in the design, material selection, and manufacturing of robot exoskeletons for the lower limbs. A lower limb robot exoskeleton is being considered as the case study in the present research and, thus, existing lower limb rehabilitation robots are discussed through the lens of manufacturing materials and methods. Following this, design and mechanism analysis, finite element modelling and structural optimisation methods are presented for various lower limb robot exoskeletons. A survey of optimisation methods using genetic algorithms is included in this chapter. The main issues in the above research areas are discussed, which leads to the aims and objective as well as the scope of the research presented in this thesis.

2.1 Wearable Robots

Wearable rehabilitation robots are also called as robot exoskeletons, robotic orthoses, or active orthoses. These active orthoses are training robots, which are designed to work in parallel with the human body motion and have mechanical actuation to apply forces to a human limb. The first ever complete lower limb rehabilitation exoskeleton with mechanical actuators was conceptualised and developed at the Institute for Automation and Telecommunications, Yugoslavia in 1974 [43]. The University of Wisconsin prototype for gait rehabilitation was another example, which employed universal joints at the hip and ankle to provide kinematic compatibility between orthosis joints and human skeletal joints [44]. After that, various active orthoses have been developed for the purpose of rehabilitation. Other active orthoses devices such as LOKOMAT [26], HAL [45], and MIT-MANUS [46] were developed, tested in rehabilitation centres and clinics, and now are commercially available. Nevertheless, the field of active orthoses is still an active research area and there is a continuous improvement in the material, design, actuation, and functionality of such devices. In recent years, an active leg exoskeleton (ALEX) was developed. It is a robotic device from the University of Delaware for gait training of stroke survivors [47]. The lower extremity powered exoskeleton (LOPES) using Bowden cable-based actuation system is another example of a recent development [39]. Robot exoskeletons are mainly developed for the purpose of locomotor rehabilitation of stroke survivors to overcome the physical disability of the survivors. Hence, these devices must be lightweight and have ample strength to support the body weight of the patient [48].

After a review of the related literature, it has been observed that although the field of robotic rehabilitation is an emerging research field, only a small number of prototypes has been

proposed by the researchers in this field. Since the development of the first such robotic exoskeleton in 1974, only a small number of robot designs have gained the attention of physiotherapists for use in rehabilitation clinics. A possible reason could be the multidisciplinary nature of the research issues involved in the development of robot exoskeleton devices. Manufacturing materials, design, and manufacturing methods present significant challenges in the development of wearable robots, which have also been discussed in Chapter 1.

2.2 Manufacturing Materials

To date, the primary thrust of robot exoskeleton research has focused on medical applications, such as supporting mobility and rehabilitation of stroke and spinal cord injured (SCI) patients [49]. Lower limb exoskeletons for providing gait mobility assistance are of particular interest to the engineering research community as they have broader applications. Robot lower limb exoskeletons should be lightweight and easy to wear. Research in this area is shifting toward the development of lightweight materials from high-density materials. Hard and stiff materials are used to manufacture robot exoskeletons as these materials provide excessive power and preciseness. Initially, steel and its alloys have been used as the manufacturing material for a lower limb exoskeleton. LOKOMAT was developed during the late 1990s at ETH Zurich (see Figure 2.1). This is the first commercially used lower limb gait rehabilitation robot and it has been manufactured by using steel. After that, two more robot exoskeleton devices made from steel frames have been developed, named as Pneumatically Operated Gait Orthosis (POGO) and (Pelvic Assist Manipulator (PAM). These two devices were conceptualised at the Los Amigos Research and Education Institute, Downey, California (USA) to move the patient's legs with linear actuators attached to a frame placed around the subject and to assist the pelvic motion during human gait training on a treadmill [50].

In the search of lightweight robot design, aluminium has taken the place of steel due to its low density. A wearable lower extremity robot exoskeleton named CUHK-EXO was designed in Hong Kong for stroke patients (see Figure 2.2). The aluminium alloy (7075-T651) has been used as the main manufacturing material to keep the CUHK-EXO lightweight and highly stiff [51]. Aluminium 6061 has been employed in the design of a lower limb exoskeleton for the gait assistance of the elderly population [52]. More recently, titanium is rapidly replacing aluminium in the field of robot exoskeleton due to a better strength-to-weight ratio.

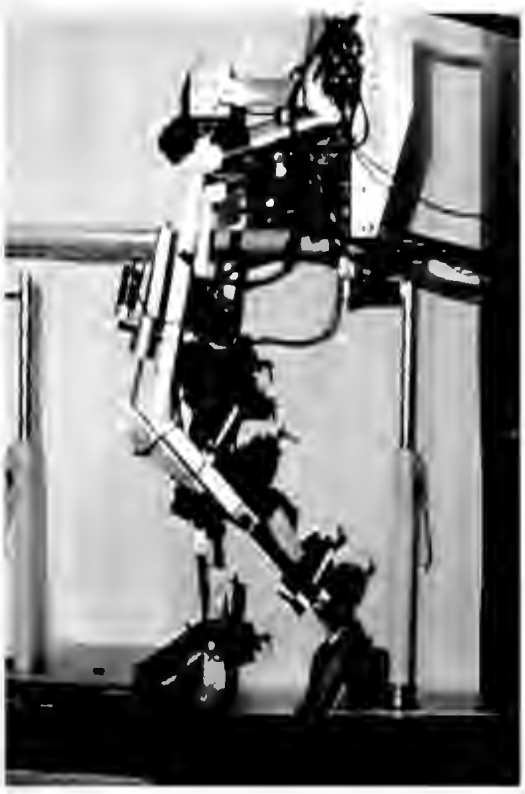

Figure 2.1 First clinical, steel prototype of the LOKOMAT system [50].

A robot exoskeleton of high-grade titanium named MINDWALKER was developed for paraplegics. In MINDWALKER the foot plates are made from carbon fibre to reduce the manufacturing cost [53]. Carbon fibre materials are gradually replacing metals to produce lightweight robot designs at lower manufacturing cost without effecting the strength of the exoskeletons.

A pneumatically operated robot knee-ankle-foot orthosis (KAFO) has been built at the University of Michigan (see Figure 2.3) [54]. It has been designed based on the concept of a lightweight mechanism and has utilised carbon polymeric composites in the design. There is a significant reduction in weight of the exoskeleton by using carbon fibre. Indego, which is lower limb robot exoskeleton, has been developed at Vanderbilt University with the goal to reduce the weight without compromising the strength of the device [55]. Indego is composed of carbon composites (see Figure 2.4). The use of carbon fibre as a replacement of aluminium has helped in reducing the weight of Indego to 27 pounds (12.25kg) without compromising the strength of the orthosis.

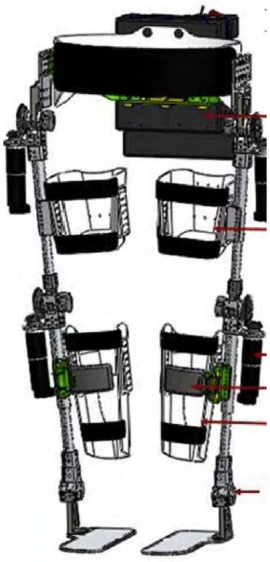

Figure 2.2 Lower limb aluminium exoskeleton CUHK-EXO [51].

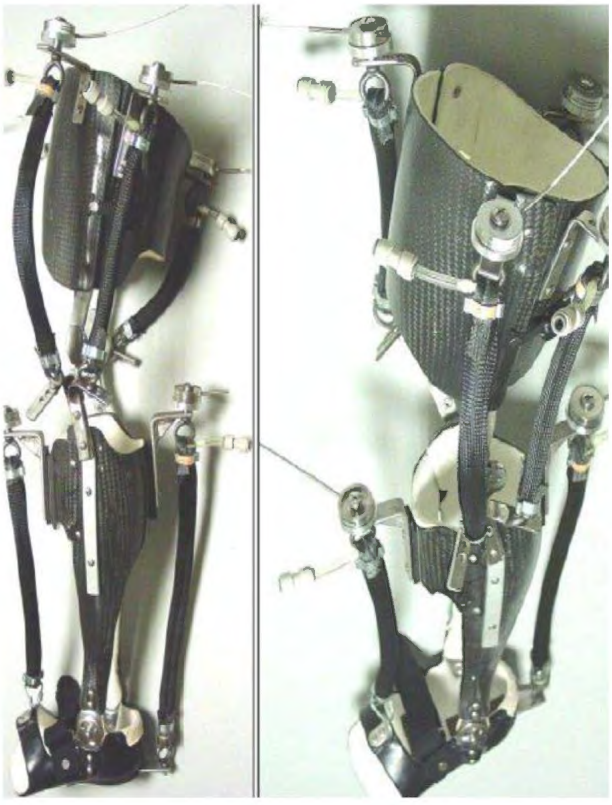

Figure 2.3 Knee-ankle-foot orthosis (KAFO) made from carbon fibre [54].

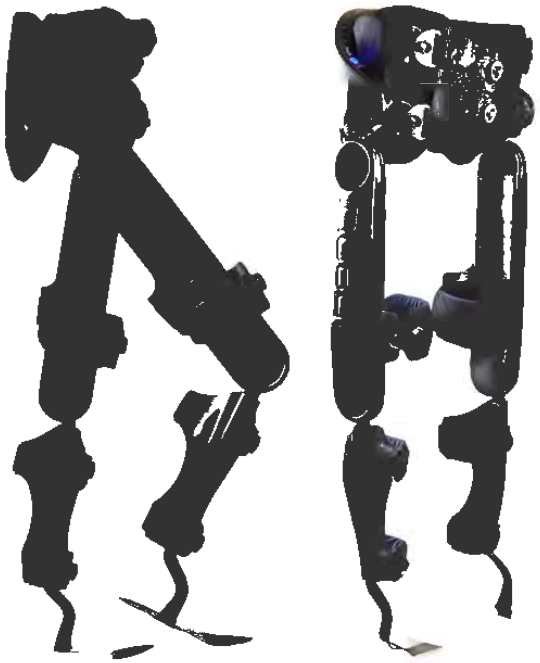

Figure 2.4 A lower limb exoskeleton Indego made from carbon composite [55].

It is clear from the above discussion that the material has a very important role to keep the robot exoskeleton lightweight, comfortable, and user friendly. However, the mechanism design is another important factor to consider as the exoskeleton robot must satisfy the coordination of robot and the human body.

2.3 Mechanism Design

The mechanical structure and mechanism design of the lower limb exoskeleton must be able to match the biomechanical requirements of the human motion in terms of ranges of motion as well as joint moments [56]. Therefore, the mechanism design of the lower limb exoskeleton robot is an important factor to consider in the development of these exoskeleton robots. Generally, the kinematics of the human leg are represented as a seven degrees of freedom (DOFs) chain. There are three rotational degrees of freedom at the hip and four at the lower leg (three at the ankle and one at the knee). However, it is evident from detailed anatomical studies that the human knee joint structure is more complex in nature, as it displays angular movement in three dimensions and translation in one dimension relative to the hip during walking. Similarly, the motion of the ankle joint is characterised by plantarflexion - dorsiflexion. Thus, in the sagittal plane, which is the dominant plane of motion during walking, the simplified structure of the lower limb with revolute joints at the knee, ankle, and the hip is shown in Figure 2.5. This simplified kinematic structure provides the basics of the kinematic design of many robot exoskeleton devices for walking assistance.

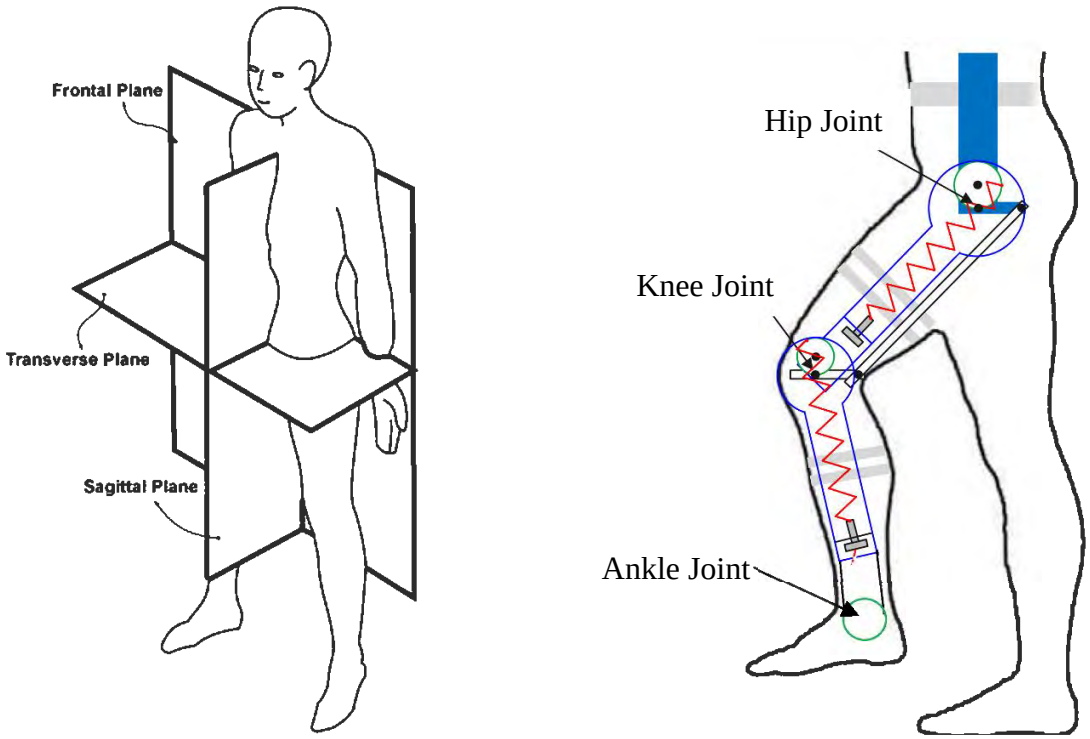

Figure 2.5 The kinematic structure of the lower leg in the sagittal plane [57].

Several research studies have been carried out utilising different mechanisms to simulate human walking [58]. An early active orthosis device has been designed by using a leg brace with a crank located at the hip to wind up a torsional spring at the knee joint to produce a reciprocating motion at the knee. This design was presented in a US patent in 1935 by Cobb and is shown in Figure 2.6 [59]. Another simple exoskeleton named “kinematic walker” has been designed, which reduces the control problems of a large number of servo systems to obtain a gait trajectory by using the kinematic coupling between the hip and the knee [60].

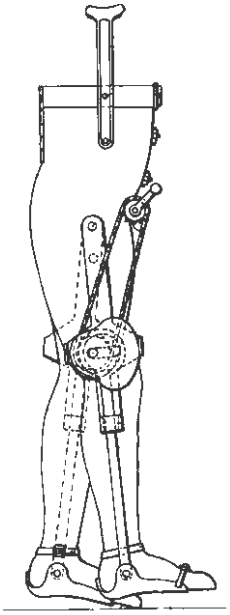

Figure 2.6 Cobb's lower leg exoskeleton [59].

The lower limb rehabilitation exoskeletons are based on anthropomorphic measurements of the human lower limb, and they are built specifically by following their natural biomechanical performance parameters. This information can be easily collected using various types of motion capture technologies available commercially. Depending on the complexity of the physiological task to be supported, a linkage topology is selected. This selection is dependent on the designer's experience, which is aided by the advent of several commercially available mechanism synthesis packages (e.g. Mehgan [61], MotionGen [62]). There are a variety of linkage mechanisms that have been developed and modified by various researchers in the field of robot design. The entire human leg has been approximated by a spatial serial Trunk Recovery Scale (TRS) chain mechanism and dimensional synthesis is used to obtain a two DOF spatial eight-bar linkage to mimic human gait cycle [63]. More recently, the design of a lower leg exoskeleton device based on a Stephenson II six-bar function generator for 11 accuracy points has been illustrated [64]. This work was further extended to present the design of an optimised Stephenson III six-bar linkage for following the natural ankle trajectory by a group of researchers [65]. It is clear from the above discussion that the Stephenson six-bar linkage mechanism is the latest development in the mechanical design of the lower limb exoskeleton. This mechanism has also been used by a group of researchers at California State University to design a lower leg exoskeleton and the dimensions were closely matched to the lower limb kinematics of the human leg [56]. Their proposed model, which was obtained by a Stephenson III six-bar linkage mechanism, is shown in Figure 2.7.

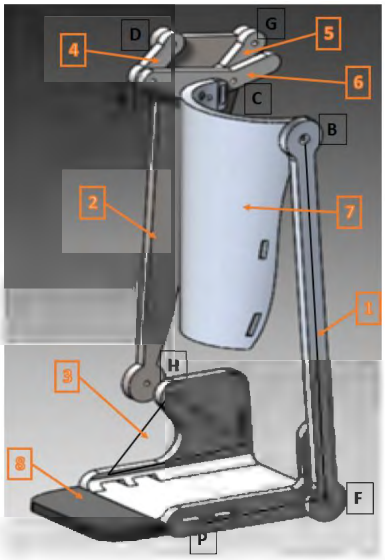

Figure 2.7 The design of a lower limb exoskeleton adapted from the six-bar linkage [56].

After the selection of a suitable mechanism for the mechanical design of the exoskeleton devices, the next stage in the development of the exoskeleton is the mechanism analysis. This is mostly done by using simulation-based approaches to save time and money in carrying out unnecessary experimental work. Hence, finite element modelling and analysis are commonly used to design and analyse the mechanisms of the lower limb robotic exoskeletons before making the prototypes of these devices.

2.4 Mechanism Analysis and Design

Design and mechanism analysis is important for obtaining a suitable structure that can perform the desired rehabilitation tasks. There are certain elements involved in obtaining a feasible structure. Hence, the mechanism analysis starts by converting the kinematic model into a 3D CAD model to conceptualise the design of the lower limb exoskeleton robot. After that, various types of design parameters are optimised to achieve a feasible mechanical structure.

2.4.1 Finite Element Modelling

The use of finite element analysis considerably eliminates the need for unnecessary experimental work, hence, resulting in saving time and resources. The finite element analysis is widely used in the design and development of various lower limb exoskeleton devices. It provides the designer the freedom of applying torques, distributed loads and external loads at the various joints of the virtual prototype models of the lower limb exoskeleton and to observe the outcomes. These protype models are developed by using certain Computer Aided Design (CAD) software that is commercially available. In the finite element modelling software, it is also possible to select different manufacturing materials in order to find a suitable material that can produce a lower limb exoskeleton with lightweight and high strength properties.

Finite Element Modelling has been carried out in the design of an ankle exoskeleton with flexion/dorsiflexion and adduction/abduction to facilitate the user's independent centre of gravity adjustment [66]. In another study, a numerical model of the patient's foot was generated and used to design an ankle–foot orthosis model using the CAD software SolidWorks. The designed model was mechanically analysed by the finite element method using the ANSYS Workbench under different static and dynamic loading conditions. The designed lower limb exoskeleton model, which is shown in Figure 2.8, has been analysed before the manufacturing process [67].

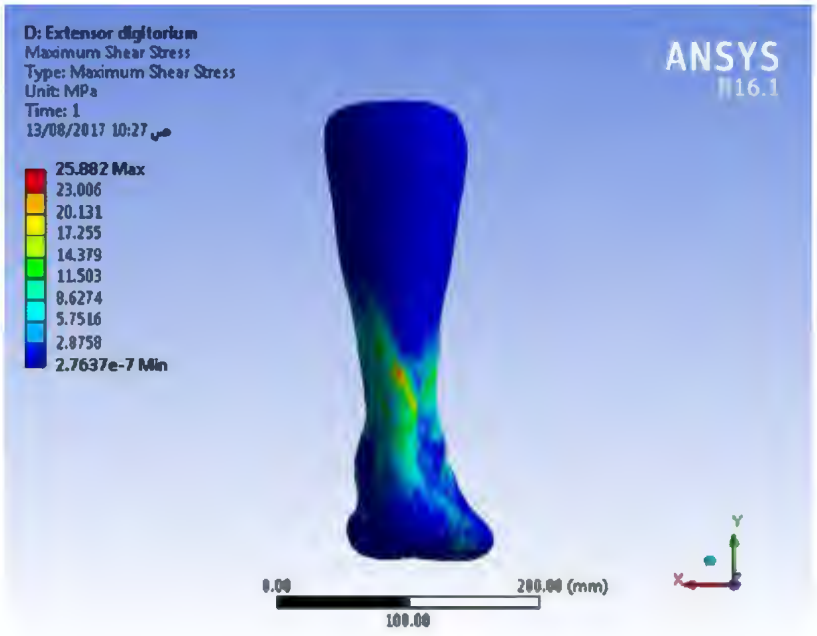

Figure 2.8 Stress distribution model of a lower limb exoskeleton [67].

The finite element analysis of a lower limb robot for walking assistance has been carried out using aluminium alloy 7075-T6. The authors have focused on the stress distribution during the application of the patient's weight, while the robot is being used [68]. The finite element analysis has been used to improve the structure to increase the weight bearing capacity of a lower limb exoskeleton [69]. In this study, the ergonomics parameters of pivotal bearing parts, such as hip and thighs, have been employed to create a 3D CAD model and, later, the model has been analysed under different loads by using Ansys. The authors presented an improved design to make the robot more efficient to work with partially paralysed patients by increasing the stability of the robot structure [70]. A robot model for gait rehabilitation has been presented in which the authors have used aluminium composite panel for the material of

its frame [71]. After design and mechanism analysis, optimisation is an important step towards the development of a lightweight and reliable structure of a lower limb robot exoskeleton.

2.4.2 Structural Optimisation

While designing a lower limb exoskeleton mechanism, it is highly recommended that its structure should be optimised to reduce the weight and improve strength [72]. Material and topology optimisation of robots is an emerging area of research as these two optimisation factors play an important role in the structural design of a robotic exoskeleton. Such optimisation is useful in saving the cost of materials, providing better mechanical performance as well as reducing the time in running unnecessary experimental work. The topology of these robots needs to be modified and optimised to improve their mechanical performance. Structural and topology optimisation are the ideal methods in the preliminary design stage to achieve the desired shapes and configuration of the robot's mechanical parts, as this process results in a suitable material distribution within the optimised area [73].

For this reason, many studies have been conducted to optimise robotic exoskeleton designs by formulating different optimisation objectives and approaches. Possible issues faced during the structural design of robot exoskeletons include a reduced workspace, increased singularity, higher actuator force requirements, etc. It has been revealed from the literature that to exploit the comprehensive potential of the robots, researchers in the past have worked on their design optimisation [74]. Several trial-and-error or exhaustive search optimisation methods were used during previous research studies to solve the different design issues of lower limb exoskeletons. Design optimisation using an exhaustive search minimisation method has been used in [75], wherein a performance index called *space utilization* is proposed to evaluate the optimal kinematic design of a linear Delta robot. To use the trial-and-error search methods, there is a need of rigorous experimental work or simulations to achieve an acceptable design. Hence, the main disadvantage of using these optimisation methods is the exponential increase of simulation time with the increase in the number of optimisation parameters. Furthermore, tuning of all design parameters simultaneously is difficult and time consuming.

Researchers worldwide have also used numerical methods to optimise lower limb robotic exoskeletons. Several performance indices, namely dexterity index, manipulability, isotropy, conditioning index, Global Conditioning Index (GCI), and global isotropy index, have been defined by different researchers and details of these indices are provided in [76]. Geometrical optimisation of a 2-DOF planar parallel robot has been performed to maximise a global mechanical advantage matrix. An exhaustive search has been performed using the

Monte Carlo method for the optimisation [77]. The structural topology optimisation of a robotic exoskeleton has been reported in [78], in which the optimisation process has been carried out using the finite element analysis method. As a result of the optimisation, a structurally optimised lightweight model of an exoskeleton has been obtained with a reduced weight of 9.92% as compared to the existing exoskeleton. In another research work, a lower limb exoskeleton has been optimised to improve the energy efficiency [79]. A more energy efficient exoskeleton structure has been obtained by the introduction of elastic elements into the structure. Here, an approach based on simultaneous optimisation of the parameters of the elastic elements and regulator parameters has been proposed. The optimisation has been performed using Sobol sequences and a nonlinear optimisation algorithm as discussed in [80]. Various optimisation algorithms have been reported in the literature for the structural optimisation of robotic exoskeletons. From these optimisation algorithms, Genetic Algorithms (GA) are mostly used to perform multi-objective design optimisation [81].

Recently, Genetic Algorithms have also been used by researchers to optimise the design of lower limb exoskeletons for gait rehabilitation. GA works with a population of points and processes simultaneously, hence, is more likely to provide a global solution [82]. In the study of [83], the design of an ankle robot for lower limb rehabilitation has been optimised. In this published work, three design stages of the ankle robot were identified and investigated and from that, six performance objectives were identified and optimised by using GA. Optimal robot link lengths have been obtained by maximising the objective function using GA. A lower limb exoskeleton rehabilitation robot design has been optimised with the main goal of achieving a lightweight structure [84]. Finite element analysis has been used to design and analyse a prototype model and an optimisation scheme has been put forward with the conditions of meeting requirements for the intensity, rigidity, vibration characteristics of rehabilitation training. The weight of the optimised exoskeleton robot has been reduced by 10%. The protype design before and after optimisation is shown in Figure 2.9.

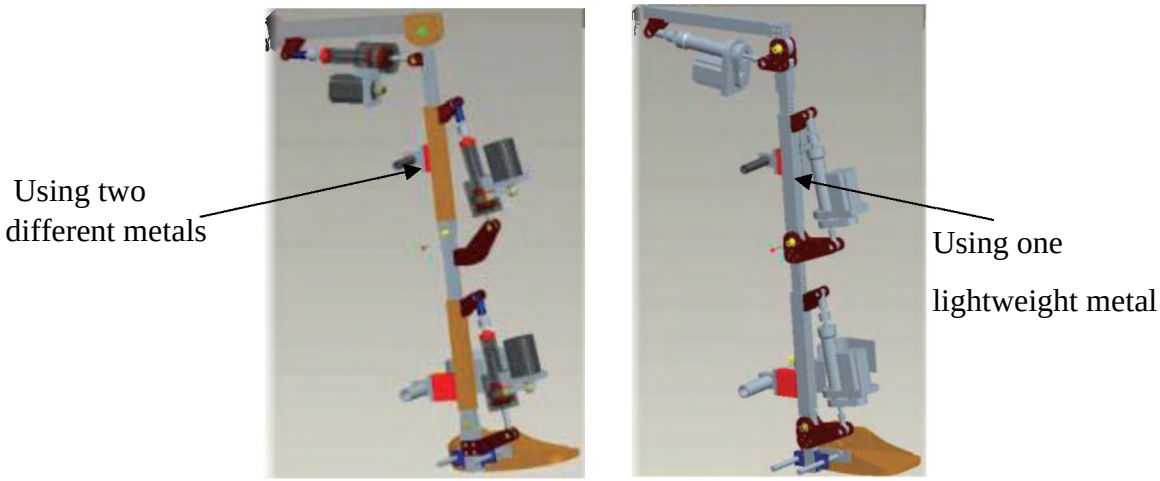

Figure 2.9 Lower limb exoskeleton with optimised weight: (a) before optimisation with two metals (b) after optimisation with a single lightweight metal structure.

The majority of the optimisation work has been carried on the design and structural aspects of the lower limb exoskeleton to make it lightweight. However, to the best of the author's knowledge, little research has been published on the material aspects of a lower limb exoskeleton. Furthermore, only a few optimisation studies have been carried out that focused on the material properties to select a suitable material for the lower limb robotic exoskeleton. The material properties, such as density, have never been used as a design objective to optimise the structure of a lower limb exoskeleton for a lightweight and highly stiff design. The joint stiffness is another important aspect to consider during the design and optimisation of a lower limb exoskeleton. Without the proper stiffness analysis during the design stage, the lower limb robot may cause chattering, which will lead to discomfort to the wearer [85]. After optimisation the next step is the manufacturing process of lower limb exoskeleton, and the choice of manufacturing process and proper actuating system is important in developing a lightweight design.

2.4.3 Manufacturing Method

Numerous manufacturing techniques and materials have been developed for lower limb exoskeletons over the last two decades, resulting in the design of a variety of robot exoskeletons for gait assistance for elderly and disabled people. Additive manufacturing (AM) is considered an ideal method for developing customized robot exoskeletons with a reduction in manufacturing costs. The potential for AM has been demonstrated for rapid and cost-effective fabrication and transformative service of the custom hip-knee-ankle-foot orthoses. The manufacturing methods are mostly selected after the material has been finalised for the design

of the robot exoskeleton, as these methods vary depending upon the selected material. Different manufacturing methods are utilised for metals and non-metallic materials [86].

Several conventional manufacturing methods, such as extrusion, Computer Numerical Control (CNC) machining, and metal casting, are used in the fabrication of lower limb robot exoskeletons. Extrusion is a metal forming process in which metal or a work piece is forced to flow through a die to reduce its cross section or convert it into the desired shape. This process is extensively used in pipe and steel rod manufacturing. The force used to extrude the work piece is compressive in nature. Metal casting is a modern process with ancient roots. In the metal casting process, metal shapes are formed by pouring molten metal into a mould cavity, where it is cooled and later extracted from the mould. The ATALANTE and Chuk-Exo robot exoskeletons were manufactured by using extrusion and CNC machining processes. The ETH Knee perturbator was manufactured by using CNC machining in combination with conventional drilling methods. The Expos, LOPES, ICRO, and ALEXIII robot exoskeletons were manufactured by metal casting, followed by CNC machining of these metal casted parts. The SCUT robot exoskeleton was manufactured by using the metal extrusion process in combination with CNC machining. Details for the various manufacturing process used for several lower limb robotic exoskeletons are provided in the Table 2.1.

Metal joining processes have also been used in combination with conventional machining methods. WPAL was manufactured by using extrusion and the welding of these extruded aluminium parts. A high cost per part, cost of CNC machining, hard to achieve uniform strength, difficulty in achieving uniform wall thickness, and poor accuracy in design and shape of the finished part are some of the disadvantages of the conventional techniques of extrusion, metal casting, and CNC machining over modern manufacturing methods such as 3D printing.

3D printing is an additive manufacturing technique, which is used for fabricating a wide range of structures and complex geometries from 3D model data and has widely been used for polymeric materials, though there is an increasing trend of using this method for metals as well. The method prints successive layers of material on top of each other. A process called stereolithography (SLA) was developed by Charles Hull in 1986 [87], which was followed by subsequent developments such as powder bed fusion, fused deposition modelling (FDM), inkjet printing, and contour crafting (CC). 3D printing, involving various methods, materials, and equipment, has seen a significant evolution over the years and can transform manufacturing processes. Additive manufacturing has seen broad applications in various industries, such as construction, prototyping, and biomedical engineering. New applications are also emerging

with the rapidly advancing research in the domain of novel materials and AM methods. Polylactic acid (PLA) and acrylonitrile butadienestyrene (ABS) are the major types of polymers used in the 3D printing of composites.

Table 2.1 The manufacturing process used for various lower limb exoskeleton.

Name of robot exoskeleton device	Manufacturing method
Ekso [88]	3D printing of individual components and joining all
Re Walk [89]	Manufactured by using 3D printing
Indego [49]	Three parts have been manufactured by selective laser sintering
HAL-Hybrid assistive limb [90]	3D printing
Atalante [47]	Extrusion, CNC machining
Chuk-Exo [51]	Extrusion, CNC machining
ETH Knee pertubator [40]	CNC machining and drilling
Expos [38, 91]	Metal Casting and CNC machining
Lokomat [92]	3D printing for casing of actuation mechanism and CNC milling for metal parts
ALEX III [93]	Casting, CNC machining
SCUT robotic exoskeleton [94]	Extrusion, CNC machining
WPAL [95]	Extrusion, joining
LOPES [39]	Metallic casting, CNC machining
MINDWALKER [53]	Extrusion, 3D printing
PAM and POGO [96]	3D printing of metallic parts and joining
ICRO [97]	Casting, CNC machining
KAFO [54]	3D printing
SR-AFO [98]	3D printing and Thermal bonding

A specific emphasis has recently been put on the use of 3D printing for ankle-foot exoskeletons [99]. It is important to mention here that 3D printing has not extensively been used and reported in the literature for the development of lower limb robot exoskeletons. The complete manufacturing process for any lower limb exoskeleton involves various processes to get the final product. A 3D printed robot hip exoskeleton was proposed in [100], in which a CNC machined aluminium part has been combined with a 3D printed polylactic acid part. As a result, a significant reduction in weight and manufacturing time has been achieved. A powder bed fusion-based manufacturing method was also utilised to develop a multi-joint robot exoskeleton for lower limb assistance [101]. The Indego robot exoskeleton was also manufactured by using 3D printing. Indgeo has both carbon polymeric parts manufactured by 3D printing and metallic parts made by conventional CNC machining methods. Similarly, the mechanical frame of Lokomat has been manufactured by using CNC machining. The casings to hide the mechanical parts of Lokomat for improved appearance have been manufactured by

using 3D printing. After manufacturing methods, the choice of the actuator is an important factor as these actuators run the robot exoskeleton devices to aid the physically disabled people.

2.4.4 Actuators

An actuator is a part of a device or machine that helps it to achieve physical movements by converting energy, often electrical, air, or hydraulic, into mechanical force. Actuator is the component in any machine that enables movement. Actuators provide mechanical torque to the lower limb of human subjects and move them on the predefined paths. Choosing a suitable actuation type for the robot exoskeleton is an important parameter to consider during the design and manufacturing stage [102]. Various types of actuators have been used by different researchers to develop various lower limb robotic exoskeletons. Out of these, the three most commonly used ones are hydraulic actuators, pneumatic actuators, and electric motors or electromagnetic actuators [103]. Prototypes of robot lower limb exoskeletons such as LOKOMAT and BLEEX [104] are powered by electromagnetic actuators [92, 105]. The actuator types used in the manufacturing of various orthoses are listed in Table 2.2.

Table 2.2 Actuators for various lower limb exoskeleton devices [106].

Name of robot exoskeleton device	Type of actuation
Ekso	Hydraulic actuators
Re Walk	DC motors with a battery unit
Indego	DC brushless motor
Rex [107]	Linear actuators
HAL-Hybrid assistive limb	Electric DC actuation
Atalante	Brushless DC motor
Exoatlat [108]	Electric actuators
Vanderbilt exoskeleton [109]	Electric actuators
Chuk-Exo	Electric actuators
ETH Knee pertubator	Brushless and flat actuators
Expos	Tendon connecting motors and pulleys
Lokomat	DC drive motor
ALEX III	DC drive motor
SCUT robotic exoskeleton	DC drive motor
WPAL	DC motor drive
LOPES	Bowden cable and SEA
NUS Knee-ankle-foot robot [110]	SEA
MINDWALKER	Spring-based SEA
ALTACRO [111]	Spring-based SEA
PAM and POGO	Pneumatic cylinders
ICRO [97]	PMA
KAFO	PMA
SR-AFO	PMA

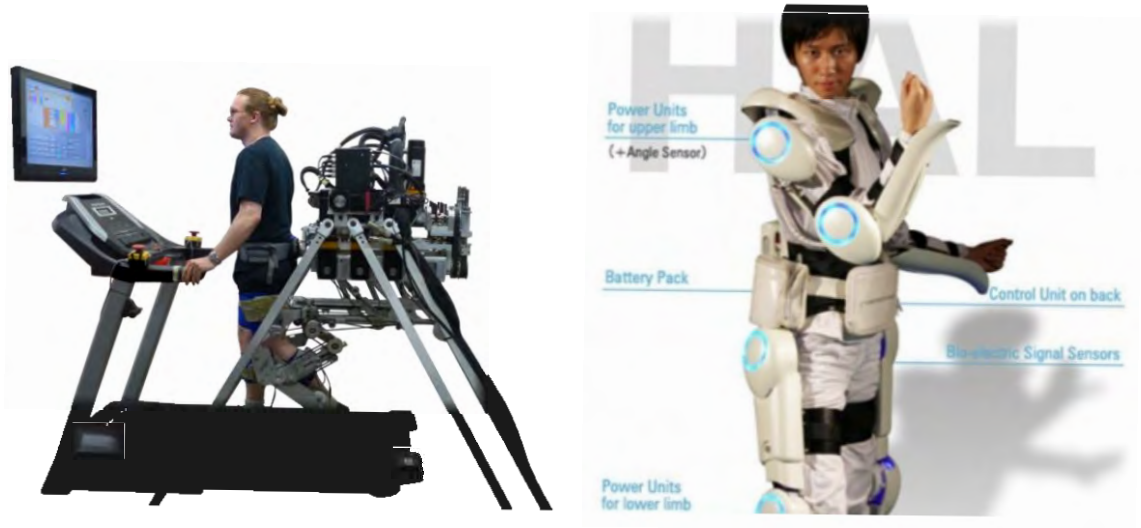

(a) (b)

Figure 2.10 Robot exoskeletons powered by electromagnetic actuators: (a) ALEX [42], (b) HAL [23].

DC motors are widely used in the actuation of lower limb rehabilitation exoskeletons. DC motors are broadly classified into two types: brushless DC motors and synchronous DC motors. The exoskeletons such as Indego [55], Re Walk, HAL (Fig. 2.10b) [112], Lokomat [92, 105], ALEX (Fig. 2.10a) [113], SCUT robotic exoskeleton [94], WPAL [114] used DC motors for actuation. The benefits of electric actuators lie in their high-power capacity, torque-to-weight ratio, and precision. Moreover, they produce less noise in comparison to pneumatic or hydraulic ones. Electromagnetic actuators are used in Exoatlat, the Vanderbilt exoskeleton [115], and CUHK-EXO [51].

Since the development of electromagnetically actuated robot lower limb exoskeletons, there has been an increasing trend among the engineering community for the development of compliant actuation concepts for these exoskeletons [102]. These compliant actuators are believed to provide safer human-robot interactions as compared to electromagnetically actuated ones. The reason for the improved safety is their inherent compliance which can absorb unexpected involuntary forces provided by the patients such as in the form of tremors. Later prototypes of lower limb robot exoskeletons have increasingly been powered by compliant actuators such as pneumatic and hydraulic. The robot exoskeleton Ekso has been actuated by a hydraulic system with the advantage of providing large output, but an additional energy supply system was needed [116]. On the other hand, exoskeletons with pneumatic actuators are known for their lightweight and compliance. These pneumatic actuators in the

form of cylinders have been used in the design of PAM and POGO exoskeletons [96]. Pneumatic actuators are compliant and have been selected due to their lightweight and high

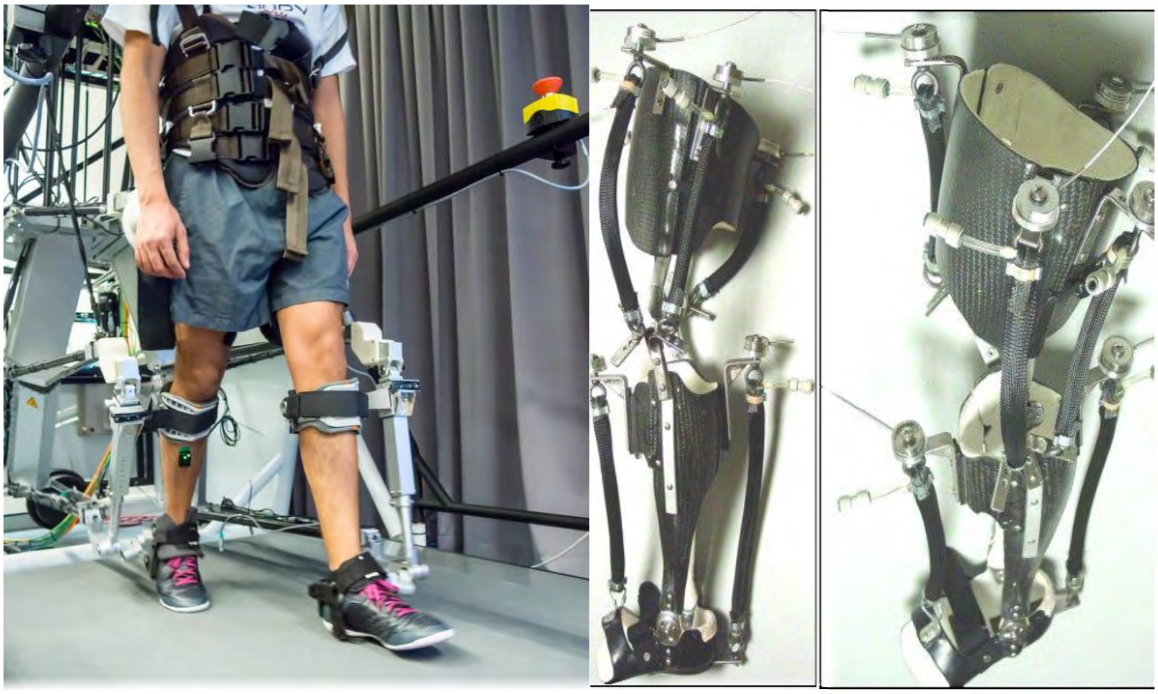

(a) (b)

Figure 2.11 Robot Exoskeletons Powered by Compliant Actuators: (a) LOPES [38], (b) KAFO [52].

power-to-weight and power-to-volume ratios as compared to electromagnetic and hydraulic actuators.

Later, various other forms of pneumatic actuators have also been developed and utilised for lower limb rehabilitation exoskeletons. The most common type of these pneumatic actuators is Pneumatic Muscle Actuators (PMA) [117]. PMA work similar to skeletal muscles, as they can only generate unidirectional pulling forces [118]. As an example, the University of Auckland has proposed a compliant robotic orthosis, which is actuated using PMA. The robot provides motions in the sagittal plane allowing for hip and knee joint rotations [97]. A knee-ankle-foot orthosis (KAFO) powered by PMA (Fig. 2.11b) for providing sagittal plane motions to the ankle joint has been developed at the University of Michigan [119]. Later, a different variant of PMA has been developed at the Vrije University Brussels and is known as pleated PMA. Pleated PMA have been utilised for the development of a knee robot exoskeleton [120]. Since the PMA can only provide unidirectional forces, they must be used in pairs for generating bidirectional forces. This presents a drawback for the control of PMA powered rehabilitation robots due to the increased complexity of the control system [121]. The usage of either

pneumatic or hydraulic actuators also make exoskeletons non-portable, heavy, and hard to manipulate. Despite their drawbacks, there are still several successful implementations of these actuators in lower limb exoskeleton systems [122].

These limitations of hydraulic and pneumatic actuators have prompted the development of new actuation concepts for the rehabilitation robots to overcome these limitations. The most recent and successfully implemented concept in the lower limb rehabilitation exoskeletons is the concept of series elastic actuators (SEA) [123]. These SEA are lightweight, compliant and provide safer human-robot interaction. They also do not produce noise like hydraulic and pneumatic actuators and can provide bidirectional forces. These SEA are constructed by combining electromagnetic actuators in series with a spring. Bowden cables have been used in combination with SEA to create "joint-less" exoskeletons and utilise the patient's natural joints instead [124]. LOPES at University of Twente (Fig. 2.11a) [39], National University of Singapore (NUS) Knee-ankle-foot robot [91], MINDWALKER [53], ALTACRO [111], and Harvard University's Exosuit [125-127] have utilised SEA as their actuation method [128]. With the elastic component, SEAs are back-driven and intrinsically compliant [126]. They work as a buffer between the limbs and the exoskeleton, which helps in reducing the impact of the externally applied shock on the subject's joints [125].

2.4.5 Reliability Analysis

A reliability analysis of the systems is useful for the development of mechanical products with the aim of computing the probability that the system functions successfully by keeping in view the various uncertainties. Various research efforts have been employed to enhance the accuracy and efficiency for the estimating the system reliability. First-order and second-order reliability methods (FORM and SORM) have been used for the estimation of the time-independent reliability [129, 130]. The analytical work has been carried out by the transformation of a limit state function (LSF) into a standard normal space. For performing the reliability assessment based on the first- or second-order Taylor expansion, a most probable point (MPP) is identified as the closest point from the failure surface to the origin. Surrogate modelling techniques [131-133] have been used to lighten the burden of expensive computational costs and approximate reliability by employing sampling methods such as Monte Carlo simulation (MCS) [134, 135] and importance sampling [136, 137]. As the performance of mechanical systems gradually degrades over time, effective time-dependent reliability analysis is of critical importance to practical robotic rehabilitation applications.

In the previously published research studies, time-dependent reliability analysis

approaches have been investigated by using various methods [138-140], which include extreme value-based methods [141, 142], out-crossing rate method [143, 144], and surrogate modelling-based technique [145, 146]. The primary target of extreme value-based methods is to identify the extreme system performance. These methods allow the use of traditional time-independent reliability analysis methods for assessing the time-dependent reliability. The reliability of any system including a robotic system is dependent on components forming that system [147]. To estimate the reliability, a logic function is used to express the relationship between the system's state and its components' states. The logic function is static, meaning that the performance configuration keeps invariant. Static reliability analysis methods including Static Fault Tree [148], Reliability Block Diagram [149], and Binary Decision Diagrams [150] are appropriate methods for conducting reliability analysis of a system.

Some dynamic reliability analysis methodologies have been developed to capture the time-dependent sate transition during the usage stage. Commonly used methods are named state transition diagrams [151, 152] , Stochastic Petri nets [153, 154], Dynamic fault tree analysis [155, 156], Go-Flow [157, 158], and Dynamic Bayesian Network [159, 160]. Many time-dependent sate transition strategies namely, transitions based on set points, competing events, simul tenuous transition/scenarios, and component influences on transition rates and dependencies have been developed from the current dynamic reliability methods [161]. Therefore, the current dynamic reliability methods focus on the trigger rules for state transition, but the correlation of different system states' evolution is rarely referred to. For the lower extremity exoskeleton, the states of joints and the end-effector are correlated due to the time sequence and error propagation. Hence, new dynamic reliability analysis methods are needed for efficiently handle the reliability of the lower extremity exoskeleton.

In recent times, deep learning has gained more popularity in the field of machine learning due to its potential advantages in handling large scale data and feature extraction. Based on the information obtained from the collected data, the deep learning framework utilises a layered structure of algorithms to make predictions, and it has been applied for classification and regression problems in various fields of practical applications [162], such as medical information processing, image processing, computer vision, robotics and control, etc. To deal with data sequences, inputs and historical information are processed in the internal memory of recurrent neural network. It is possible for vanishing and exploding gradient to occur during the training process of a deep learning neural network, such as recurrent neural networks, which significantly affect the training speed and prediction accuracy. To deal with such challenges,

the long-short term memory network (LSTM) has been introduced with a structure of multiple gates to control the information flow, and it has been successfully applied in speech recognition, natural language processing, and condition-based maintenance. The LSTM-based neural network has great potential for robot applications. The reliability analysis for the lower limb rehabilitation robots, in which many design parameters are involved, can be performed with improved accuracy by using this approach.

From the literature, it was found that most of the reliability studies have been carried out with properly actuated rehabilitation robot systems, such as Berkeley Lower Extremity Exoskeleton (BLEEX) [163]. However, the reliability testing of an underactuated mechanism is equally important, as this mechanism gives the robot designer and engineers a freedom of producing lightweight robot exoskeletons. To the best of the author's knowledge, there is no research study published for a sequential time-dependent reliability analysis of an underactuated robot system used for gait rehabilitation. Hence, there is a research gap because of the unavailability of such a reliability analysis method for an underactuated mechanism for a lower limb exoskeleton. From the discussion presented in Section 2.4, some research gaps were identified, which leads to set the research aims of this research work.

2.5 Research Gaps and Objectives

From the literature review, there are certain research gaps in the material selection, design, and analysis of lower limb robot exoskeletons. These gaps are listed below:

1. In mechanism design, there is no previously published research study, to the author's best knowledge, on rehabilitation robots that is underactuated with linkage-based mechanism. There are various studies on linkage-based mechanisms [64, 65], but these mechanisms are properly actuated, which increases the overall weight of the robot exoskeleton.
2. Material selection is an important part for decreasing the overall mass of the exoskeleton. The material should have good strength to weight ratio. Most of the commercially available exoskeletons for gait rehabilitation are made up of heavy metal metals such as, aluminium or steel [106]. Hence, there is a need to explore a light weight and high strength material.
3. Topology and design optimisation are the terms that are alternately used [164]. Optimisation to reduce the overall mass of the robotic exoskeletons is also important. Various structural optimisation studies have been undertaken for lower limb exoskeletons using different optimisation approaches such as nonlinear

optimisation algorithm [80]. A lower limb exoskeleton rehabilitation robot design has been optimised by using Genetic Algorithm (GA) with the main goal of achieving a lightweight structure [84]. However, to the author's best knowledge there is a missing trend to perform both material and topology optimisation by using a GA as the author could not find any published research data on this type of optimisation.

4. The choice of suitable manufacturing technique also plays an important role towards the development of a reliable structure of a robot exoskeleton. In recent times, most exoskeleton devices have been fabricated using 3D printers [80, 96]. Casting techniques are not much used in the previously published research as this technique has several benefits over 3D printing [165] and they must, therefore, be explored in the manufacturing of lower limb exoskeleton.
5. At last, the reliability analysis – an important part of the present research – is used to determine the reliability of the designed system of a lower limb robot. From the literature, it was found that most of the reliability studies by using machine learning (ML) have been carried out with properly actuated rehabilitation robots [163]. However, the reliability analysis of underactuated systems must be explored to fill the research gap.

These gaps will be addressed by this research work. The main aim of this research is to develop a lower limb robot exoskeleton, which is comfortable and lightweight but must be strong enough to support the weight of the human body for a longer period. The research objectives to achieve this research aim are given below.

2.5.1 Mechanism Design of an Underactuated Gait Robot

An underactuated mechanism will be designed for the lower limb gait rehabilitation robot. The biomechanics of human gait will be studied to obtain the naturalistic human leg motion.

2.5.2 Material Selection and Finite Element Modelling of the Proposed Gait Robot

After mechanism design, the next step towards the development of a lower limb exoskeleton robot is the material selection. which is the second research objective. The material choice plays an important role in the determination of exoskeleton weight, strength, and reliability. Various materials will be compared, and a suitable lightweight and high strength material will be selected. Three materials with different properties will be analysed and characterised by using finite element analysis.

2.5.3 Topology Optimisation

The optimisation will be carried out to make the structure as lightweight as possible without effecting the strength of the designed robot structure. This includes both material and topology optimisation. The materials that are currently used in the manufacturing of the lower limb exoskeletons will be optimised and a manufacturing material will be selected, which will be used to fabricate the robotic prototype.

2.5.4 Manufacturing and Evaluation of the Gait Robot

Another objective of this research work is the physical development of the lower limb exoskeleton robot prototype by using an additive manufacturing method. A combination of moulding and CNC cutting will be used to develop the prototype. The material properties will be evaluated.

2.5.5 Reliability Analysis of the Designed Gait Rehabilitation Robot

The final objective of this research study is the reliability analysis of the designed lower limb exoskeleton. Keeping in view the complexity of reliability analysis and the involvement of many factors, a machine learning based approach will be used to derive the time-dependent reliability of the designed underactuated lower limb robot.

2.6 Scope of Thesis

This thesis covers a broad scope of the design mechanism, manufacturing materials, and prototype realisation of an underactuated lower limb exoskeleton robot. The mechanism was designed according to the Stephenson six-bar linkage. This mechanism was chosen due to its advantage of using just one actuator to move the lower limb exoskeleton robot. There are other mechanisms widely used on a commercial scale in the design of lower limb exoskeleton, but they are beyond the scope of this thesis. The mechanism design provides the movement in the sagittal plane with just one DOF. The human trials were not included in this research work as these are beyond the scope of this research project. Force compliance was not considered in this research as this mechanism was selected to keep the robot lightweight by using only one actuator.

Secondly, a comparison of different manufacturing materials for the lower limb exoskeleton will be carried out based on cost and the strength-to-weight ratio. There may be some other expensive materials available with better properties, but these will not be discussed in this thesis.

Finally, a manufacturing process for assembling the lower limb exoskeleton device will be selected, which is simple, fast, and accurate. Several other manufacturing

methods are available and used but these are beyond the scope of this thesis. In addition, the development of control strategies as well as evaluation of the developed robot exoskeleton with human subjects is also beyond the scope of this thesis.

2.7 Chapter Summary

This chapter presented a comprehensive review on the research issues, which are relevant to the development of lower limb robot exoskeleton for gait rehabilitation. The focus of the review was placed on aspects such as wearable robots; manufacturing materials; mechanism design and analysis; material and structural optimisation and stiffness analysis. In this chapter, a discussion on the work done by previous researchers is presented to draw motivations for the present research. The review of the actuators and the manufacturing methods for the fabrication of various previously developed exoskeleton robots is presented in this chapter.

Research gaps have been explored while working on the development of a lower limb gait rehabilitation robot. From the discussion, it was found that the above-mentioned research aspects needed further investigation. From the research gaps identified, the main goal of the research has been defined and the steps to achieve the overall research aim in the form of research objectives have been presented. Finally, the scope of thesis has been presented.

CHAPTER 3 MECHANISM AND CONCEPTUAL DESIGN

Lower limb robot exoskeletons have demonstrated their effectiveness in post-stroke gait rehabilitation therapy. There is a continuous research effort in the improvement of existing rehabilitation exoskeletons in terms of ease-of-use and innovative design. There is a slow adaptation of the linkage-based mechanism in the design of lower limb exoskeletons due to design difficulties. The primary difficulty in the design of exoskeletons utilising linkage-based mechanism is that the movement of one link is based on the other link. This makes it difficult to set the precise dimensions of the links and the position of fixed joints to produce the target trajectory motions [166]. Moreover, in a linkage-based design mechanism, the customisation of the linkage lengths according to the height of different people is difficult as it may require more computational resources during iterative calculations.

However, when it comes to the lightweight and energy efficient design of robot exoskeletons, the linkage-based mechanisms offer multiple advantages. The main advantage of these mechanisms is that a single actuator can move all the joints of the lower limb exoskeleton, which contributes significantly to reducing the weight and manufacturing cost of these lower limb exoskeleton robots. This mechanism offers the best solution to develop an under-actuated robot exoskeleton as every DOF of the lower limb motion does not need a separate actuator. The properly actuated robotic exoskeletons use at least one actuator to power every single DOF, which results in the increase of the overall weight as well as energy consumption of the exoskeleton [167]. In linkage-based mechanisms, Stephenson II four-bar, Stephenson II six-bar, Stephenson III four-bar, and Stephenson III six-bar linkages are commonly used for design of lower limb exoskeletons [65, 168].

Lower limb robotic applications of Stephenson four-bar linkage mechanisms have some drawbacks. The desired gait path can only be matched approximately and the accurate trajectory of the human lower limb is difficult to obtain [25]. There has been an improvement in the transmission efficiency and smoothing in the knee joint torque curve for the six-bar linkage mechanism as compared to a four-bar linkage [169]. The reduction of the weight has always been an important consideration of the lower limb exoskeleton devices following the linkage-based mechanism. The six-bar linkage mechanism has been used to design a lower exoskeleton by using steel as the manufacturing material and it weighed more than 30kg, which is not suitable for the rehabilitation task and difficult to carry for a patient [170]. Another lower limb exoskeleton of stainless steel has been designed with six actuators to control different degrees of freedom, which was very heavy in weight and not comfortable for a person having

a spinal cord injury (SCI) [171]. An underactuated lower limb exoskeleton of steel following the linkage-based mechanism has been designed and tested for the gait rehabilitation, but was also bulky [56]. Hence, to the author's best knowledge, there has been no research study published in which a lightweight and high strength material, i.e., carbon reinforced fibre, has been considered for designing a lower limb exoskeleton following an underactuated Stephenson III six-bar linkage mechanism. A six-bar mechanism was chosen because a lightweight and high strength material with that mechanism has not been tested before. And this mechanism had been tested with a lightweight and high-strength material and no such study had been published before as most of the previously published research either use aluminium or steel for development of lower limb robots using linkage-based mechanism.

In this chapter, an overview of the biomechanics of the human lower limb is presented, followed by the mechanism and conceptual design of the proposed lower limb exoskeleton. The parameters of the linkage-based mechanism are discussed for the development of a lower limb robot exoskeleton. A discussion on design specifications is provided, followed by a section on the conceptual design and development of the lower limb rehabilitation robot. The use of various commercially available materials for the manufacturing of the lower limb exoskeleton is also discussed along with the weight estimation.

3.1 Lower Limb Biomechanics

The main joints of the human lower limb skeleton are hip, knee, and ankle as shown in Figure 3.1. The hip joint has three rotational DOFs and its movement is characterised by the hip flexion/extension, hip abduction/adduction, and hip internal/external rotational motions. The hip joint is considered as a ball-and-socket joint. The knee joint has two rotational DOF and is considered a condyloid joint. The motions at this joint are flexion/extension and internal/external rotations. Finally, the ankle joint has three rotational DOF. The three degrees of motion at the ankle joint are referred to as dorsiflexion/plantarflexion, inversion/eversion and adduction/abduction [172, 173]. The typical range of motion required for a healthy person at various degrees of freedom at different joints is presented in the Table 3.1.

Table 3.1 Typical range of motion of human lower limb joints[174].

Joint	Type of motion	Required range
Hip	flexion/extension	110º-120º/10º-15º
	abduction/adduction	45º/15º-25º
	internal/external rotation	30º-45º/40º-60º

Knee	flexion/extension	120º-150º/0º-15º
	Internal/external rotation	10º/30º-40º
Ankle	Dorsiflexion/ Plantarflexion	20º-30º/38º-46º
	Inversion/ Eversion	15º-22º/10º-17º
	Adduction/ Abduction	22º-36º/15º-26º

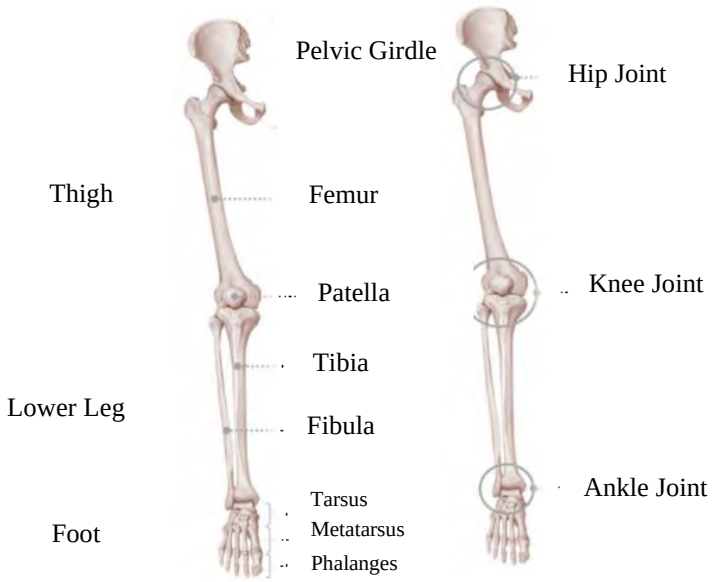

Figure 3.1 Human lower limb skeletal system [175].

3.1.1 Gait Cycle

There are two basic conditions that must be fulfilled for human walking. The first condition is the application of continuous ground reaction forces to support the body weight. Secondly, the periodic motion of each foot from one position of support to the next position in the direction of progression is needed [176]. A Gait Cycle (GC) is typically defined as the interval between two successive occurrences of the same event, beginning with the heel strike of one foot and ending at the next heel strike of the same foot (Figure 3.2). It is defined in terms of time interval and is usually expressed as a percentage of gait events taking place. Walking consists of a cycle of repeated events of foot strike and foot off. The event of foot strike usually begins with heel strike and is an indication of load bearing. Foot off begins with the toe pressing against the ground while preparing for load transfer to the contra lateral limb. The human GC has four

main events, which are: foot strike (FS), opposite foot off (OFO), opposite foot strike (OFS), and foot off (FO) [177].

The GC is divided into two main divisions, one is the stance phase and the other one is the swing phase. The swing phase represents the portion of the gait cycle when the foot is off the ground. The stance phase begins at heel-strike when the heel touches the floor and ends at toe-off when the same foot rises from the ground surface. Both stance and swing phases are further subdivided into many sub-phases as shown in Figure 3.2. After the GC, the planes and axis division of the human body are important to understand for the design of a mechanism of the lower limb robot exoskeleton.

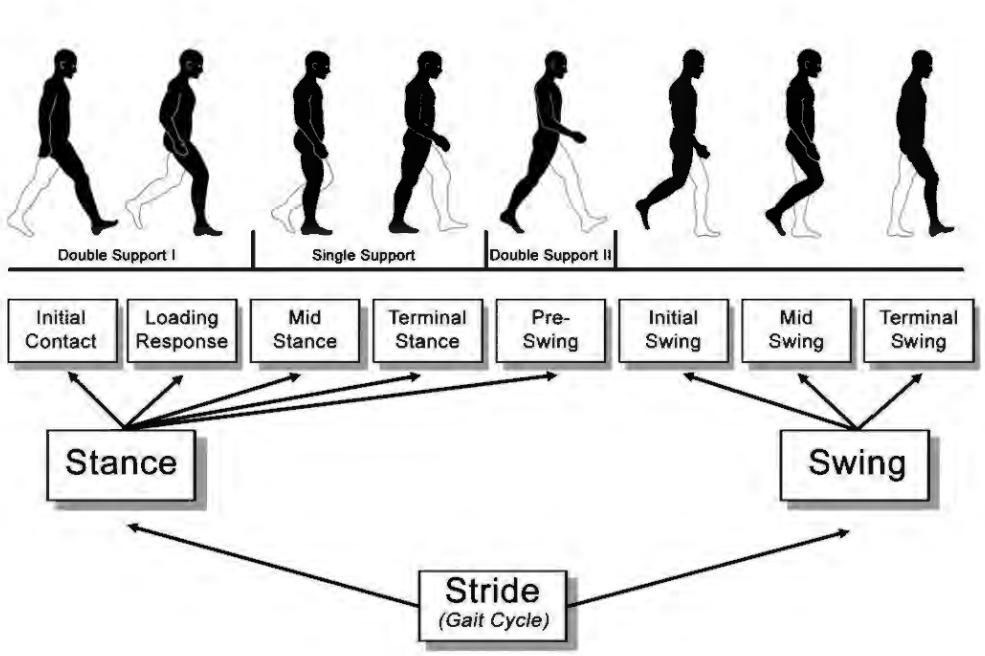

Figure 3.2 Phases of the gait cycle (GC) [178].

3.1.2 Planes and Axis Division

The three planes, which divide the human body into six parts, are shown in Figure 3.3. The detailed description of these planes is given below:

- The sagittal plane splits human body into two halves, right half and left half. Movements occur about the mediolateral axis running side to side through the centre of mass of the human body.
- The frontal or coronal plane splits the human body into front and back halves. Movements

  occur about the anteroposterior axis that runs anterior and posterior from the plane.

- The transverse or horizontal plane splits the human body to create upper and lower halves. Movements occurring in this plane are primarily rotations about a longitudinal axis.

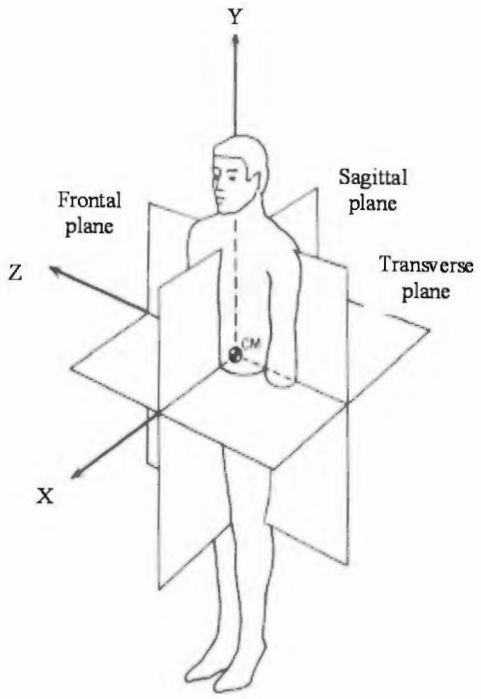

Figure 3.3 Plane and Axis for the division of human body [179].

Although the movements of knee joints occur in all three planes (sagittal, coronal, and transverse), most of the motions during the gait cycle occur in the sagittal plane, when the knee joint flexes or extends body [179]. Therefore, in the present research work, only the sagittal plane is considered for the design of the mechanism for a lower limb robot for gait rehabilitation. To design the lower limb exoskeleton linkage mechanism, it is important to understand the lower limb anatomy as well as the axis of division of the human body. The mechanism design for the lower limb exoskeleton is disused in the following sections.

3.2 Mechanism Design

In this work, a Stephenson III six-bar linkage is used to design a lower limb gait robot. The mechanism consists of two four-bar linkages, which constitute together the six-bar linkage, where one of the four-bar linkages drives another one [180]. However, the central benefit of using this linkage/mechanism as an underactuated mechanism for providing naturalistic walking experience has not been explored so far. It is possible to achieve flexibility by employing a lower number of actuators than the DOFs of a mechanism. Hence, the six-bar

linkage mechanism is considered an ideal one for designing a underactuated robot for lower limb rehabilitation.

3.2.1 Linkage Mechanism and Parameters

The initial mechanism design and its linkage parameters are synthesized with the use of the GIM software® [181], which is a specialised software for the synthesis and analysis of mechanisms. The idea for the mechanism design by using GIM software was taken from in previously published research work [56]. GIM is a registered software created by the COMPMECH Research Group. The GIM software was freely downloaded from the COMPMECH web site via the following link: www.ehu.es/compmech/software. GIM is mainly oriented to the field of kinematic analysis, motion simulation and dimensional synthesis of planar mechanisms [182]. It also includes other modules for workspace and singularity evaluation, and the static analysis of mechanical structures. The main widow for creating the geometry module is shown in Figure 3.4.

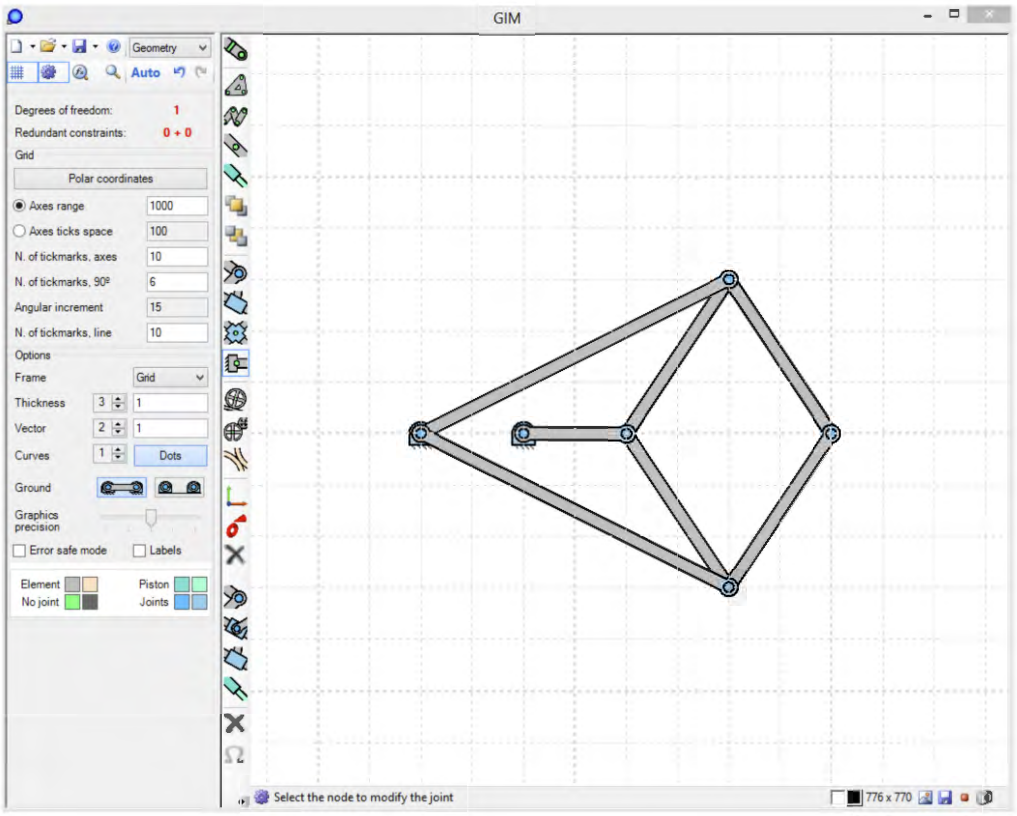

Figure 3.4 Main window of Geometry module of the GIM software.

All links in the mechanism are designed to be connected by pin-type flexible couplings and, as a result, the mechanism consists of two ternary (CDE and GEH) and four binary links (Figure 3.5 (a) & (b)). The proposed mechanism has three fixed pivots at joints A, B, and J.

The link between joints A and D rotates in an anticlockwise direction pivoting at A. This link serves as the driving link for the whole system and so is called a crank. Link BC or L5 is the rocker. The link CD is the coupler link on which the first coupler joint E is being placed. The first four-bar linkage with coupler joint E is acting as a crank part for the second four-bar mechanism, where link L1 is the second rocker. Joint H is the second coupler joint in the structure. Coupler joints E and H in the mechanism correspond to the knee and ankle joint, respectively. The simulated trajectory paths for the knee and ankle joints are shown in Figure 3.5 (a). The assignment of variables for each link and rotational joint is shown in Figure 3.5 (b).

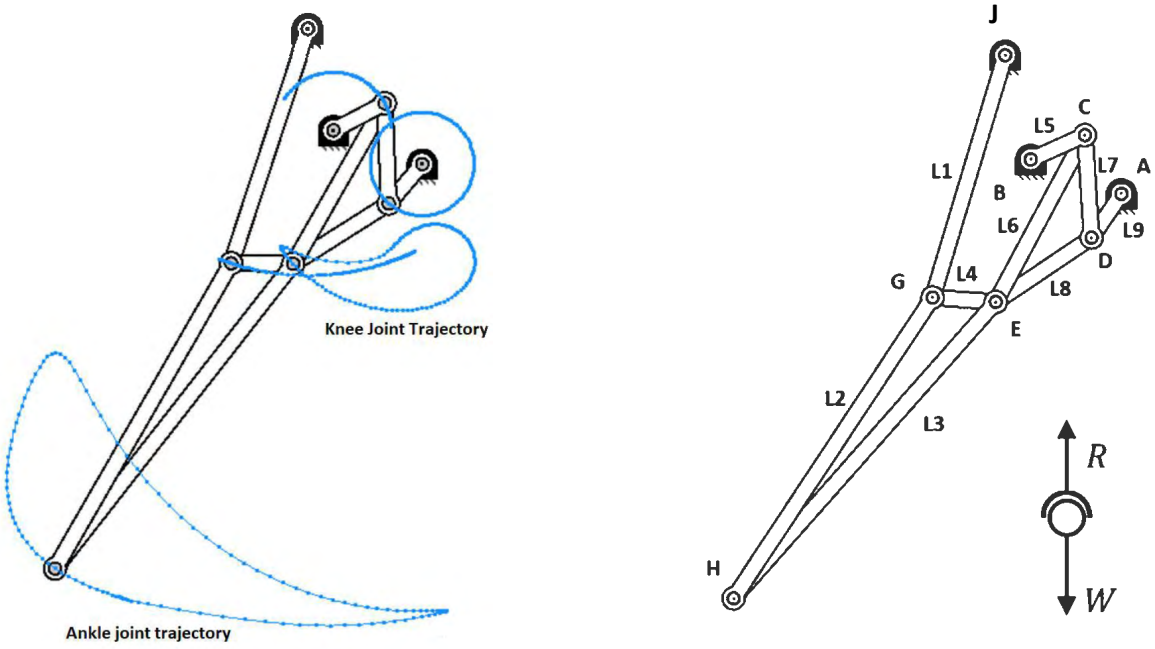

(a) (b)

Figure 3.5 Simulation of the mechanism in the GIM software environment: (a) motion trajectory, (b) assigned variables for different link lengths [183].

3.2.2 Linkage lengths and dimensions

The lengths of the links are denoted by L1-L9. The required link dimensions are selected and synthesized in a manner such that the desired trajectories for gait motion are achieved at the joints. The length of these links in metres are given in Table 3.2. These lengths were used to construct a conceptual design of a lower limb exoskeleton model by using a professional CAD software. The formation of a three-dimensional (3D) prototype model of a lower limb exoskeleton is discussed in the next section of this chapter.

Table 3.2 The link dimensions of the mechanism synthesized from GIM® software [183].

Linkage Variables	Length (m)
L1	0.37
L2	0.530
L3	0.581
L4	0.923
L5	0.087
L6	0.278
L7	0.151
L8	0.170
L9	0.078

3.3 Prototype Model of the Lower Limb Robot Exoskeleton

In this section, the 3D CAD model of a prototype of the lower limb exoskeleton is discussed. A commercially available CAD modelling software named SolidWorks® is used to produce that model.

3.3.1 Design of Prototype Components and Model

To begin with, the whole lower limb exoskeleton was divided into various components i.e., hip, knee, shank, and ankle. Each component was separately designed as shown in Figure 3.6. The SolidWorks® has the capability to join all these components in the form of the assembly to create a full prototype model. While analysing the bulk structure, there will be an error in the simulation software if exceedingly small features are added. Therefore, in this model, the connecting accessories (screws, nuts) are omitted to reduce chances of error during finite element analysis. This also helps in avoiding areas of high stress concentration, which normally occur at edges and small design details [84].

(a) Hip section

(b) Ankle section

(c) Shank section (d) Knee section

Figure 3.6 Components of lower limb exoskeleton.

Figure 3.7 shows the CAD model of the complete lower limb exoskeleton. Various sections of the lower limb exoskeleton are also annotated in Figure 3.7. Commonly used manufacturing materials were compared, and the weight prediction was carried out for various materials. Three commonly used lower limb exoskeleton materials were compared to select the most suitable lightweight and high strength material for the lower limb robot exoskeleton.

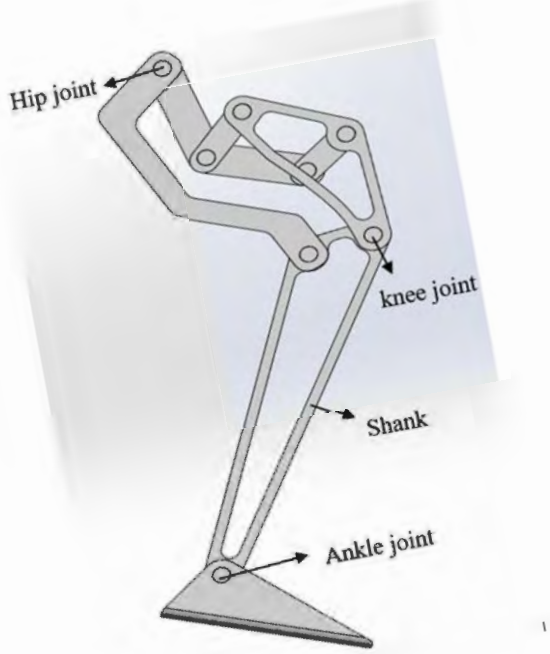

Figure 3.7 The 3D CAD model of underactuated lower limb exoskeleton.

3.3.2 Weight Prediction of Exoskeleton Model

After the design stage, the selection of a lightweight and high strength material is of primary importance, as a high strength material can provide better stiffness at the joints of the exoskeleton robot. To address that, three materials, namely structural steel, aluminium and carbon reinforced fibre, were tested for the lightweight model. The first two materials are commonly used, whereas the third one is still at the research stage to be used for rehabilitation robots [184]. Economic considerations are an important factor to consider before developing

any exoskeleton device. Hence, expensive materials, such as titanium were avoided. The use of these materials in the manufacturing of previously designed exoskeleton devices is discussed in Chapter 2 of this thesis.

For the present study, the weight of the designed robotic exoskeleton was predicted by the SolidWorks® software. In the SolidWorks toolbox, a specific tool, known as "mass properties," is available to calculate the weight of the designed structure. This tool's commands are shown in Figure 3.8.

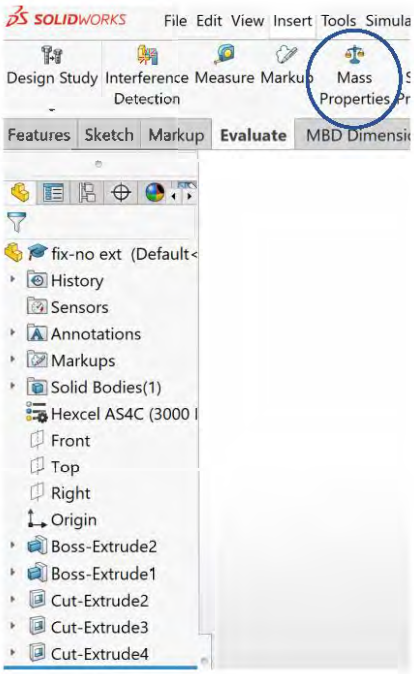

Figure 3.8 Mass properties tool for weight calculation of the lower limb exoskeleton.

The weight of the designed exoskeleton using the three materials was calculated and graphically represented in Figure 3.9. The calculated mass for the structural steel prototype model is 10.5kg, while for aluminium and carbon reinforced fibre, it is 3.70kg, and 2.43kg respectively. Based on this comparison, the carbon reinforced fibre model is the lightest one, which makes it a suitable one for manufacturing a robot exoskeleton for lower limb rehabilitation. The exoskeleton designed model of carbon reinforced fibre was 76 % and 34% lighter as compared to structural steel and aluminium, respectively. This calculated weight is further optimised by optimising the area of links (L1-L9). The topology optimisation is carried out and will be discussed in detail in the next chapter of this thesis.

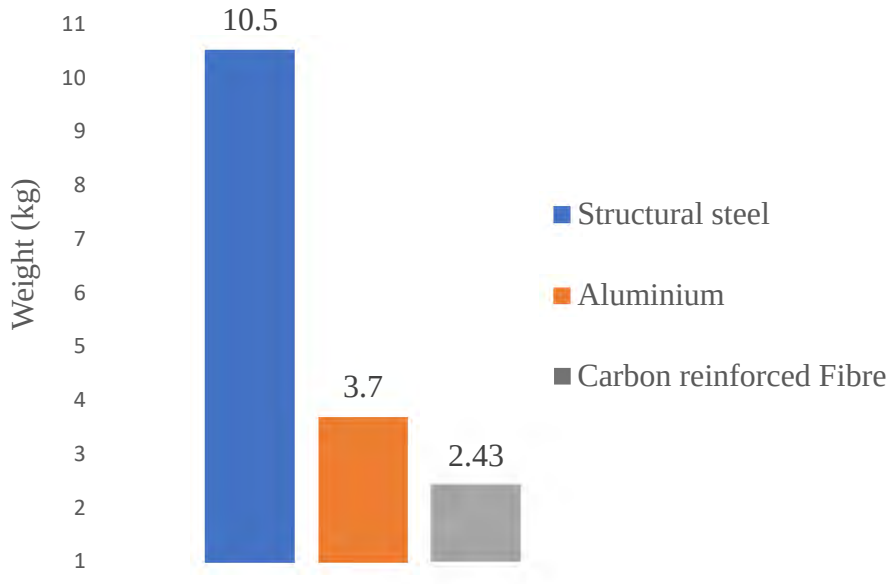

Figure 3.9 Calculated mass of exoskeleton for different materials.

3.3.3 Exoskeleton Mechanism Analysis in Matlab

After the modelling in SolidWorks® (2022 version) and the GIM software®, a functional feasibility analysis of the proposed design is carried out in the Simscape Multibody® software, which is available in the Matlab® environment in R2022b version (Figure 3.10). Here, the gait robot design is appended with position and force sensors to obtain real-time sensor data while the robot is moved on desired trajectories. The gait robot's capabilities in terms of traversing through the required workspace, along commanded trajectories with opposite joint torques is evaluated. To complete the mechanism analysis, a simple PID controller is designed that writes the commanded joint velocity on the motor hardware interface in terms of electric currents. The position and torque sensors data from the robot can be read from the sensors readout blocks that are included in the overall Simscape model (Figure 3.10) and the same data can be either displayed or stored in files as desired for further analysis. In Figure 3.10, the block on the right side (W) shows the global coordinate system and block marked with C shows the mechanism that was designed by GIM software. Further, f(x)=0 shows the externally applied forces are zero. The centre block with Conn1, 2, and 3 shows robotic system with actuators and sensors in it. Subsequent to the sensor data analysis, if there is a need to make changes to the robot design to comply with the desired specifications, it is possible to return to the CAD model and

make the necessary changes. After that the robot design can be analysed again using the GIM software and later the entire system equipped with sensors in Simscape can be further validated.

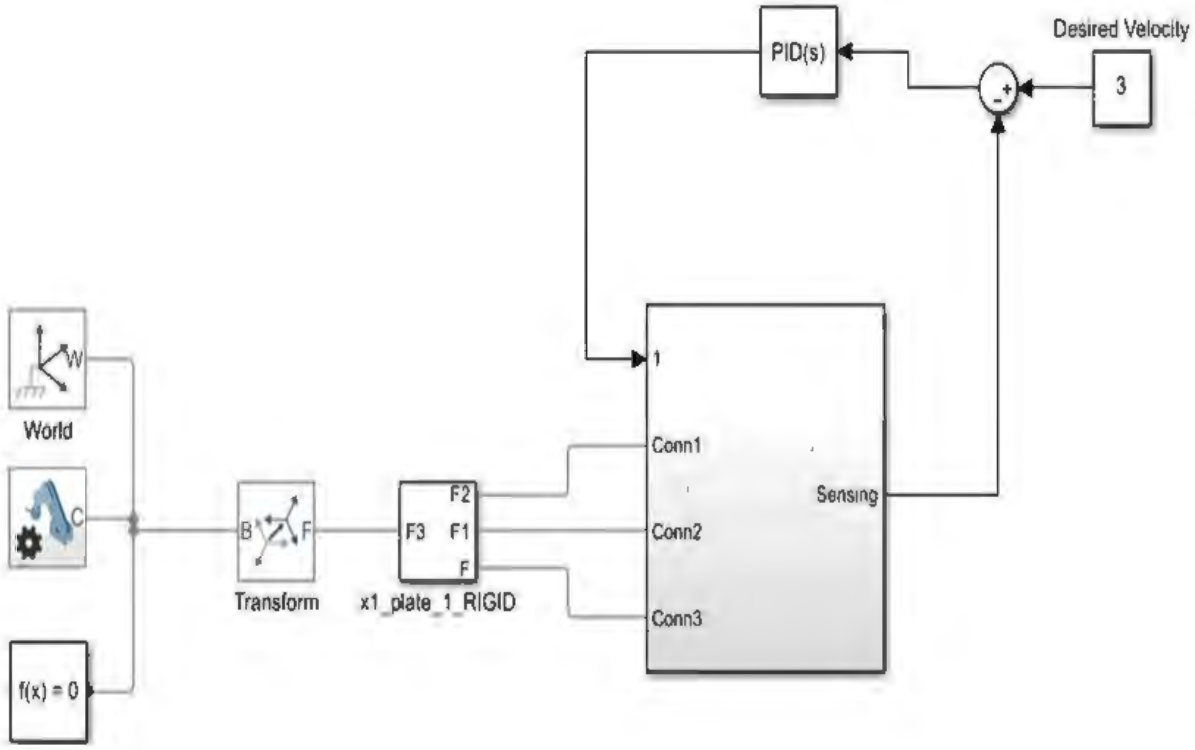

Figure 3.10 Flow chart for the simulation and optimisation. The centre block shows the robotic system with actuators and sensors.

3.4 Chapter Summary

This chapter started with a discussion of a linkage-based mechanism and its advantages over other mechanisms for lower limb rehabilitation robot exoskeleton design. After that, the biomechanics of human lower limb were discussed in detail along with the DOFs of various parts of the human lower limb. The human gait cycle and planes and axes for the division of human body were discussed. The parameters of the linkage mechanism were obtained and discussed in this chapter. The 3D CAD modelling for the various components of the lower limb exoskeleton and their assembly is presented. The weight calculation of the exoskeleton model for different manufacturing materials was carried out and the material, which can give the lightest exoskeleton, was identified. Finally, the flow chart for exoskeleton mechanism analysis in Matlab was presented.

After mechanism design and CAD modelling for suitable material selection, the next step towards the development of a lightweight lower limb exoskeleton is the Finite Element

Modelling. The objective of finite element modelling is to apply the human leg load at different components of the lower limb exoskeleton and to carry out the topology optimisation of the exoskeleton for a further reduction of weight. The finite element modelling and topology optimisation are presented in the following chapter.

CHAPTER 4 FINITE ELEMENT MODELLING AND OPTIMISATION

This chapter deals with the finite element modelling and the optimisation for the further reduction of weight of the designed lower limb robot exoskeleton. The finite element modelling is carried out, followed by the topology optimisation to optimise the area of the linkages that were designed as a six-bar linkage in the previous chapter. The workflow for finite element analysis and various optimisations is shown in Figure 4.1. This chapter discusses the details of finite element modelling and optimisation for the development of lower limb exoskeleton.

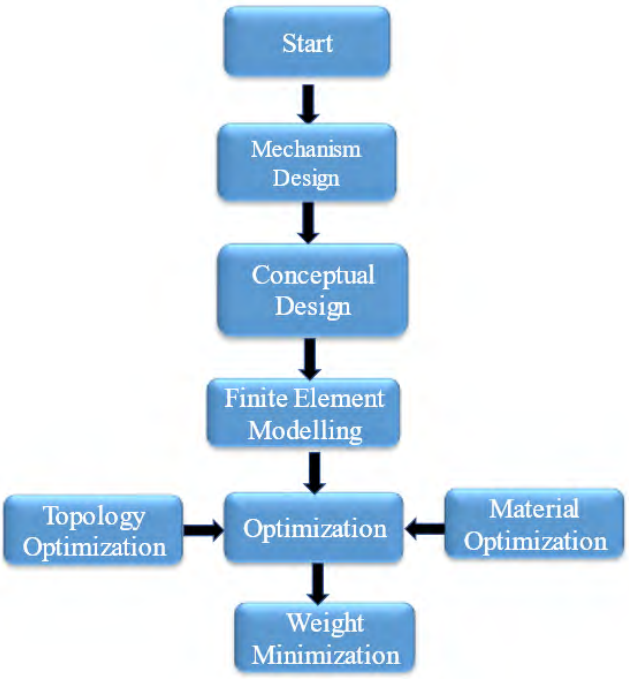

Figure 4.1 Flow chart for the simulation and optimisation.

4.1 Finite Element Modelling

Finite element modelling and analysis have commonly been used for the numerical solution of the complex stress problems. It is possible to solve a complicated structure to obtained various stress properties by using finite element analysis. A robot is an example of a complicated structure in which many mechanism links and joint are involved. Structural analysis is carried out by finite element modelling, which is the most common analysis to characterise the various parameters at the design stage. Finite element analysis is widely used in robotics to achieve an improved design and to rectify any design errors [185]. This type of analysis is mostly carried out on the 3D CAD models by using purpose-built, specialised software. Some commonly used

software packages for finite element modelling are known as Nastran, ANSYS, NISA, and STAAD-PRO.

In the finite element modelling environment, it is possible to apply torque, force, and many other mechanical and material properties to the CAD model. Despite the great power of finite element analysis, the disadvantages of computer solutions must be kept in mind when using this and similar methods: they do not necessarily reveal how the stresses are influenced by important problem variables such as material properties and geometrical features, and errors in input data can produce wildly incorrect results that may be overlooked by the analyst. Hence, the simulation results must be compared with some experimental analysis to obtain a proper solution of the designed problem. Perhaps, the most important function of theoretical modelling is that of sharpening the designer's intuition; users of finite element codes should plan their strategy toward this end, supplementing the computer simulation with as much closed-form and experimental analysis as possible. [186]. In practice, a finite element analysis usually consists of three principal steps given below.

4.1.1 Pre-processing

The first step in the finite element analysis is the division of the 3D model geometry into a finite number of subregions known as elements, which are connected at certain regions known as nodes. At some nodes, there are displacements and others have prescribed loads for the certain structure. This process of dividing the model into nodes and elements is known as meshing. These models, also known as mesh models, are extremely time consuming when using codes and manual methods. In finite element analysis, these can be done conventionally as part of a computerised drafting and design process, which means that these codes are already added to the software interface and, hence, the manual writing of code is not needed [187].

4.1.2 Analysis

The second step is solving the mesh model obtained during pre-processing by using a linear or nonlinear algebraic equation [188] .

$$K_{ij}U_j = f_i \tag{4.1}$$

Where U and f are the displacements and externally applied forces at the nodal points. The formation of the K matrix is dependent on the type of problem intended to solve. Commercially available finite element analysis packages have a large number of element libraries, which are useful to solve a wide range of problems. One of principal advantages of

finite element analysis is that many problem types can be addressed by merely specifying the appropriate element types from the library [189].

4.1.3 Post-processing

This is the final step to obtain the results from finite element analysis, but these results must be validated by some sort of experimental results. This stage gives the user a listing of displacements and stresses at discrete positions within the model. The modern software uses graphical displays, which is helpful to visualise the results. A typical postprocessor display overlays coloured contours representing stress levels on the model, showing a full-field picture of the experimental results [190]. Hence, finite element analysis is useful tool to save time and resources in running the unnecessary experimental work. However, some experiments are still needed to some extent to validate the results obtained from finite element modelling.

In the present work, the finite element analysis is performed on the 3D prototype model, which was described in the previous chapter of this thesis. As a next step, the designed model is analysed via a commercially available finite element analysis software and analysis details are given in the next section.

4.2 Finite Element Modelling of the Lower Limb Robotic Exoskeleton

In this section, the finite element modelling of the 3D CAD model of lower limb exoskeleton is presented. In finite element analysis, the static structural analysis is carried out to obtain the stress distribution model of the lower limb exoskeleton model for the identification of areas under higher stresses. The finite element analysis is carried out on the model shown in Figure 3.7 in the previous chapter of this thesis. The software used for the analysis is Ansys®, which is a well-known, commercially available finite element analysis software, and this has been extensively used for analysing lower limb exoskeletons by previous researchers [84, 191, 192]. The modelling starts by importing the CAD model as an initial graphics exchange specification (IGES) before meshing is carried out.

4.2.1 Model Meshing

Meshing of the model, which is the pre-processing stage for the finite element analysis is carried out in the Ansys® workbench. The meshing size is an important parameter to consider and must be selected carefully. Too large a meshing size may leave some areas in a complex structure unsolved and a meshing that is too small increases the computational time to solve the modelled structure. In this work, meshing is carried out by using the meshing commands

and adjusting the size of elements from the settings available in the Ansys® work bench tool as shown in Figure 4.2.

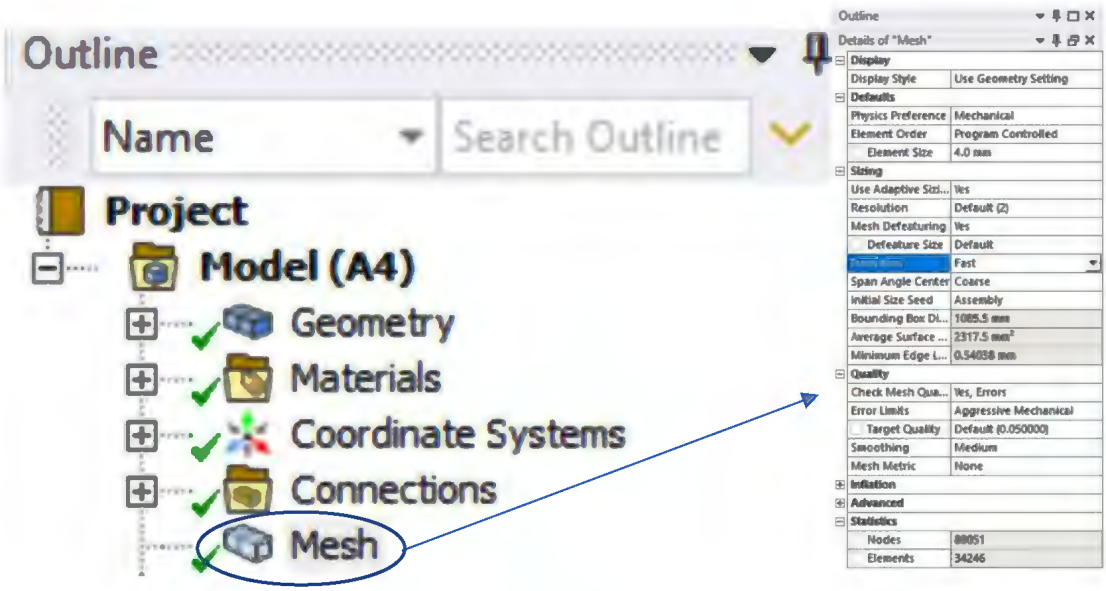

Figure 4.2 Meshing tool in the Ansys® workbench.

The meshing model was obtained by using an element size of 4mm, which was selected for the analysis. This element size was selected for meshing in Ansys® workbench on the basis of the work previously performed on the finite element analysis of lower limb exoskeleton [193]. The various parameters for meshing of a lower limb exoskeleton model are also given in Figure 4.2. The exoskeleton model uses the Solid187 and Solid45 mixed unit and, as a result, the model was divided into 89,051 nodes and 34,246 elements. The meshing model of the designed lower limb exoskeleton is shown in Figure 4.3.

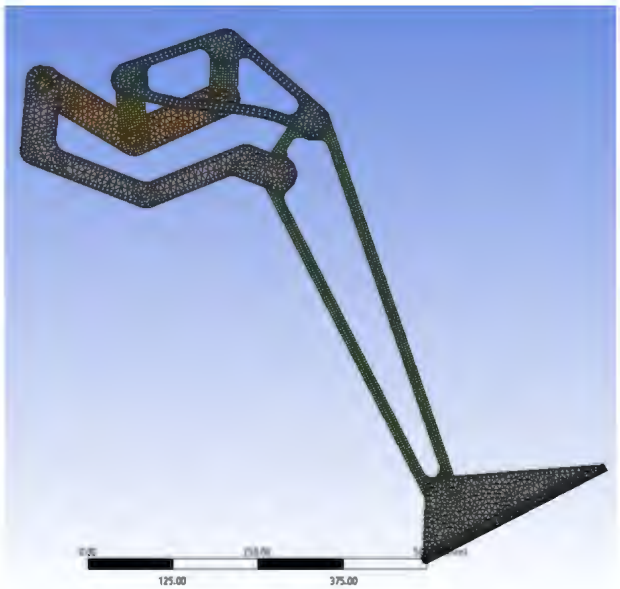

Figure 4.3 Meshing model of the designed lower limb exoskeleton.

4.2.2 Application of Material Properties:

After meshing, the next stage is the application of material properties. The material properties are also important as the present study compares the material properties of three commonly used materials (Aluminium Alloy, Structural Steel, and Carbon Fibre Reinforced composite). The properties of each material were applied to the mesh model. Ansys® includes the material library from which the material properties were acquired. Hence, the materials were selected and applied to the model and the properties are shown in Table 4.1.

Table 4.1 Material Properties of various materials used in finite element analysis.

Properties	**Aluminium Alloy**	**Structural Steel**	**Carbon Fibre Reinforced**
Young's Modulus (Pa)	7.1×10^{10}	2.0×10^{11}	9.49×10^{10}
Poisson's Ratio	0.33	0.33	0.32
Compressive yield strength (Pa)	2.8×10^{8}	2.5×10^{8}	3.04×10^{8}
Bulk Modulus (Pa)	6.9×10^{10}	1.67×10^{11}	8.78×10^{9}
Shear Modulus (Pa)	2.67×10^{10}	7.69×10^{9}	3.60×10^{10}
Tensile yield strength (Pa)	2.8×10^{8}	2.5×10^{8}	5.07×10^{8}
Density (kg/m^3)	2770	7850	1750
Ultimate Tensile Strength (Pa)	3.1×10^{8}	4.6×10^{8}	5.03×10^{8}

These materials and their properties are used as the input for finite element modelling to obtain the stress distribution model. By comparison, the carbon reinforced fibre has the lowest density and highest tensile strength, which makes it a suitable material for manufacturing the lower limb robot exoskeleton for gait rehabilitation. After material properties, the next step in finite element modelling is the application of load and torque, which is discussed below.

4.2.3 Mechanical Load Analysis

In the overall gait robot system, the exoskeleton mechanism is fixed on a linkage-based mechanism, which supports the pelvis motions passively by moving up and down with the body's centre of gravity in the vertical direction. The application of standard earth gravity to the exoskeleton model is shown in Figure 4.4(a). In mechanical load analysis, it is assumed that the designed exoskeleton is meant to be attached to the human leg during usage and, therefore, the distribution of the human body mass was another factor to consider. Hence, the distributed mass was applied to the exoskeleton, assuming the hypothetical subject's mass as 70kg [194]. The mass was applied at the thigh, leg, and foot sections of the lower limb

exoskeleton that was designed for static analysis. The details of the distributed mass applied at various links of the lower limb are provided in Table 4.2.

Table 4.2 Human lower limb mass properties[195].

Link	Mass(kg)
Foot	1.00
Shank	3.32
Thigh	8.00
Pelvis	9.00

After the application of the distributed mass, the torque application is another important parameter to consider. The designed mechanism is underactuated, so only one actuator was used to move all the lower limb components. The designed exoskeleton has only one DC motor, attached at its hip joint to apply torque. A torque of 60 Nm was applied on the model of lower limb exoskeleton and the same amount of torque will be applied to the physical model. Hence, the simulation is applied to the designed mesh model to simulate the test conditions in the Ansys® workbench and is shown in Figure 4.4(b).

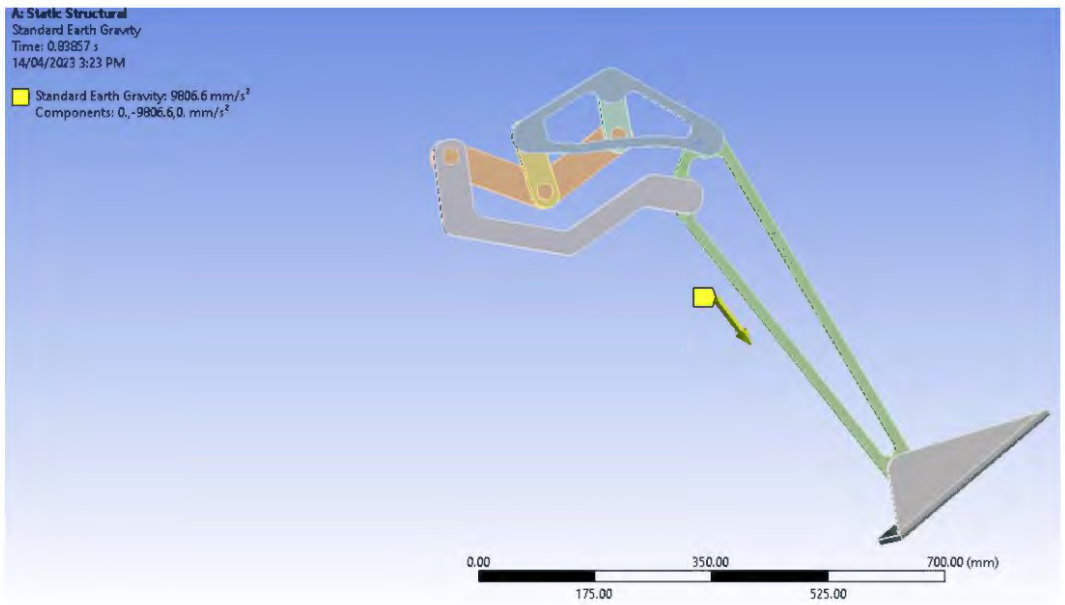

(a)

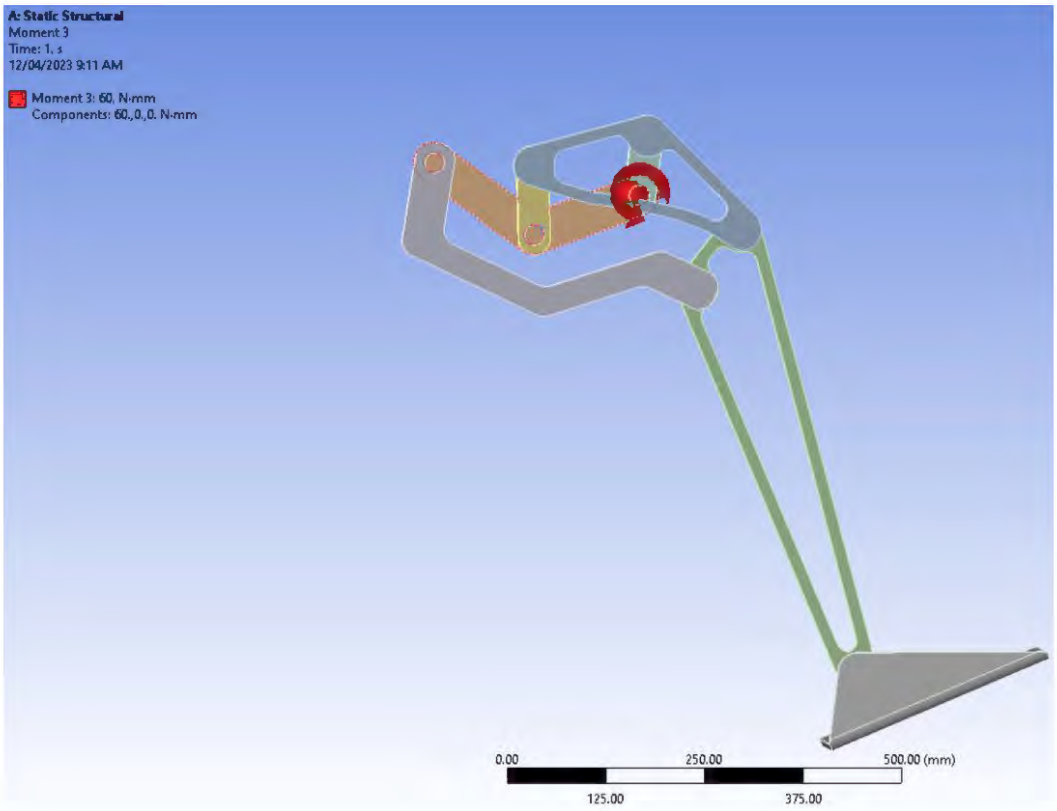

(b)

Figure 4.4 Standard gravity (a) and torque application (b) to the designed exoskeleton model.

4.2.4 Static Structural Analysis

After the application of mass, torque, and standard earth gravity, which are known as boundary conditions, the post-processing was carried out as the final stage of finite element modelling. In this step, the static analysis was carried out in the Ansys® work bench to assess the stability of the designed exoskeleton model as well as to visualise the areas of stress concentration in the designed 3D CAD model. The main goal behind performing the analysis was to obtain the areas of high stress concentrations on the gait rehabilitation exoskeleton. The stress-distribution model obtained as the result of finite element modelling is shown in Figure 4.5. It is clear from the figure that the maximum stress is at the upper end of the shank and just above the knee section, which means that this structure needs to be optimised for better performance and durability with the lowest possible mass. The stress concertation areas are the same as obtained in prior research while performing the static analysis of a lower extremity exoskeleton [196]. As stated previously in this chapter, the simulation results can sometimes be incorrect; therefore, an experimental evaluation is necessary to get the accurate results. As the output of

static structural analysis, the values of equivalent Von Mises stress, total deformation, equivalent elastic strain, and strain energy for three different materials are shown in Table 4.3.

Table 4.3 Results of the static structural analysis of different materials.

Results from static analysis	**Aluminium Alloy**	**Structural Steel**	**Carbon Fibre Reinforced**
Von Mises stress (MPa)	9.517	18.135	7.71
Equivalent elastic strain (mm)	$1.34x10^{-4}$	$9.1x10^{-5}$	$8.12x10^{-5}$
Total deformation (mm)	0.840	0.80	0.41
Strain energy (mJ)	0.0174	0.018	$9.3x10^{-3}$

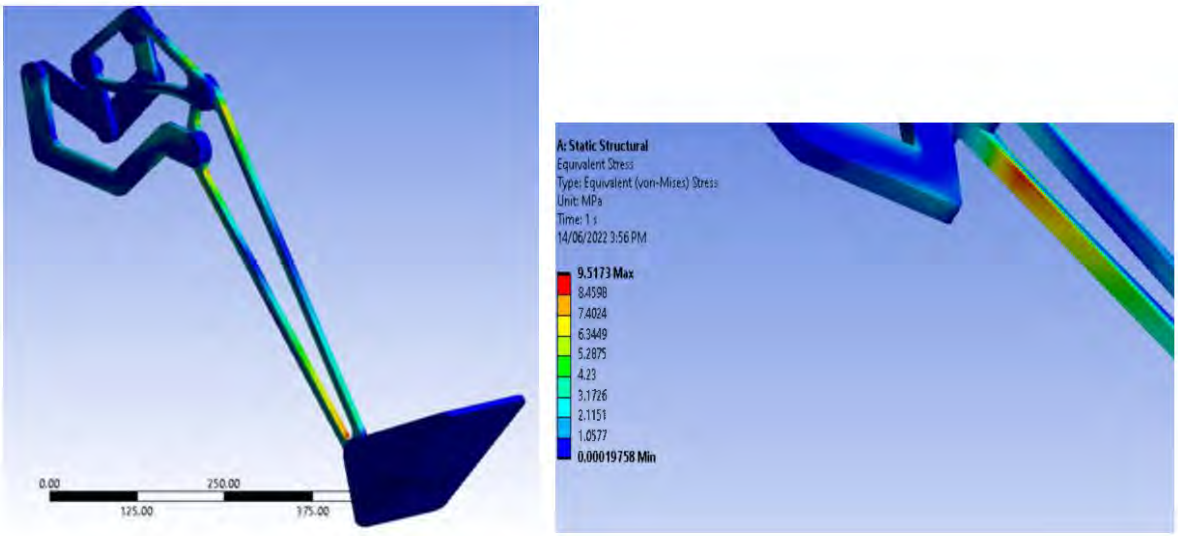

Figure 4.5 Stress distribution model of the designed lower limb exoskeleton.

From the comparison of the three materials under the same mechanical loading, the maximum Von Mises stress was first obtained for structural steel, followed by aluminium, and then carbon fibre. The main drawback of steel is its high density; hence, the exoskeleton will be heavier and difficult to carry for users. Carbon fibre is replacing the metallic alloys as a robotic fabrication material due to a better strength-to-weight ratio. After finite element analysis, optimisation is the next stage towards development of a lightweight design of a lower limb robot exoskeleton. To obtain a lightweight structure, material and topology optimisation were carried out and are discussed in the following section.

4.3 Optimisation of Lower Limb Exoskeleton

The rapid increase of computational resources available in the past few years has made it easy to optimise complex structures, such as robot structures with complex designs. Structural optimisation is a simulation-driven design technique that lets teams identify and explore high-

potential designs – and reject low-potential ones – earlier in development cycles. Manufacturers can use structural optimisation to enhance their product designs and generate lightweight, manufacturable concepts. Topology optimisation is considered as a branch of structural optimisation to optimise various shape and design parameters in order to obtain a lightweight design of a robotic exoskeleton.

4.3.1 Topology and Material Optimisation

The wearable robot design is expected to be compact, compliant, lightweight and, at the same time, it is required to be highly stiff and strong. Since these requirements were conflicting, it is necessary to carry out optimisation of the robot design to establish a trade-off between the design objectives. Structural topology optimisation is essential to get the desired shapes and configuration of the robot's mechanical parts as this process results in a suitable material distribution within the optimised area [197]. In the present work, the material and topology optimisation were carried out to further optimise the robot exoskeleton design. In the optimisation scheme, a multi-mode single-objective Genetic Algorithm was used for the weight minimisation by reducing the cross-sectional area of the exoskeleton links.

From the result of the static structural analysis, it is observed that the designed exoskeleton has a large space for the structural optimisation. In view of the existing model, the foot section is not bearing much stress, so it can be optimised to achieve a good optimal structure at the lowest possible cost. The topology optimisation is carried out in MATLAB®. The single objective optimisation was carried out by using a multi-mode genetic algorithm with an objective to minimize the overall mass**.** The objective function is described as:

$$M = L \sum_{i=1}^{9} \sum_{j=1}^{3} \rho_j \, K_i \, A_i \tag{4.2}$$

where K_i is the set of normalised lengths where the length of i^{th} link is obtained after diving it by the length of link L9. These link lengths are given in Table 3.2 in the previous chapter. In other words, all link lengths are normalised considering the length of the smallest link (which is L9 in the present case) as unity. Thus, the normalised set of link lengths can be written as $K_i = (4.48, 6.81, 7.47, 1.196, 1.12, 3.57, 1.94, 2.18, 1)^T$. Further, ρ_j is the density for the chosen material in kg/m^3, and L is the nominal length of links (L1-L9), which is $0.07772\ metres$. From Equation (4.2), it is evident that to minimise the overall mass of the exoskeleton, the cross-sectional area of each segment should be considered as the design variable. Considering uniform cross-sections of the links L_{6-8} and L_{2-4}, the design variables reduce to five instead of nine that were considered earlier as given below:

$$1.2 \times 10^{-4} \leq A_1, A_4, A_5, A_7, A_9 \leq 6 \times 10^{-4} \quad (4.3)$$

The force applied on the mechanism presented in Figure 3.5 in the previous chapter was analytically calculated by using various principles of trigonometry and these values are used as constraints for optimisation. The coordinates A, B, and J are fixed pivots of the mechanism. Point A was assumed to be the origin of the coordinate system. Then, the coordinates for B and J were obtained from GIM simulation software. The angles that were assumed to calculate the coordinates of the joints of the mechanism and to calculate the force and torque at the knee and ankle joints are shown in Figure 4.6. The coordinates of all the points of the six-bar linkage mechanism are shown in Table 4.4.

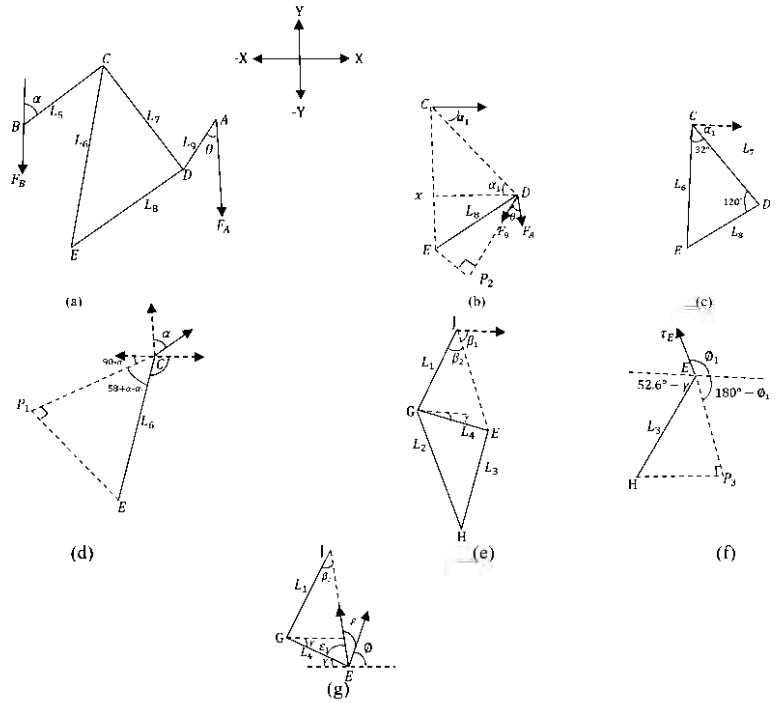

Figure 4.6 The angles assumptions used to solve the mechanism.

Table 4.4 Coordinates of the joints of the designed mechanism.

Joint	X coordinate (mm)	Y coordinate (mm)
A	0	0
B	-133.2	50.6
C	$-133.2 + L_5 \sin\alpha$	$50.6 + L_5 \cos\alpha$
D	$-L_9 \sin\theta$	$-L_9 \cos\theta$
E	$C_x + L_6 \cos(32 + \alpha_1)$	$C_y - L_6 \sin(32 + \alpha_1)$
J	-170.7	203.4
G	$-170.7 + L_1 \times \cos(\beta_1 + \beta_2)$	$203.4 + L_1 \times \sin(\beta_1 + \beta_2)$

The principles of trigonometry were used to determine the values of forces F_A and F_B and torque at the knee joint (τ_E). The values as represented by the given equations:

Force in L_9 $$(AD) = F_9 = F_A \sec\theta \quad (4.4)$$

Force in L_5 $$(BC) = F_5 = F_B \sec\alpha \quad (4.5)$$

Force in L_1 $$\tau_E \cos\varepsilon \cos\beta_2 \quad (4.6)$$

From the mathematical calculations, τ_E which is the torque applied at knee joint can be calculated as:

$$\tau_E = (F_9 \times EP_2) + (F_5 \times EP_1) \quad (4.7)$$

The values obtained from the above relations were used as the constraints for the topology optimisation. The stress applied on the various links of the designed exoskeleton were obtained and exerted in MATLAB as the constraints for optimisation. The equations are given below:

For Aluminium

$$\text{Syc} - \frac{193.06\tau_E \cos\varepsilon \cos\beta_2}{3.5 \times 10^{-4}} \geq 0, \quad (4.8)$$

$$\text{Syc} - \frac{193.06(F_A \sec\theta \times EP_2) + (F_B \sec\alpha \times EP_1)}{1.5 \times 10^{-4}} \geq 0, \quad (4.9)$$

$$Syt - \frac{193.06F_B \sec\alpha}{4 \times 10^{-4}} \geq 0, \quad (4.10)$$

$$\text{Syc} - \frac{193.06F_B \sec\alpha - F_A \sec\theta}{1.5 \times 10^{-4}} \geq 0, \quad (4.11)$$

$$\text{Syt} - \frac{193.06F_A \sec\theta}{4 \times 10^{-4}} \geq 0 \quad (4.12)$$

For steel

$$\text{Syc} - \frac{254.8\tau_E \cos\varepsilon \cos\beta_2}{3.5 \times 10^{-4}} \geq 0, \quad (4.13)$$

$$\text{Syc} - \frac{254.8(F_A \sec\theta \times EP_2) + (F_B \sec\alpha \times EP_1)}{1.5 \times 10^{-4}} \geq 0, \tag{4.14}$$

$$\text{Syt} - \frac{254.8F_B \sec\alpha}{4 \times 10^{-4}} \geq 0, \tag{4.15}$$

$$\text{Syc} - \frac{254.8\ F_B \sec\alpha - F_A \sec\theta}{1.5 \times 10^{-4}} \geq 0, \tag{4.16}$$

$$\text{Syt} - \frac{254.8F_A \sec\theta}{4 \times 10^{-4}} \geq\ 0 \tag{4.17}$$

For carbon fibre

$$\text{Syc} - \frac{180.32\tau_E \cos\varepsilon \cos\beta_2}{3.5 \times 10^{-4}} \geq 0, \tag{4.18}$$

$$\text{Syc} - \frac{180.32(F_A \sec\theta \times EP_2) + (F_B \sec\alpha \times EP_1)}{1.5 \times 10^{-4}} \geq 0, \tag{4.19}$$

$$\text{Syt} - \frac{180.32F_B \sec\alpha}{4 \times 10^{-4}} \geq 0, \tag{4.20}$$

$$\text{Syc} - \frac{180.32\ F_B \sec\alpha - F_A \sec\theta}{1.5 \times 10^{-4}} \geq 0, \tag{4.21}$$

$$\text{Syt} - \frac{180.32F_A \sec\theta}{4 \times 10^{-4}} \geq 0 \tag{4.22}$$

where F_A, and F_B are forces exerted along A and B components of the exoskeleton as shown in Figure 3.5 in the previous chapter and τ_E is the torque applied. The angles θ, α and β were the angles between different links ($L_1 - L_9$) of the mechanism that were assumed for the analytical solution to find the stress on each link to use in the optimisation algorithm. Syt and Syc are the tensile and compressive strength of various materials, respectively, used for the exoskeleton.

The application of the Genetic Algorithm for the minimisation of the weight of the prototype along with pseudocode is given Table 4.5. Applying the algorithm presented in Table 4.5, gives M^* the minimised mass for the exoskeleton for the material j^* provided the linear

constraints in equation (4.3) and non-linear constraints in equation (4.8-4.22) based on the material. The algorithm also yields the optimised cross-sectional area A_i^* for j^* material. This algorithm can be modified for yielding the minimised weight and optimised set of design variables for any collection of materials [183] .

Table 4.5 Algorithm for minimisation of prototype's weight.

Algorithm: Pseudocode describing the application of Genetic Algorithm for minimisation of the weight of the prototype	
Objective:	Minimise (1) for 3 materials
Input:	K_i where $i = 1,2,\dots,9$, ρ_j where $j = 1,\dots,3$ and L
1	Setting up linear constraints for A_i
2	Initialise $M^*, j^*, A_i^* = 0$
3	**for** $j = 1,\dots,3$ **do**:
4	Calculate non-linear constraints conditions based on the material type (eq 4.4,4.5,4.6)
5	Calculate M_j
6	if $M_j < M^*$ then
7	$M^* \leftarrow M_J$
8	Update j^* and A_i^* with j and A_i respectively
Output:	M^* and s^* (the minimum weight M^* for material s^*)

For the current application, the selection of suitable GA parameters was of utmost importance since the algorithm was subjected to linear and non-linear constraints. The maximum generations value was set to be 900 but the algorithm was programmed to stop if the average relative change in the best fitness function value over 50 generations was diminutive ($< 1 \times 10^{-6}$). The constraint tolerance was set to 0.001 and the crossover fraction was 0.8. The algorithm was set to evaluate fitness and constraint functions in series rather than parallel. With these parameters, the algorithm was run to find the optimised cross-section area for all links of the exoskeleton and the materials.

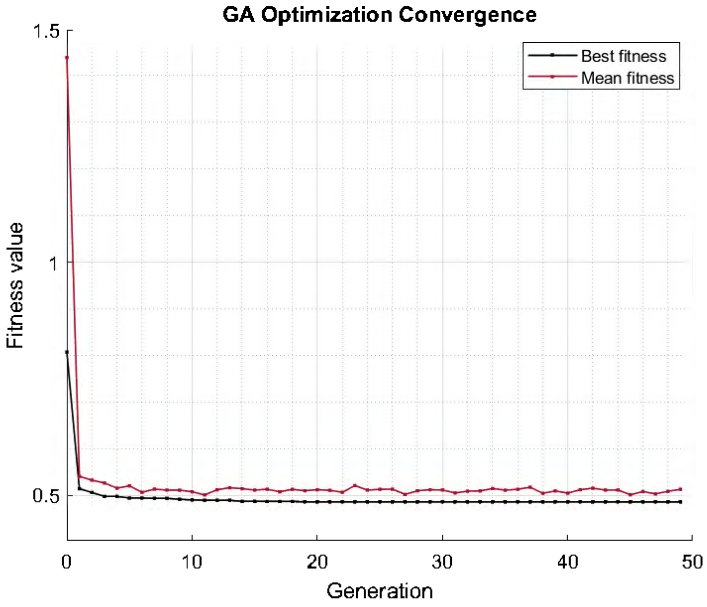

Figure 4.7 Convergence of the GA optimisation algorithm.

The convergence of the genetic algorithm-based optimisation is shown in Figure 4.7. The best fitness value (overall mass of one of the exoskeleton legs) from GA optimisation is found to be 0.486 with a mean of 0.513 The duration of each optimisation for different materials, the values for design variables and the best fitness values are provided in Table 4.6 below.

Table 4.6 The duration, optimal design variables, and the best fitness values for different materials.

Material	Duration (s)	A1 $(10^{-4}m^2)$	A4 $(10^{-4}m^2)$	A5 $(10^{-4}m^2)$	A7 $(10^{-4}m^2)$	A9 $(10^{-4}m^2)$	Best Value (kg)
Aluminium	21.39	1.55	1.21	1.55	1.40	1.47	0.541
Steel	21.90	1.21	1.22	1.29	1.20	1.26	0.494
Carbon Fibre	21.93	1.24	1.24	1.70	1.40	1.73	0.485

4.3.2 Optimisation Outputs

The weight minimisation of the prototype model was the main objective to run the optimisation algorithm. This objective was achieved by reduction of cross-sectional area of the various link, which were joined in the linkage-based mechanism for a lower limb exoskeleton. The area of cross-section denoted by (A_1- A_9) for the links $L_1 - L_9$ is given in Table 4.7. From the table, the decrease in optimised area is observed, which will ultimately decrease the weight of the

lower limb exoskeleton model designed for various materials. These areas of cross-section were kept same for all the three materials that were compared to select the most suitable material for manufacturing the lower limb exoskeleton. Hence, a sufficient decrease was obtained, and this decrease is uniform for the various materials as the same structure was modelled for all the materials. The result for the weight minimisation, which was the main objective behind the optimisation, are discussed in the following section.

Table 4.7 Cross-sectional area of the links before and after optimisation.

	Area before Optimisation (m^2)	Area after Optimisation (m^2)
A_1	3.5×10^{-4}	1.27×10^{-4}
A_2	1.5×10^{-4}	1.38×10^{-4}
A_3	1.5×10^{-4}	1.21×10^{-4}
A_4	1.5×10^{-4}	1.25×10^{-4}
A_5	4.0×10^{-4}	1.48×10^{-4}
A_6	1.5×10^{-4}	1.40×10^{-4}
A_7	1.5×10^{-4}	1.49×10^{-4}
A_8	1.5×10^{-4}	1.20×10^{-4}
A_9	4.0×10^{-4}	2.09×10^{-4}

4.3.3 Weight Minimisation

Weight minimisation, which was the primary optimisation target, was achieved by using a multi-mode single objective algorithm. The reduction in the overall weight of the lower limb exoskeleton after optimisation for three different materials is shown in Table 4.8. The weight of the exoskeletons has been reduced by 30% for all materials that were investigated. A graphical representation of the decrease in the weight as the result of optimisation is shown in Figure 4.8. The topology optimisation shows, for some links, this decrease is noticeable and for others the value is almost the same. The reason behind this is that the areas showing less change are not bearing force when the force is applied on the exoskeleton in the form of the human body mass. The calculated weight is the mass of the exoskeleton estimated by using SolidWorks. The mass estimated for carbon fibre is the lowest of all three materials, which makes it a suitable material for the lower limb exoskeleton.

Table 4.8 Comparison between estimated and optimised weight.

Materials	Calculated weight (kg)	Optimised weight (kg)
Aluminium	3.70	2.58
Structural steel	10.5	7.30
Carbon fibre	2.42	1.63

The comparison of weight (Table 4.8) shows that the calculated weight for structural steel exoskeleton is 10.5kg, for aluminium it is 3.70kg, and for carbon fibre it is 2.42kg. The minimum weight is estimated for carbon fibre, which is 77 % and 34 % lower than the estimated weight for steel and aluminium exoskeletons, respectively. As a result of the topology optimisation, the weight was reduced by 30 % and the optimised weight came out to be 7.30kg for steel, 2.58kg for aluminium, and 1.63kg for carbon fibre. Hence, optimisation by Genetic Algorithm is a very useful tool for overall reduction in the exoskeleton's weight for different materials.

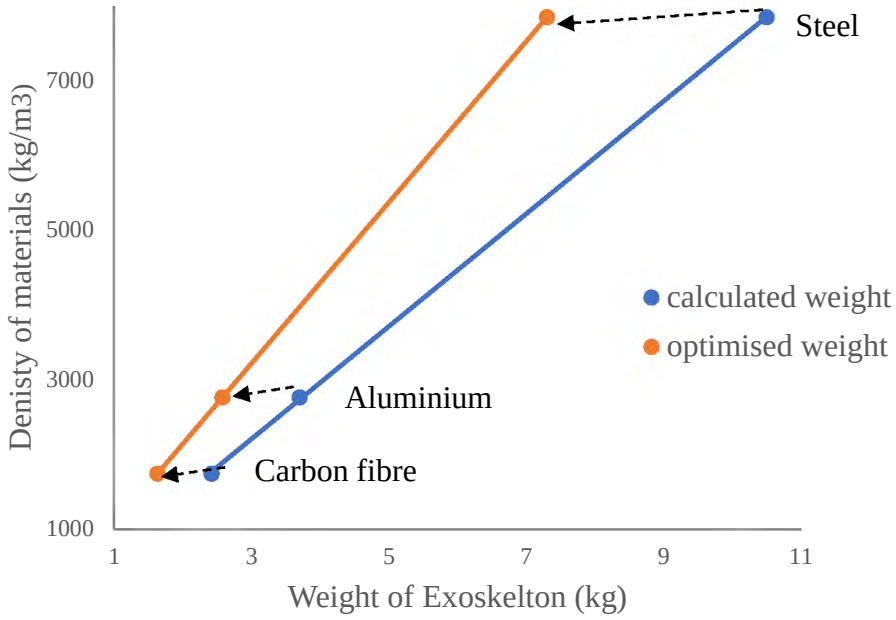

Figure 4.8 Comparison of calculated vs optimised weights for three varied materials.

4.4 Chapter Summary

This chapter presented information about two main steps toward the development of a lightweight and high strength robotic exoskeleton device (finite element modelling and optimisation). In the first section, finite element analysis was presented for different materials to obtain the stress distribution model of the lower limb exoskeleton. Various steps of finite

element modelling were discussed to achieve the stress distribution model and the most suitable material for the manufacturing of lower limb exoskeleton by the comparison of three commonly used materials. After that, the topology and material optimisation were presented, and the optimisation objectives was discussed. The optimisation algorithm to achieve the objective was also presented and discussed in this chapter. In the end, the minimised weight was given for the robotic exoskeleton prototype model and these optimised cross-sectional areas of various links will be used to build a physical prototype model of the lower limb robot exoskeleton.

From the optimisation results shown above, carbon reinforced fibre came out as the most suitable material for manufacturing the lower limb robot exoskeleton. However, the carbon reinforced fibre shows anisotropic material behaviour, which means this material shows different properties in difference directions of applied force [198]. Chapter 5 provides the detailed explanation about the anisotropic nature of this material and which fibre orientation would be the most suitable one to manufacture a lower limb robot exoskeleton. Hence, in the next chapter, the steps towards the manufacturing process to build an exoskeleton protype will be discussed in detail. The manufacturing process was started from the material testing and the detailed information about the material testing will be provided in Chapter 5.

CHAPTER 5 MATERIAL CHARACTERISATION FOR LOWER LIMB EXOSKELETON

After optimisation and finite element modelling, the next stage is the material characterisation for the prototyping of exoskeleton. The material used to manufacture the actual prototype model must be lightweight and at the same time it must have a good strength to carry the human body weight for longer periods of time. Carbon reinforced fibre was found to be a suitable material out of three materials compared during the mechanical load analysis, which was presented in the previous chapter. Hence, the material properties such as ultimate tensile strength, yield strength and elastic modulus must be experimentally obtained before starting the manufacturing process of the lower limb robot exoskeleton.

Carbon reinforced fibre is a type of composite material, which is extremely strong and lightweight. These fibres can be expensive to produce but now are commonly used for the applications where a high strength-to-weight ratio and stiffness are required. In rehabilitation robot applications, the weight reduction and high stiffness are the preliminary design requirements and to meet these requirements, carbon fibre polymers are gradually replacing the metals [199]. The carbon reinforced fibre that was used in the present work to design the lower limb exoskeleton was tested for the material properties before using this material for the fabrication of the various components of the lower limb exoskeleton as shown in Figure 3.6.

The material properties of carbon reinforced fibre composite like any other composite material can vary if different orientations are used while stacking the material to form the desired shape. Hence, these composite materials can be used for various application where varied material properties are needed [200]. In this work, the material properties were tested for different fibre orientations to assess the most suitable orientation of the fibre laminates for obtaining the best strength without increasing the material cost. Before performing the lab analysis, an optimal criterion for fiber orientation was defined by using Hashin's Failure Criteria. This chapter discusses the material characterisation as a function of fibre orientation of an anisotropic material to choose the most suitable orientation, which can give the most reliable structure. The flow chart for the various steps involved in the material characterisation is shown by Figure 5.1.

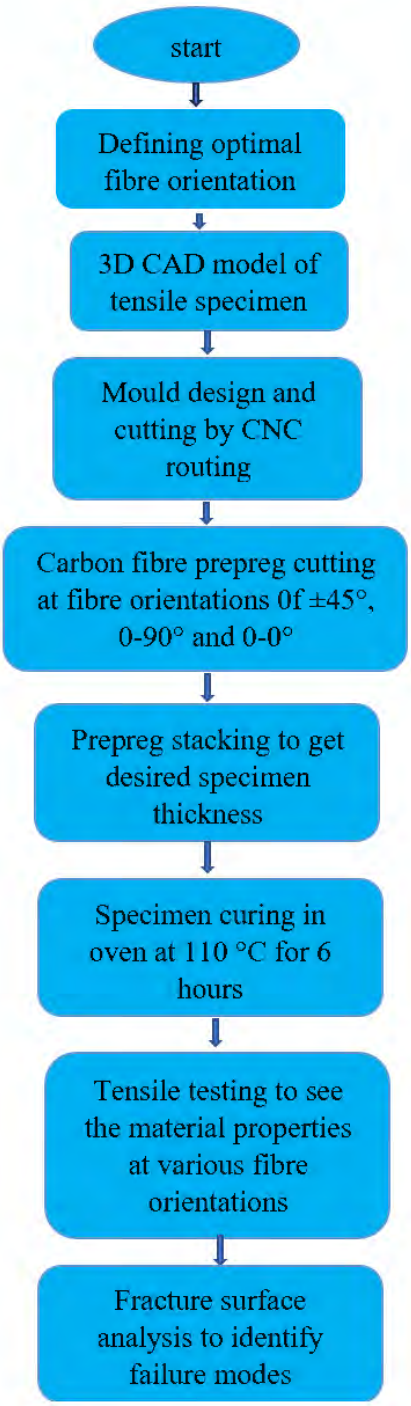

Figure 5.1 Workflow for the materials characterisation as a function of fire orientations.

5.1 Hashin's Failure Criteria

For defining the optimal criteria for fibre orientation, Hashin's Failure Criteria is considered. These criteria are developed based on observed failure modes also explored in Hashin-Roten criteria. There are four distinct failure modes: matrix tensile, matrix compressive, fibre tensile, and fibre compressive. The Hashin's Failure Criteria governs all these modes which interact in terms of stresses and strength properties [201]. Hashin's failure criteria is an interacting failure criterion which evaluates the different failure modes for various stress components. They are

involving four failure modes are related to the fibre and matrix failures. Further, Hashin's Failure Criteria can be used to select point-wise design for fibre orientation by means of optimality conditions [202] . The literature mentions several other optimality conditions for fibre orientations. Optimality conditions based on Hill [203] and Tsai-Wu [204] criteria were derived in [205] that proved that based on material properties and loading, the orientations other than principal stresses can minimize the failure criteria. However, these studies do not demonstrate practical optimisation algorithms based on the derived optimality condition. The optimisation algorithm of the optimality condition based on Hashin's Failure criteria presented in [206]. The optimality conditions are analytically derived and used to minimize the Hashin's failure criteria in all four modes (matrix tensile/compressive and fibre tensile/compressive). The developed algorithm was adopted to find the optimum fibre orientation for the fabrication of the lower limb exoskeleton.

In this research work, fibre fabrication at unidirectional(0^o) and bidirectional orientations (0-$90^o$and $\pm45^o$) were considered. The local material orientation can be defined in one of two ways: First, the fibre reinforcement direction in which the equivalent properties are fibre dominated. Secondly, the direction perpendicular to the fibre reinforcement direction and is referred to as the matrix direction as the equivalent points are matrix dominated. The main reason behind using these three orientations is the availability of the carbon fibre material, as it was only possible to obtain these three fibre orientations from commercially available prepregs. From the previously published research, it was clear that other orientations will show the properties like these three orientations [207]. In present work, σ_{11} refers to the direct stress in fiber reinforcement direction; σ_{22} refers to the direct stress component in matrix direction; and τ_{12} is the shear stress component between the fiber reinforcement and the matrix direction. The Hashin's failure criteria can thus be defined as:

$$F^{Yt} = \left(\frac{\sigma_{22}}{Y_t}\right)^2 + \left(\frac{\tau_{12}}{s_{12}}\right)^2 = 1 \tag{5.1}$$

This equation governs the failure according to matrix tensile mode where $\sigma_{22} > 0$. When $\sigma_{22} < 0$, failure occurs according to matrix compressive mode:

$$F^{Yc} = \left(\frac{\sigma_{22}}{2S_{23}}\right)^2 + \left[\left(\frac{Y_c}{2S_{23}}\right)^2 - 1\right] + \left(\frac{\tau_{12}}{s_{12}}\right)^2 = 1 \tag{5.2}$$

Similarly, the failure according to fibre tensile mode occurs when $\sigma_{11} > 0$:

$$F^{Xt} = \left(\frac{\sigma_{11}}{X_t}\right)^2 + \left(\frac{\tau_{12}}{s_{12}}\right)^2 = 1 \tag{5.3}$$

When $\sigma_{11} < 0$, the failure occurs according to fiber compressive mode:

$$F^{Xc} = \frac{\sigma_{11}}{-X_c} = 1 \tag{5.4}$$

In Equations (5.1) to (5.4), X_t and X_c are tensile and compressive strengths in fibre direction; Y_t and Y_c are tensile and compressive strengths in matrix direction; S_{12} is the in-plane sheer strength and S_{23} is the out-of-plane sheer strength. The relations for plane stress transformations can be written in terms principal stress $(\sigma_{1p}\ and\ \sigma_{2p})$ the orientation (β) measured from the principal stress direction (σ_{1p}) as:

$$\sigma_{11} = \frac{1}{2}\left[(\sigma_{1p} + \sigma_{2p}) + (\sigma_{1p} - \sigma_{2p})\cos 2\beta\right] \tag{5.5}$$

$$\sigma_{22} = \frac{1}{2}\left[(\sigma_{1p} + \sigma_{2p}) - (\sigma_{1p} - \sigma_{2p})\cos 2\beta\right] \tag{5.6}$$

$$\tau_{12} = -\frac{1}{2}(\sigma_{1p} - \sigma_{2p})\sin 2\beta \tag{5.7}$$

5.1.1 Optimisation

For optimisation, all the failures in different modes were considered together to determine the failure of the material. For each mode, the failure criteria were defined in terms of Equations 5.5, 5.6, and 5.7. Thus, Equations 5.1, 5.2, 5.3, and 5.4 can be rewritten as [208]:

$$F^{Yt}(\beta) = \frac{1}{4Y_t^2}\left[\sigma_{1p} + \sigma_{2p} - \cos 2\beta(\sigma_{1p} - \sigma_{2p})\right]^2 + \frac{1}{4S_{12}^2}\sin^2 2\beta(\sigma_{1p} - \sigma_{2p})^2 \tag{5.8}$$

$$F^{Yc}(\beta) = \frac{1}{16S_{23}^2}\left[\sigma_{1p} + \sigma_{2p} - \cos 2\beta(\sigma_{1p} - \sigma_{2p})\right]^2 + \frac{1}{4S_{12}^2}\sin^2 2\beta(\sigma_{1p} - \sigma_{2p})^2 + \frac{c_{Y_c}}{2Y_c}\left[\sigma_{1p} + \sigma_{2p} - \cos 2\beta(\sigma_{1p} - \sigma_{2p})\right] \tag{5.9}$$

$$F^{Xt}(\beta) = \frac{1}{4X_t^2}\left[\sigma_{1p} + \sigma_{2p} + \cos 2\beta(\sigma_{1p} - \sigma_{2p})\right]^2 + \frac{1}{4S_{12}^2}\left[\sin 2\beta\,(\sigma_{1p} - \sigma_{2p})\right]^2 \tag{5.10}$$

$$F^{Xc}(\beta) = \frac{1}{-2X_c}\left[(\sigma_{1p} + \sigma_{1p}) + (\sigma_{1p} - \sigma_{2p})\cos 2\beta\right] \tag{5.11}$$

The Global Optimisation was performed using the Genetic Algorithm. The aim is to minimize combined failure probability using Hashin's Failure Criteria, to increase the probability of success. A mathematical objective function is formulated to minimize the failure probability based on Hashin's failure criteria. The objective function considers stress, strain, and material properties as input parameters and returns the failure probability. The optimisation task is to find stress and strain values that minimize this objective function, while the

orientation angle serves as a variable that the optimisation algorithm adjusts. A global optimisation approach is employed using the Genetic Algorithm provided by MATLAB's Optimisation Toolbox. The GA seeks to find the optimal stress, strain, and orientation values that minimize the failure probability. The GA is configured with settings such as a maximum number of generations, population size, and plot functions to visualize the optimisation progress. The material properties used for the optimisations are shown in Table 5.1 along with the bounds for the Genetic Algorithm [209]. An iterative process was implemented to find the optimal stress and strain values for each orientation.

Table 5.1 Material properties and bounds for Genetic Algorithm [209].

Variable	Value
Young's modulus for laminate	100 GPa
Young's modulus for matrix	5 GPa
Volume fraction of fibres	0.6
Fibre Tensile Strength	150 MPa
Matrix Tensile Strength	30 MPa
Fibre-Matrix Shear Strength	30 MPa
Lower bound for Stress	0
Upper bound for Stress	1000
Lower bond for strain	0
Upper bond for strain	0.02

Figure 5.2 shows the convergence of the failure probability over 20 iterations. The algorithm was programmed to cease when the average decrease of the last 10 iterations was less than 10^{-20}. This was achieved by the 20^{th} iteration in each case. The least failure probability and the mean values are also summarized in Table 5.2. At a glance, the $90°$

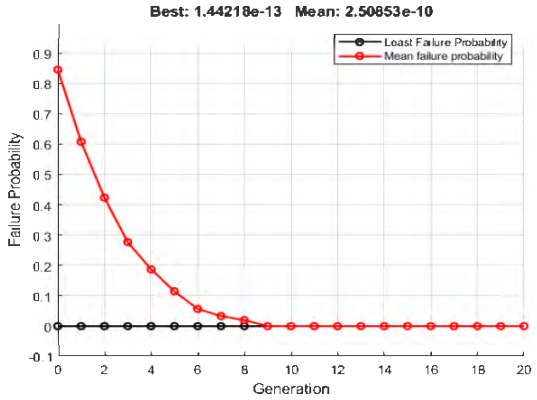

(a)

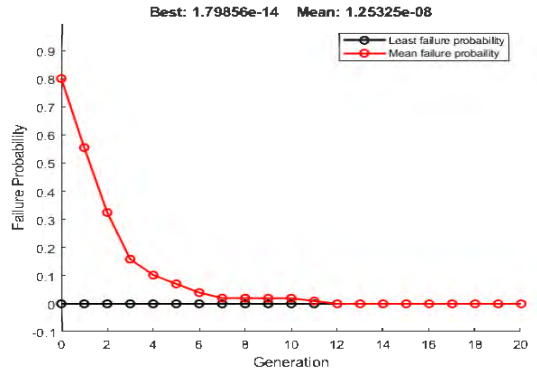

(b)

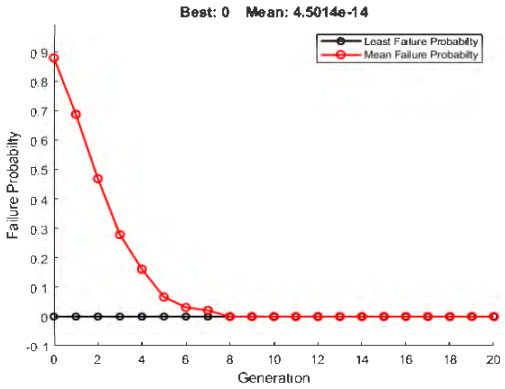

(c)

Figure 5.2 Failure probability over 20 iterations of GA for (a) 0°, (b) $\pm 45°$, and (c) $0 - 90°$. The best and mean failure probabilities are shown for each orientation.

orientation has the least failure probability which is very close to 45° orientation's failure probability. Therefore, further analysis was required to ascertain the best possible orientation for prototype fabrication.

Table 5.2 Least and Mean Failure Probabilities for various orientations.

Fibre orientation	Least Failure Probability	Mean Failure Probability
$0°$	1.4×10^{-13}	2.5×10^{-10}
$\pm 45°$	1.8×10^{-14}	1.2×10^{-8}
$0 - 90°$	0	4.5×10^{-14}

Tensile testing was carried out to get the most suitable fibre orientation to fabricate the lower limb exoskeleton for gait rehabilitation. The details of tensile lab testing procedure starting from the specimen design for tensile testing is discussed in the following section.

5.2 Tensile Testing

Tensile testing to find the monotonic tensile properties is a destructive test process that provides information about the tensile strength, yield strength, and ductility of the metallic and composite materials. It measures the force required to break a metal, composite, or plastic specimen and the extent to which the specimen stretches or elongates to that breaking point [210]. The specimen preparation is the first step to carry out tensile testing, as the specimen for tensile testing must follow the standard shape and design set by American society of testing materials (ASTM) [211]. The various required steps in the specimen preparation are presented in the sections below.

5.2.1 Specimen 3D Model

To start the tensile testing, the first step was to prepare a specimen model according to the ASTM D638 standard [211], which is the standard testing procedure to get the monotonic tensile properties of composites and plastics. The specimen model was drawn using SolidWorks ®. The designed specimen has an overall length of 165mm with a gauge length of 57mm. The gauge width of 13mm was selected with a thickness of 3mm. All these dimensions were the standard values obtained from the above-mentioned ASTM standard. The dimensions of the designed specimen and a 3D CAD model are shown in Figure 5.3.

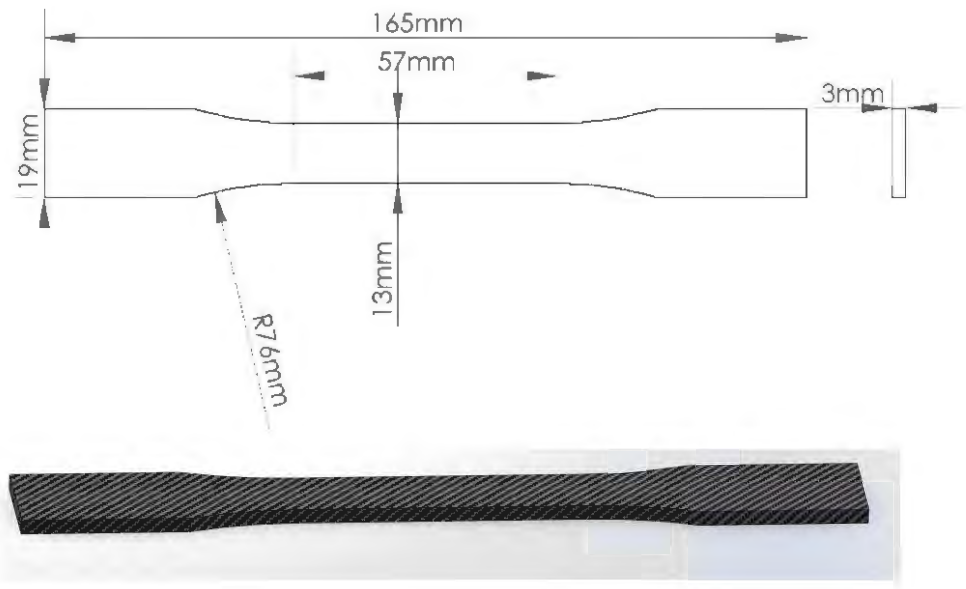

Figure 5.3 Specimen dimensions and 3D CAD Model used for tensile testing.

After preparation of the CAD model, a carbon fibre specimen was moulded to create a physical specimen for tensile testing. As mentioned earlier, the anisotropic behaviour of carbon fibre was the main material characterisation goal. Moulding was a suitable method to design the specimen with desired fibre orientations without the need of a highly specialised and expensive 3D printing technology. Although more labour cost was involved in the creation of the specimen, the test specimen could be created accurately with the desired fibre orientations, which was difficult to achieve with other shaping and fabrication techniques. The process of specimen design was carried out at the material manufacturing and testing laboratory at Faculty of Arts and Design, University of Canberra. To start the moulding process, mould preparation was the first step.

5.2.2 Mould Preparation

The mould or metallic die for the specimen design was obtained to achieve the desired thickness and shape of the tensile specimen. The mould drawing was prepared to create four specimens at a time, so that the structure uniformity of the designed specimen for each fibre orientation could be maintained. The drawing of the mould is shown in Figure 5.4, which was subsequently converted to G code to feed the information to CNC cutting machine. Aluminium sheets were used in the mould preparation to keep mould lightweight and reduce the heating cost for heating the carbon fibre specimen.

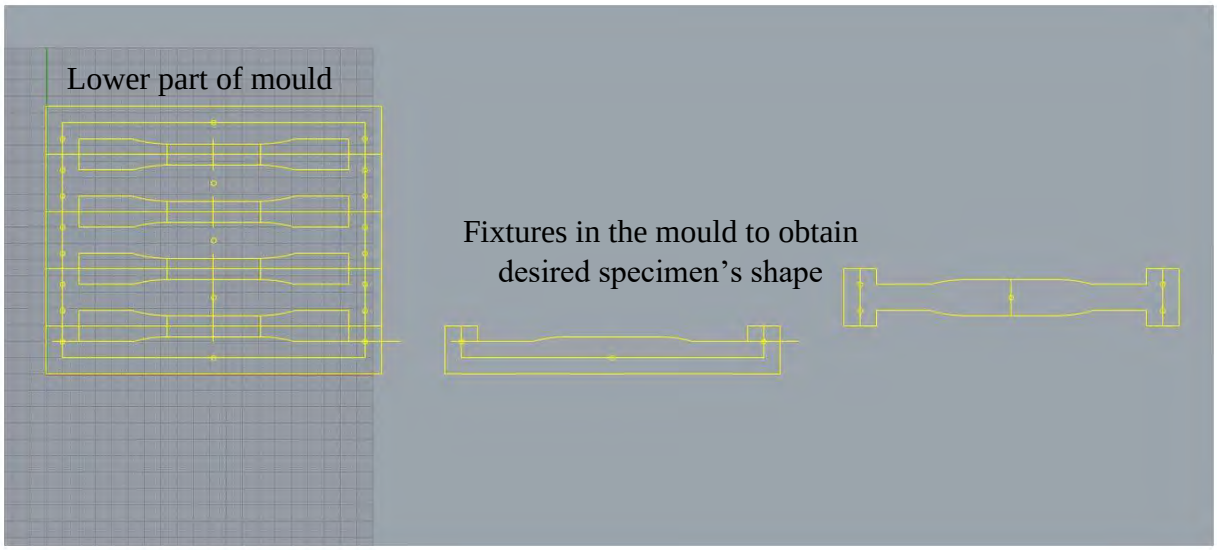

Figure 5.4 Mould drawing drawn by SolidWorks® to fabricate the carbon fibre specimen.

The process of cutting the aluminium sheets to create the mould for specimen production was carried out by using a MULITCAM SL2515v CNC routing machine with eight place tool chargers. The CNC routing machine (see Figure 5.5) uses a special software known as Enroute for feeding different commands for cutting metallic, non-metallic, wooden, composite materials sheets with a maximum thickness of 55mm. For the present work, two aluminium sheets were cut having a thickness of 3mm and 10mm, respectively.

Figure 5.5 MULITCAM SL2515v CNC routing machine at the University of Canberra.

The designed mould is assembled by using screws and the designed mould consists of two parts as shown in Figure 5.6. The 3mm sheet was selected to enable the creation of a specimen with a thickness of 3mm, which was previously discussed in section 5.2.1. The 10mm sheet was used as upper part of the mould to press the carbon fibre prepregs stacked in the lower part of the mould to remove the entrapped air. Before proceeding to the next step, the

mould was uniformly covered with a layer of the mould release solvent to avoid sticking of the carbon fibre specimen after they have fully cured.

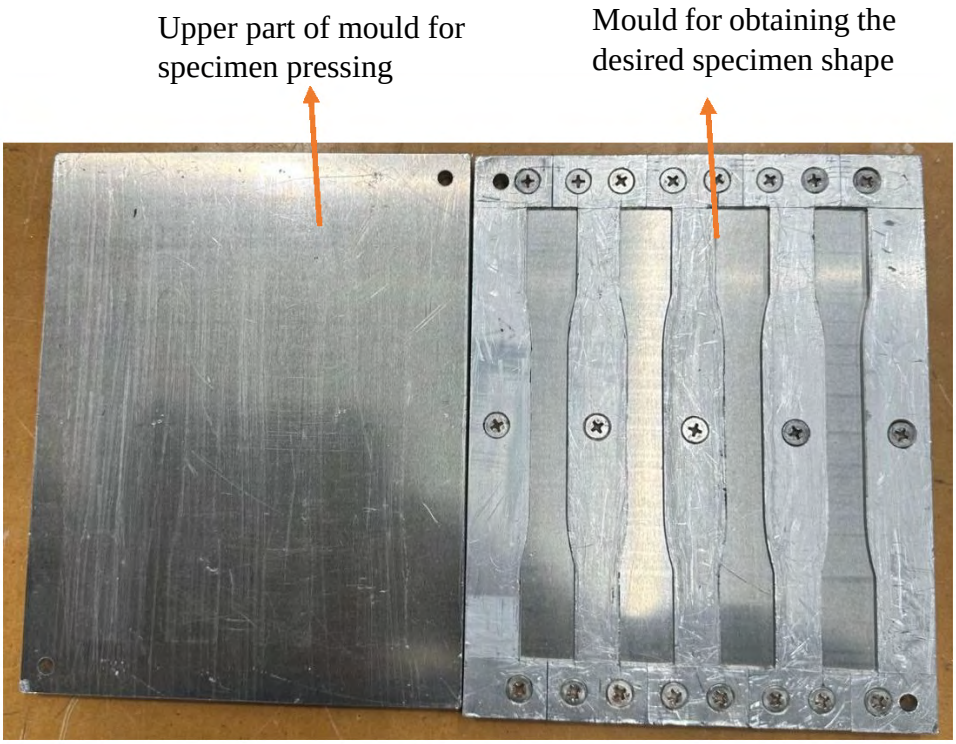

Figure 5.6 Mould of aluminium used to prepare carbon fibre tensile specimen.

5.2.3 Specimen Preparation at Different Fibre Orientations

Specimen preparation for monotonic tensile testing was carried out as the next stage of this research work. The specimen was obtained from the sheets of carbon fibre prepregs with a resin on it. These prepregs were purchased from Haining Anjie Composite material C0. LTD and having a shelf life of 12 months at a storage temperature of 23 °C. The resin properties are shown in Table 5.3, which were provided by the supplier of these carbon fibre prepregs. There are two types of prepregs (unidirectional and bidirectional) that were used with the same resin content of 40 % and the same thickness of 0.24mm. The sheets were cut into three different fibre orientations as shown in Figure 5.7. A 3k twill bidirectional carbon prepreg was used to assemble the specimens at ±45° and 0-90° specimen orientations, whereas a unidirectional prepreg was used to obtain the specimen with a 0-0°fibre orientation. The main reason behind using these three orientations is the availability of the carbon fibre material, as it was only possible to obtain these three fibre orientations from commercially available prepregs. From

the previously published research, it was clear that other orientations will show the properties like these three orientations .

Table 5.3 Epoxy resin properties (at 25 °C) used in the carbon fibre prepreg.

Viscosity (mPs)	Density (g/cm^3)	Epoxy index (eq/kg)	Solid content (%)
700	1.05	2.90	53

(a) (b) (c)

Figure 5.7 Different fibre orientations of specimens designed for tension test: (a) 0-90°, (b) ±45°, and (c) 0-0°.

The process of cutting the prepreg sheets to the desired specimen shape was carried out manually as shown in Figure 5.8. A normal paper cutting blade was used to cut the prepregs and stack them over one another. The bi-diretional prepregs were cut at the specified angles to obtain the different fibre orientations of ±45° and 0-90°. In order to achieve a thickness of 3mm for the standard tensile specimen, 12 sheets were layered for each specimen. The mould was pre-heated to a temperature of 60°C for 30 minutes before the layering process started. This process of preheating removed any moisture from the mould surface that can cause voids and may lead to false tensile testing results [212].

Figure 5.8 Cutting of carbon fibre prepreg to desired specimen shape.

The process of stacking the specimen to create the desired specimen thickness is shown in Figure 5.9. For each speciem, 12 layers of prepreg were used and great care was taaking to ensure that these prepreg sheets were properly pressed to remove any air bubbles before curing them. The upper alumimium plate was tightened with screws and the entire mould was put into the oven for curing.

Figure 5.9 Stacking of prepreg layers to achieve the desired thickness.

After stacking into the mould, the prepregs were cured at temperature of 110°C for six hours to create the hardened specimens of carbon fibre, which were used for the monotonic tensile testing to assess the material properties at various fibre orientations. The curing of the specimen was carried out by using a specially designed air-circulating oven. The oven was specially designed by a company named as LSM which designs special ovens for curing the carbon fibre prepregs at various temperature cycles (see Figure 5.10). The curing temperature data was provided by the company, which depends on the desired thickness of the final product.

Figure 5.10 Air circulating oven to cure carbon fibre specimen.

The mould was placed in the oven and two thermocouples were attached with the moulds containing the carbon fibre specimen inside. Thermocouples give accurate

measurements of the mould temperature, which was necessary for the proper curing cycle of the specimen. The position of the mould inside the oven along with the thermocouples attached is shown in Figure 5.11. After heating the specimens harden as the glass transition temperature for the resin was achieved.

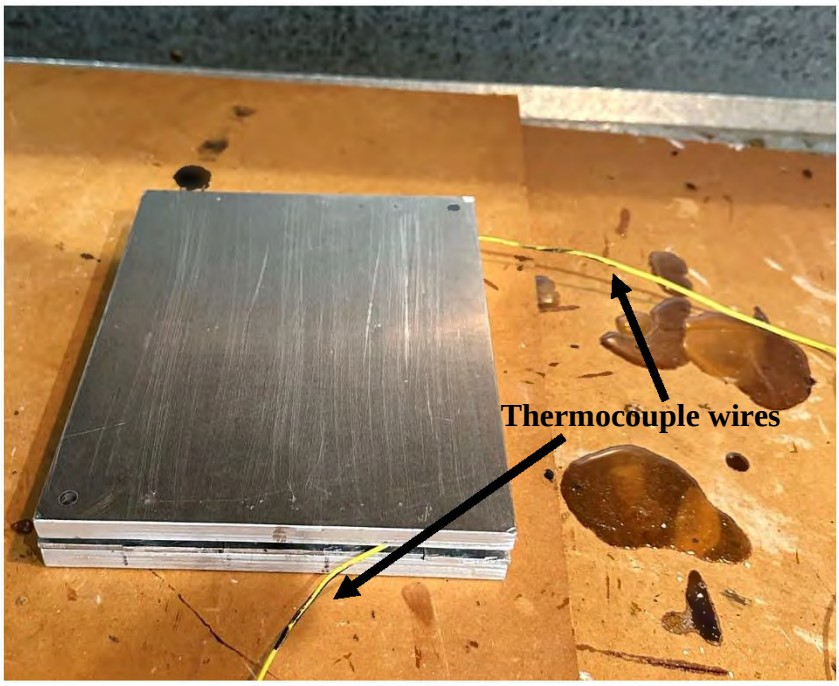

Figure 5.11 Specimen inside the heating oven for curing.

After removal from the oven, the specimens were taken out of the mould and cleaned by washing with warm water for five minutes to remove any unwanted melted surfaces, which can affect the tensile properties and leads to false results. The final specimens for different fibre orientations obtained after the complete curing cycles are shown in Figure 5.12. After that, tensile testing was the next stage to assess the monotonic tensile properties of the carbon fibre specimen at different fibre orientations to select the most suitable orientation for manufacturing the lower limb robot exoskeleton designed for gait rehabilitation.

Figure 5.12 Tensile testing specimens at various fibre orientations.

5.2.4 Tensile Testing Equipment

Tension tests were carried out according to the ASTM D638 standard [211], which is the standard testing procedure to get tensile properties of plastics and composites. The tensile tests for each fibre orientations were carried out using a 100 kN SHIMADZU tensile machine with a camera attached to assess the increase in length under the applied force. The tests were carried out with a testing speed of 2mm/min to determine the mean ultimate tensile stress (UTS), yield stress, and effective modulus of elasticity along the longitudinal loading direction for each fibre orientation. Four specimens of each orientation were tested until fracture occurred. Before testing each specimen was marked with the marking sticker (see Figure 5.13) to capture the gauge length by a camera attached to the tensile machine. The equipment used for the tension tests holding the test specimen is shown in Figure 5.14.

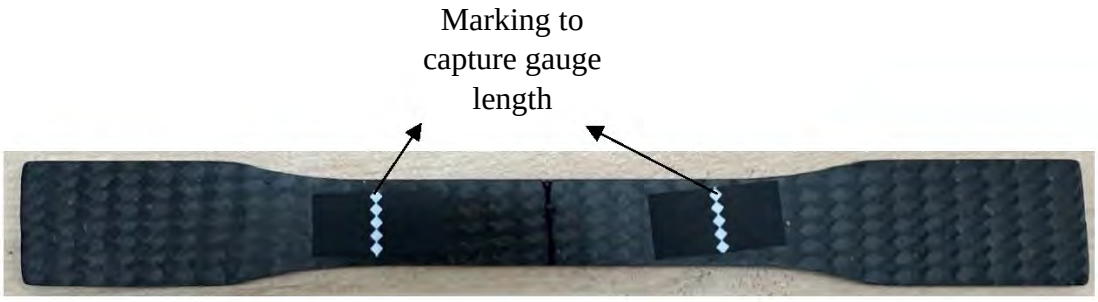

Figure 5.13 Marking stickers on tensile specimen to visually capture gauge length.

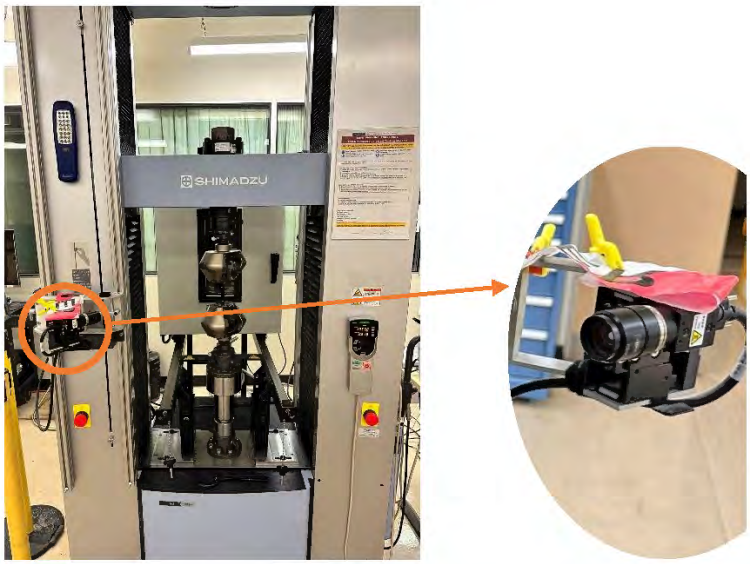

(a)

(b)

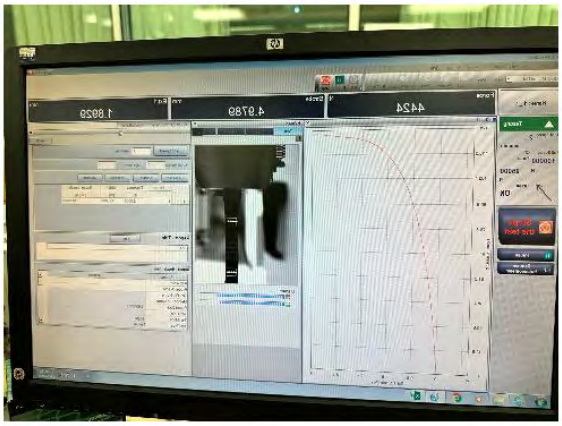

(c)

Figure 5.14 (a) SHIMADZU 100 kN tensile testing machine with camera, (b) specimen in the tensile testing machine, and (c) software interface.

The force applied to the specimen until failure, as obtained from the test data of the machine, was converted into stress by using the following equation:

$$\sigma = \frac{F}{A} \tag{5.5}$$

where F is the force applied to the specimen until fracture and A is the area of the cross-section of the specimen. The strain (ϵ), which is the change in length of the specimen under an applied force, was calculated by the following equation:

$$\epsilon = \frac{\Delta l}{l_0} \tag{5.6}$$

where Δl is the change in length and it is captured by a camera and calculated by a software interface available with the tensile testing equipment with the tensile testing machine and l_0 is the original gauge length of the specimen.

5.2.5 Tensile Test Results

The test results in the form of a stress-strain curve obtained from the monotonic tensile testing for each fibre orientation is shown in Figures (5.15-5.17), while Figure 5.18 shows a combined $\sigma - \epsilon$ curve for different fibre orientations. The effective elastic modulus for each specimen tested was calculated from the slope of the linear portion of the stress-strain curves, i.e., $\Delta\sigma/\Delta\epsilon$. The yield strength was calculated by using the 0.2% offset method, which is the standard

procedure for obtaining the value of yield stress if the material shows the yielding phenomena [213]. The monotonic tensile response observed for representative specimen types indicated dissimilarities regarding both strength and fracture strain for different fibre orientations. From the comparison of the stress-strain curves, the carbon reinforced fibre with a fibre orientation of ±45° showed a sufficiently better stress-strain behaviour than other orientations and a nice ductile facture occurred and a strain of 0.22 was obtained prior to failure. In contrast, the specimens with an orientation of 0-90° and 0-0° showed a brittle failure without any yielding and a very low strain of 0.012 and 0.008.

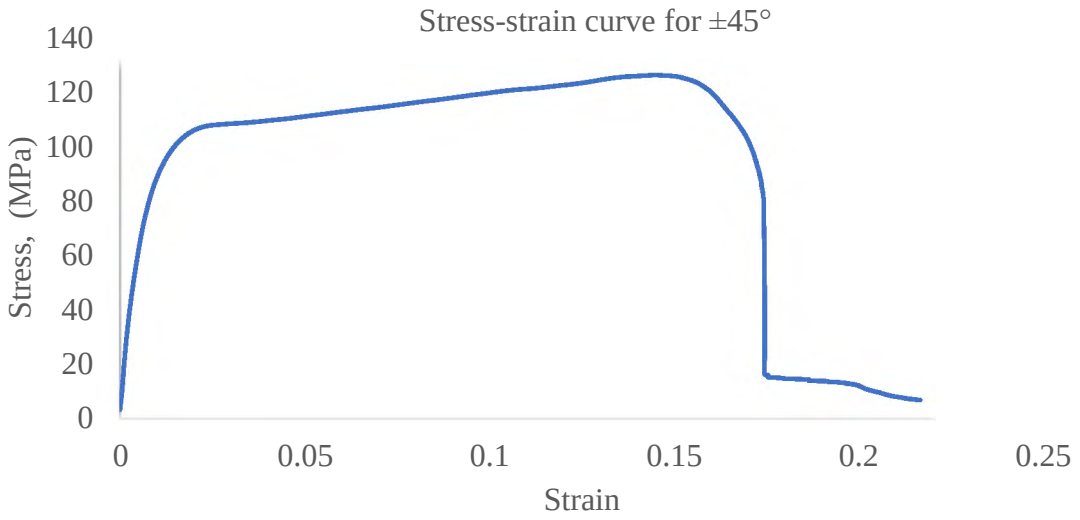

Figure 5.15 Stress-strain curve for the ±45° fibre orientation.

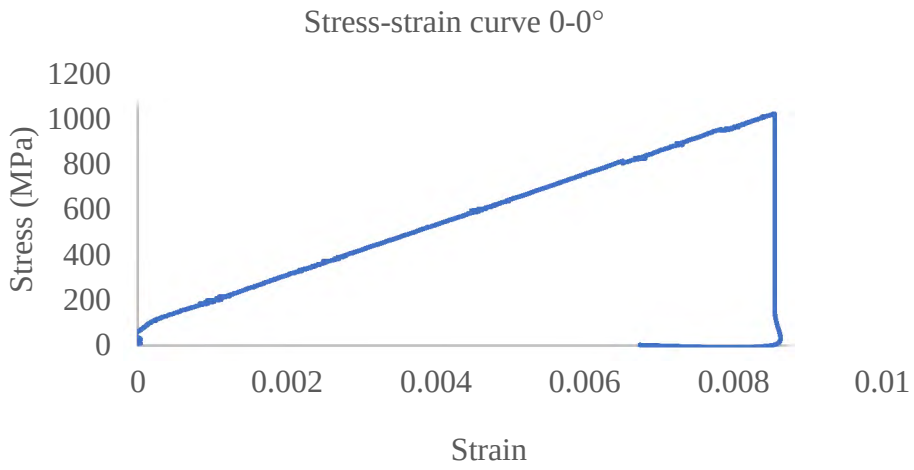

Figure 5.16 Stress-strain curve for the 0-0° fibre orientation.

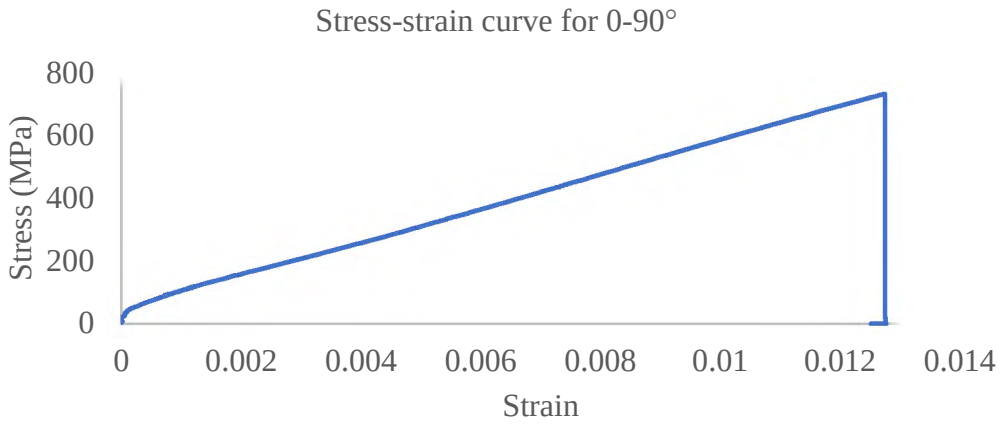

Figure 5.17 Stress-strain curve for the 0-90° fibre orientation.

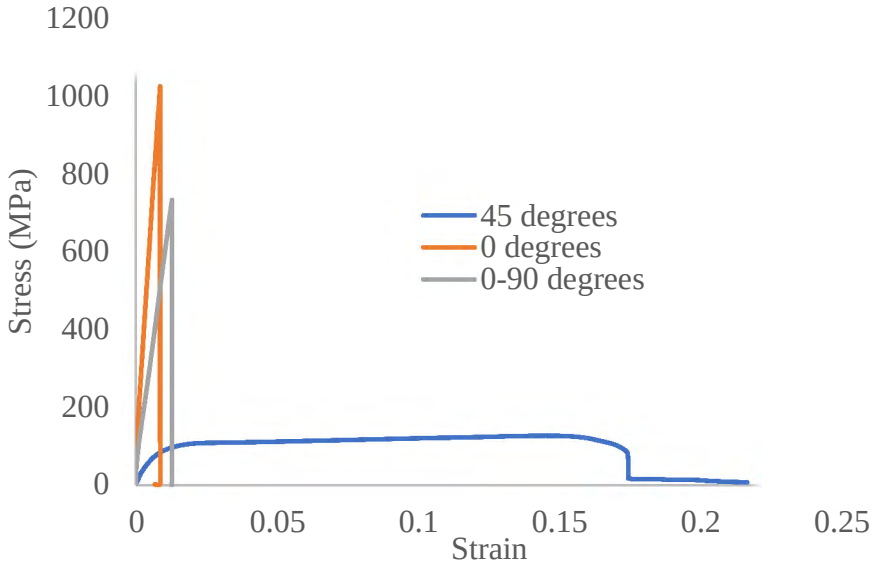

Figure 5.18 Combined stress-strain curve for all three fibre orientations.

A summary of the resulting tensile strength yield strength and elastic modulus is presented in Table 5.4. For the fibre orientation of ±45°, a tensile strength of 123.15 MPa was obtained, which is much lower than the values of 731.84 MPa and 1023.94 MPa for the 0-90° and 0-0° fibre orientations, respectively. Similarly, due to the anisotropic behaviour of carbon fibre, there was a difference in Young's Modulus and the maximum value of 111.69GPa was obtained for unidirectional (0-0°) followed by 0-90°and the minimum value was obtained for ±45°. However, the yielding was observed only in the specimen with the ±45° fibre orientations. Looking at the strain results, the maximum strain was obtained in the specimen with the ±45° fibre orientation laminates, while the other two fibre orientations were not showing any considerable strain or elongation before failure.

Table 5.4 Monotonic tensile properties at various fibre orientations.

Fibre orientations	Tensile strength (MPa)	Yield strength (MPa)	Young's Modulus (GPa)	Strain (%)
Twill (±45°)	123.15	85.91	13.20	21.98
Twill (0-90°)	731.84	No yielding	53.78	1.20
Uni-directional (0-0°)	1023.94	No yielding	111.69	0.85

Hence, it is clear from the analysis that the material used is highly anisotropic and the highest tensile strength was obtained for the unidirectional carbon fibre orientation. However, the yielding is an important factor to consider while considering robotics applications. In the fibre orientations of 0-0° and 0-90°, there is no yielding, meaning that these fibre orientations are not suitable to design a lower exoskeleton due to their brittle behaviour because a long product life is needed. Materials failing earlier due to low endurance to fatigue or cyclic stress are not suitable [214]. The carbon reinforced with fibre orientations of ±45° is the most suitable for the present work due to a ductile behaviour and an acceptable tensile and yield strength. This fibre orientation (±45) also showed the longest fatigue life when compared to other orientations in an experimental study published by a group of researchers from the Department of Mechanical Engineering, Bucknell University, Lewisburg, United States [207].

To the author's best knowledge, the application of Hashin's Failure Criteria and its experimental validation has not previously been reported in any published research work to find a most suitable fibre orientation in robotic applications. From the optimisation, the fibre orientation of 0-90º appeared to be the most suitable with least failure probability but very close to ±45º orientation. However, experimental results indicated the best orientation is ±45º to get the most reliable structure. The experimental results are considered to be good and in accordance with the previously published research work [207]. Hence, a fibre orientation of ±45º is used to fabricate the prototype. The fracture surface analysis after the tensile testing is also important and it was carried out to identify different failure modes in the specimens designed at various fibre orientations.

5.3 Fracture Surface Analysis

Inspection of the fractured specimens from monotonic tensile testing highlights the failure modes as a function of fibre variation. The fracture surface after specimen failure for various fibre orientations is shown in Figure 5.19. It was observed from a macroscopic analysis that

the unidirectional specimen (0-0°) consistently failed along the bond between the fibres (Figure 5.19(a)). The failure mode was brittle without showing any necking and elongation, as can be observed in the stress-strain curve data. A similar brittle behaviour was seen in the specimen with the 0-90°fibre orientation. As can be seen in Figure 5.19(b), there is a brittle fracture without any necking, which is an indication of a rapid fracture without showing any yielding. However, Figure 5.19(c) shows the necking area of a fracture surface of the specimen with the ±45° degree fibre orientation. This necking behaviour shows a purely ductile fracture and there was a good amount of strain before the specimen failed under tensile loading.

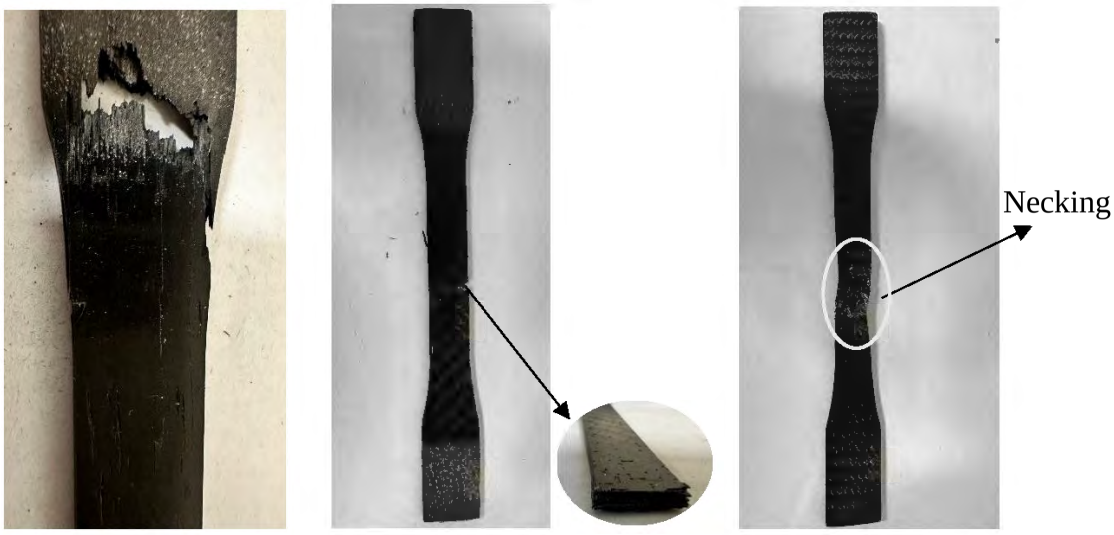

Figure 5.19 Fracture surfaces after tensile testing at different fibre orientations (a) 0-0°, (b) 0-90°, and (c) ±45°.

From the surface analysis, it can be concluded that the fibre orientation of ±45° has a greater tendency to bear the cyclic loading as the behaviour is ductile. The ductile materials can survive for longer under an applied cyclic loading as compared to brittle materials and the degradation taking place during a longer period, which contributes to a more reliable structure [215]. Hence, in the next stage to fabricate a lower limb exoskeleton, the fibre orientation of ±45° was selected and bigger sheets of carbon reinforced fibre were obtained, which were precisely cut by a CNC routing machine to manufacture the different components of the exoskeleton.

5.4 Chapter Summary

This chapter presented the material characterisation to make a lower limb robot exoskeleton. From the previous chapter, based on simulation and optimisation results, the carbon reinforced fibre was found to be the most suitable material in comparison with steel and aluminium.

Carbon reinforced fibre is a composite material with highly anisotropic behaviour, which means the fibre orientations greatly influence the material properties. Hence, to find a suitable fibre orientation, the material properties at various fibre orientations were tested and documented in this chapter. Various stages of the material testing, starting from the mould design for specimen preparation, were presented in this chapter. Furthermore, the results of tensile testing for various fibre orientations in the form of stress-strain curves were discussed. Finally, a macroscopic analysis of the fracture surfaces confirmed a ductile behaviour for a fibre orientation of ±45°, which makes this orientation the most suitable one to manufacture the components of a lightweight and reliable lower limb robotic exoskeleton.

The lower limb exoskeleton was fabricated after joining the various components, which are cut from the carbon fibre moulded at ±45° fibre orientations. The process of cutting of various components and joining the components to get the full lower limb exoskeleton actuated by a single DC motor is discussed in the following chapter. The reliability analysis of the designed lower limb exoskeleton by using a machine learning based approach is also presented in the next chapter of this thesis.

CHAPTER 6 ROBOT FABRICATION AND ASSEMBLY

This chapter describes the fabrication and assembly process to obtain a physical prototype of the lower limb robot exoskeleton for gait rehabilitation. From the previous chapter, it was concluded that carbon fibre with a fibre orientation of ±45° was the most suitable material configuration to fabricate a reliable design without increasing the weight of lower limb exoskeleton, which is the primary design concern. Hence, this chapter explains the various steps involved in the complete construction of the lower limb exoskeleton that was previously designed by following the Stephenson III six-bar linkage mechanism, and an optimised material and optimised robot topology was obtained. In this chapter, the various steps involved in joining the robot components are discussed, starting from the carbon fibre sheets cutting. The weight comparison between the simulated and a physical prototype is also presented in this chapter.

To fabricate a prototype of lower limb exoskeleton more than one fabrication technique is needed to be employed. Hence, several steps are involved to get the desired prototype structure. The complete description of manufacturing methods is discussed in detail in chapter 2 section 2.4.3. In present research work, the process of carbon fibre sheets casting, CNC cutting, and cold pressing are used. Initially, the 3D CAD model of the lower limb exoskeleton that has been designed and explained in detail in Chapter 3 was converted into a physical prototype by using carbon fibre material. To do so, the various components of that model drawing, i.e., hip, shank, and ankle were converted into the drawing exchange format (DXF) required for the CNC cutting from carbon fibre sheets. The sheets were cut and joined together to obtain a prototype assembly of a lower limb exoskeleton. The joining process involves various metal forming process such as, cold press, cutting, and grinding to get a good assembly of the lower limb exoskeleton.

Secondly, a suitable actuator is attached to provide a torque to the various joints of the designed exoskeleton to move the lower limb exoskeleton. A complete description of the direct current (DC) motor actuator is provided in this chapter along with the controller attached to adjust the speed for different users. The properties of the DC motor actuator are presented in this chapter.

A complete workflow of the events presented in this chapter, starting from cutting the carbon fibre sheets and ending with the complete assembly of the robot exoskeleton is shown in Figure 6.1.

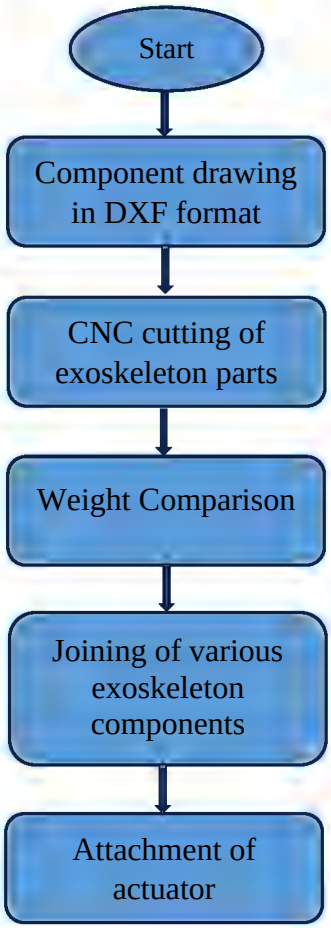

Figure 6.1 Workflow for exoskeleton fabrication and assembly.

6.1 Cutting and Milling of Various Components

Sheets of carbon fibre reinforced polymer (CPRF) with a fibre orientation of ±45° were used as this orientation was found to result in the most reliable structure of the lower limb robotic exoskeleton. The cutting process of these sheets was started from the drawing of the various components of the lower limb exoskeleton in the Drawing Exchange Format (DXF) by using SolidWorks®. This drawing format was used as an input to a CNC router machine to cut the carbon fibre reinforced sheet into various components of the designed lower limb exoskeleton. The DXF drawings for each component such as hip, knee, shank, and ankle are shown in Figure 6.2.

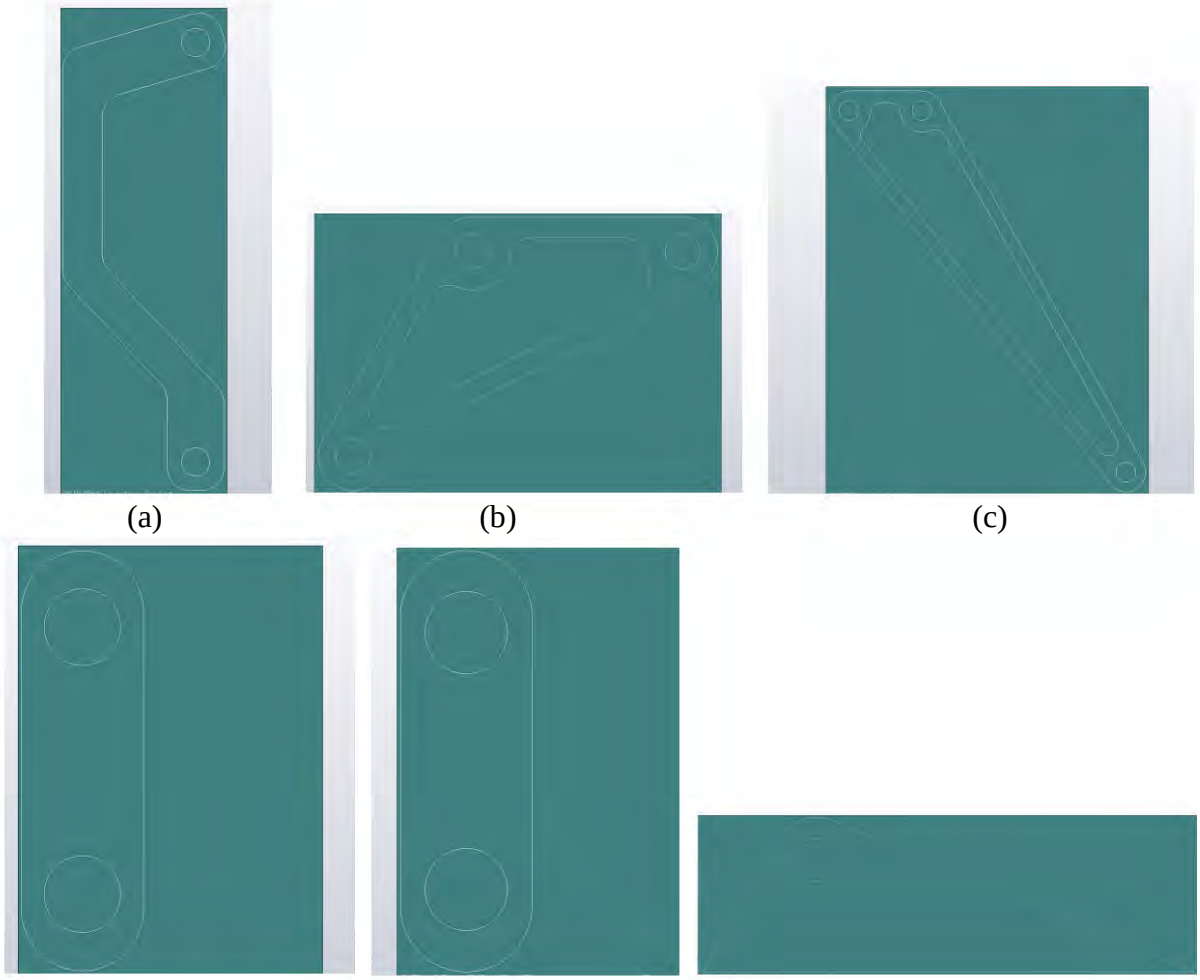

Figure 6.2 Drawing of various components of the lower limb exoskeleton in DXF format for CNC machining.

After drawing the components, the machining properties for each component were important to define to achieve an accurate cut by the milling machine. An important step was to get the correct G code for every component, so as to obtain the desirable and accurate sizes for the holes. To do so, the SolidWorks® CAM toolbox was used, which provides information about the different tools and their function for CNC machines. The G code was then obtained from SolidWorks® and then input into the milling machine.

6.1.1 Equipment Used for Component Design

The fabrication of various components of the lower limb exoskeleton design from a sheet of carbon reinforced fibre polymer (CRFP) at a fibre orientation of ±45° was carried out by using a TORMAC 770 MX CNC milling machine. This machine is a 110-volt single phase machine and requires a 15Amp dedicated circuit. This machine has a spindle power of 1.5hp and can

rotate at a maximum speed of 10,000rpm. The machine dimensions along with the machine picture are shown in Figure 6.3.

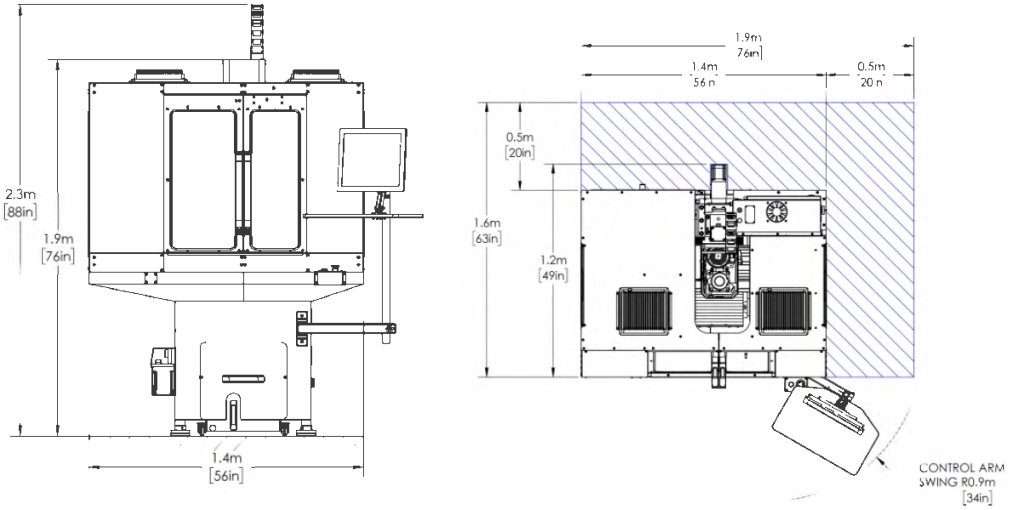

(a)

(b)

Figure 6.3 TORMAC 770 MX CNC milling machine: (a) machine footprint, (b) machine with PathPilot® controller.

The dimensions of the machine table are $660 \times 230mm$ and it is made from cast iron with hand-scraped hydrodynamic ways and tapered adjustment gibs. The machine was powered by PathPilot® controller, which offers a browser-based, full-featured simulator support up to 4-axis continuous machining. The software interface of this controller has the ability of creating usable G-code from the part drawing obtained from SolidWorks®. The desired shapes of the various components of the lower limb exoskeletons were obtained by

using various shaping features of milling and drilling by the CNC router machine before the work proceeded to the next stage of assembling the components.

6.1.2 Component Fabrication

The CNC milling machine that was used for the prototyping of the various components of the designed lower limb exoskeleton produced the desired components of carbon reinforced fibre. The components, which are shown in Figure 6.4, were precisely formed, so that the desired assembly of the exoskeleton model was possible without having any machining defects. The uniformity of various holes in different components was important to avoid any damage during the cold pressing of the stainless-steel ball bearings. The ball-bearings act as the joints to censure frictionless movement of the various links, through which the shafts of stainless steel were placed.

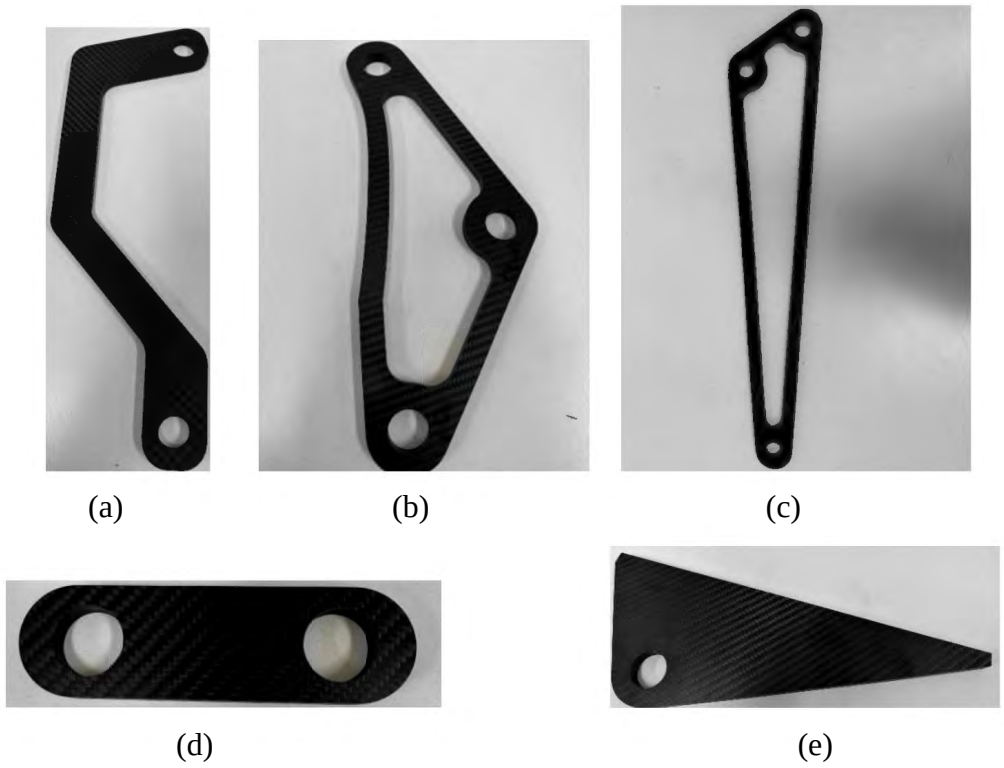

Figure 6.4 Components of the designed lower limb exoskeleton fabricated from CRFP.

6.1.3. Components Assembly

The process of assembling the lower limb robot exoskeleton began with the process of cold pressing the ball bearings into the various components. To start that process, the metal sleeves were cut from a stainless-steel pipe by using an electric disc cutter. Next, the cut metal sleeves were grinded by using electric disc grinder to remove any uneven surfaces (Figure 6.5(b)). The process of cutting and grinding the metal sleeves along with a sleeve and bearing is shown in Figure 6.5. The metal was manually pressed into the holes drilled at the various components to

avoid damaging the carbon fibre components. This process was carried out by using a hand press equipment as shown in Figure 6.6.

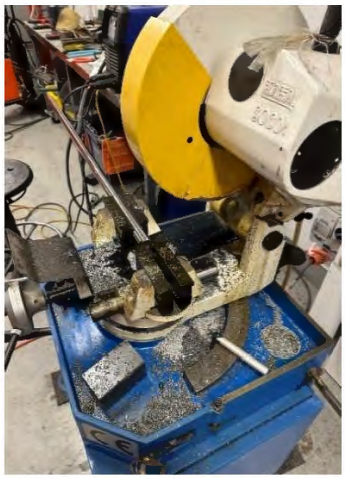

(a)

(b)

(c)

(d)

Figure 6.5 Process of sleeves cutting: (a) sleeves cutting, (b) and (c) griding and (d) sleeve and bearing.

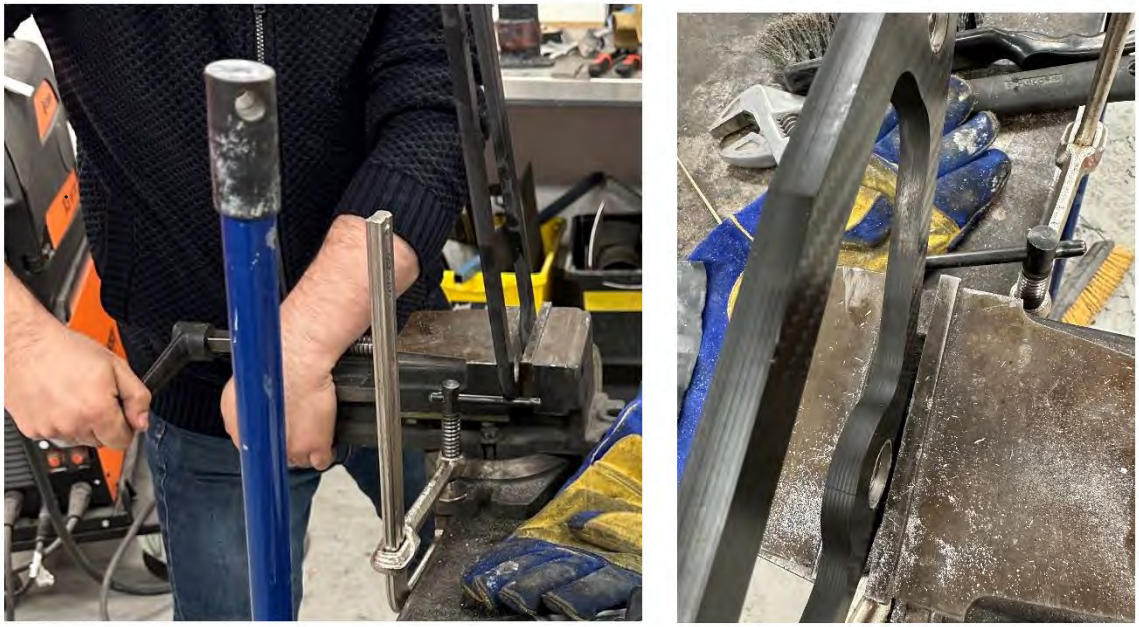

Figure 6.6 Pressing of metal sleeves and ball bearings to the different components of the exoskeleton.

After that, the various components of the lower limb exoskeleton were joined together to form a full lower limb exoskeleton by inserting the metallic shafts for frictionless movement. The actuation is an important parameter to consider while designing a lower limb robot exoskeleton and is described below.

6.1.3 DC Motor Actuator

The next stage of the present work was to add motorised movement to the lower limb exoskeleton model with the help of a suitable actuator, which can provide the desired torque. This section describes a suitable actuator, namely a DC motor actuator, that was used to run the linkage-based mechanism that was designed based on the Stephenson III six-bar linkage mechanism. As previously described in section 3.2 of chapter 3, the designed mechanism was underactuated and only one DC motor actuator was used to apply the torque and to move the lower limb exoskeleton in the sagittal plane. The DC motor used was a bipolar motor and the motor circuit along with the motor picture is as shown in Figure 6.7. The detailed specifications of the DC motor actuator are given in Table 6.1.

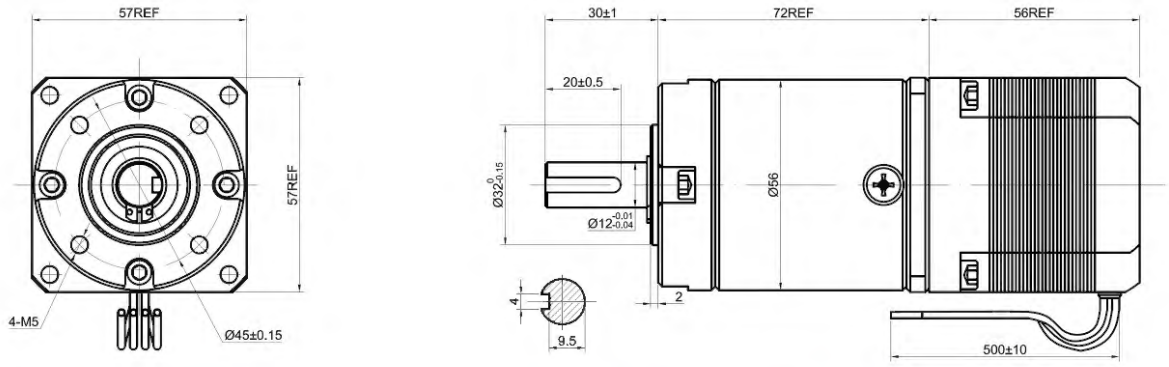

(a)

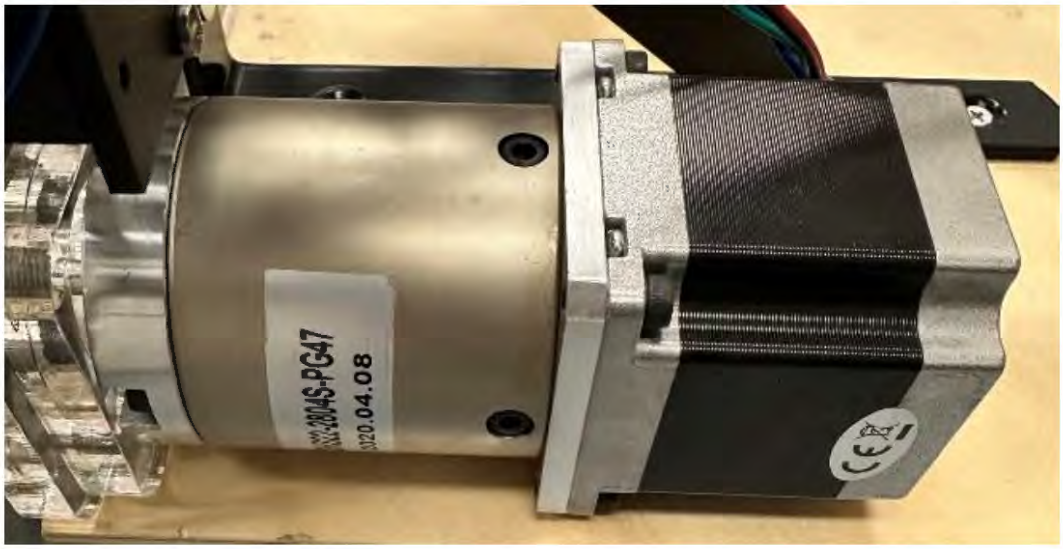

(b)

Figure 6.7 DC motor actuator used for the lower limb exoskeleton: (a) motor circuit and (b) actual motor picture.

Table 6.1 DC motor specifications.

Amp/phase	2.80
Resistance/phase (Ohm) at 25 °C	0.90±10%
Inductance/phase (mH) at 1kHz	2.50±20%
Efficiency	73%
Max. Permissible Torque (Nm)	40
Moment Permissible Torque (Nm)	60
Ambient Temperature (°C)	-10~50

The rotation of the DC motor was controlled by a controller attached to the motor. The motor shaft was rotated with a speed of 3 revolutions per minute (RPM). This speed was selected to avoid the singularity of the designed linkage-based mechanism. In one complete

motor rotation, the complete gait cycle of the human lower limb was completed. The complete model of the exoskeleton manufactured from carbon reinforced fibre is shown in Figure 6.8.

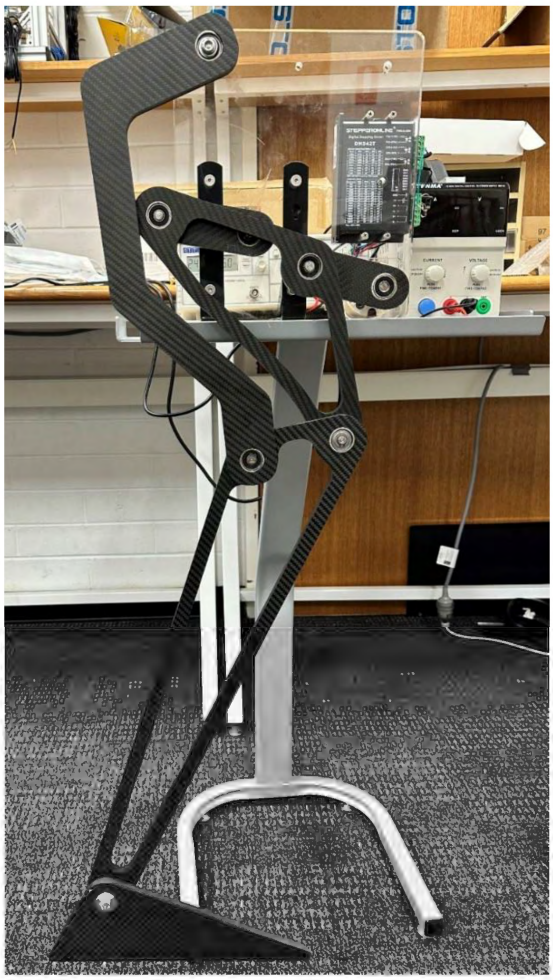

Figure 6.8 Fabricated model of the designed lower limb exoskeleton.

The weight of the exoskeleton was measured to compare it with the predicted and the optimised weight of the digital twin that was obtained by Finite Element Modelling in Chapters 3 and 4 in this thesis. The weight comparison is presented in the following section.

6.2 Weight Comparison

This weight comparison between the simulated and fabricated exoskeleton is important to assess the accuracy of the simulation results. Recapitulating earlier chapters in this thesis, initially, three different materials were chosen from which one was selected based on good mechanical and weight bearing properties with an optimal weight. Hence, the weight comparison was carried between the digital twin of the lower robot exoskeleton designed by using SolidWorks® and the fabricated physical model. Optimisation (see Chapter 4) was carried out to further reduce the weight of the designed lower limb exoskeleton without

effecting the mechanical properties and the manufacturing was carried out following the dimensions of the optimised model. The weight comparison between the simulated, optimised and the fabricated exoskeleton model is shown in Table 6.2.

Table 6.2 weight comparison of various exoskeleton models.

Exoskeleton Model	Weight (kg)
3D CAD Model	2.43
Optimised model	1.63
Fabricated Model	1.84

From the weight comparison, it was found that there is a very small difference between the optimised and fabricated models. The weight of the fabricated lower limb exoskeleton is slightly higher as compared to the optimised one with a difference of only 11%. This small difference indicates a good weight estimation of the optimised model obtained by using a Genetic Algorithm. The difference of 11 % between a simulated and fabricated or the actual model is considered to be an optimal one [216]. Hence, it can be said that the optimisation and the CAD model were designed in an ideal way, and that good results were obtained from there by keeping the experimental work to the minimum possible level. After the process of assembly of the exoskeleton prototype is completed, the reliability testing is another important stage of the research work, and it is presented in the next section.

6.3 Chapter Summary

This chapter presented the fabrication process of lower limb exoskeleton. Various steps involved in the fabrication of the prototype are discussed in detail in this chapter. The fabrication was carried out with the lightest material and processes involved in cutting and joining the various components of the lower limb exoskeleton were presented and discussed. A suitable lightweight actuation method was presented, which was employed to move the lower limb robot exoskeleton to obtain the desired motion. In the end of this chapter, a weight comparison was presented between the digital twin of the lower robot exoskeleton designed by using SolidWorks® and the fabricated physical model. In the next stage of this research, a reliability analysis is carried out to observe that whether the design system is safe and reliable in the long run.

CHAPTER 7 RELIABILITY ANALYSIS

A reliability analysis is presented to determine the system's safety of the designed lower limb robotic exoskeleton. As system reliability is a complex subject, a long short-term memory (LSTM)-augmented deep learning framework was used for time-dependent reliability analysis of dynamic systems. The reason behind the use of LSTM based approach is that a robotic system is also a dynamic system, so this approach appeared to be the most suitable one [217]. An LSTM-augmented deep neural network algorithm is designed to estimate the time-dependent reliability of joint displacement and the positions of the end-effector first. After decoupling time sequence and failures correlation due to error propagation, the original reliability problem is then transferred to a series of time-dependent reliability models. The time-dependent system reliability analysis is, finally, realised by calculating the conditional probability, which is the common practice for estimating the reliability [144]. The lower limb exoskeleton model, which was fabricated by using carbon reinforced fibre as the manufacturing material with the highest strength-to-weight ratio, was tested for reliability. The lower limb robotic exoskeleton must have a long life, so that the users can use it for long periods of time without any damage. The failure of any exoskeleton component is potentially dangerous for the person using it and can cause injury as well as the financial burden on the wearers to repair or replace it with a new one. Lower limb exoskeletons are considered as engineering systems performing various tasks and uncertainty is ubiquitous in engineering systems during their lifecycle.

The details about various reliability methods and the use of machine learning to employ these methods is discussed in detail in Chapter 2 of this thesis. In this research work, a LSTM-augmented deep learning framework is developed for time-dependent reliability analysis of dynamic systems. A set of local-limit state functions are defined based on the natural responses. The LSTM network is then trained to learn the time-dependent behaviour of the dynamic system that is the lower limb exoskeleton for each local-limit state function. After training multiple such LSTM surrogates for the local-limit state function, the global surrogate model is defined using a feedforward neural network to predict the overall forced response of the system.

Three such units are created each for the hip, knee, and the ankle joint, respectively. The sequential time-dependent reliability of the system is then determined by employing the concepts of conditional probability. By considering the lower limb exoskeleton a dynamic

system, the modelling is the first step for the reliability analysis by using a LSTM-augmented deep learning approach.

7.1.1 System Modelling for Time-Dependent Reliability Analysis

A dynamic system can be modelled as:

$$\dot{x_s}(t) = f[x_s(t), z(t)] \tag{7.1}$$

where $x_s(t)$ is the state variable and $z(t) = [z_1(t), z_2(t), \dots, z_k(t)]$ is the stochastic process. Hence, $z(t)$ can be modelled as a Gaussian process:

$$z(t) \sim N\big(\mu_z(t), \sigma_z(t)\big) \tag{7.2}$$

Once the uncertainties are quantified, the reliability analysis can be performed for the system, which is based on the kinematic accuracy during a given time interval. Hence, the limit state function is defined as the failure criterion dependent on all the variables with uncertainties. For a traditional time-dependent reliability analysis, the system response for the current time step can be written as:

$$G(x_s(t), z(t), t), \exists t \in [0, T] \tag{7.3}$$

Here, $G(\cdot)$ represents the system response and $[0, T]$ represents the system life cycle. A failure event occurs when the response at any time falls below a threshold ε, which can be defined as the margin of error. The time-dependent limit state function $g(\cdot)$ can now be defined as:

$$g(x, z(t), t) = G(x_s(t), z(t), t) - \varepsilon \leq 0, \exists t \in [0, T] \tag{7.4}$$

Therefore, the probability of failure over a period of $[0, T]$ can now be defined as:

$$P_f(0, T) = \Pr(g(x, z(t), t) \leq 0), \exists t \in [0, T] \tag{7.5}$$

The probability density function of the LSF is then determined using the LSTM network. A set of local limit state functions is first introduced by sampling time-independent random variables. An LSTM network is then trained to learn the time-dependent behaviour of the dynamic system for each local limit state function. For each sample, an indicator function is defined to classify it as safe and failure:

$$I_f = \begin{cases} 1, & \min\limits_{1 \leq t \leq s} \hat{g}(x, z(t), t) \leq \varepsilon \\ 0, & otherwise \end{cases} \tag{7.6}$$

Here, $\hat{g}(x, z(t), t)$ represents the response prediction at time instant t, and ε represents the permissible margin of error. From Equation (7.6) shows that a failure sample will be identified

when the worst performance over a given period is less than ε, which is defined for hip, knee, and ankle separately. After evaluating a total N samples, a time-dependent probability function can be reduced to:

$$P_f(0,T) \approx \frac{N_f}{N} \tag{7.7}$$

Here, N_f represents the failure samples over the decided period.

7.1.2 LSTM-augmented Deep Learning Framework

The framework here handles both the time-dependent and time-independent uncertainties for the reliability analysis of a dynamic system. Multiple local LSTM models are first constructed to learn the local-limit state functions that are identified by sampling the time-independent random space. Then, forced response predictions are collected from these local LSTM models and further utilised to train a feedforward neural network. A response surface of the validation loss with respect to the number of neurons can be established by using regression analysis. The architecture of the FNN is determined by searching for the minimum validation loss. The finalised FNN is considered as the global surrogate to predict the time-dependent behaviour of the dynamic systems and the time-dependent reliability of the system can then be approximated.

7.1.3 LSTM-based Learning of System Dynamics

The LSTM network belongs to a family of recurrent neural networks and consists of a chain of repeating modules of neural networks. For the long-term memory, three gates are used in the repeating module, namely, input, output and forget gate. The information flow, which is represented by the cell state, is at the core of the LSTM idea. Because of the structure of the gates, LSTMs can add information to the cell and forget information, which is no longer useful. The forget gate's output can be expressed as:

$$f_t = \sigma\left(W_f z_t + R_f h_{t-1} + b_f\right) \tag{7.8}$$

Here, W_f, R_f and b_f are input weights, recurrent weights, and bias, respectively, and h_{t-1} represents the previous hidden state. The sigmoid function is used since the output of this non-linear function is between 0 and 1. The input gate is used to determine the updated state and a hyperbolic tangent layer adds a vector of candidate values to the state:

$$\begin{cases} i_t = \sigma(W_i z_t + R_i h_{t-1} + b_i) \\ \widetilde{C}_t = \tanh(W_c z_t + R_c h_{t-1} + b_c) \end{cases} \tag{7.9}$$

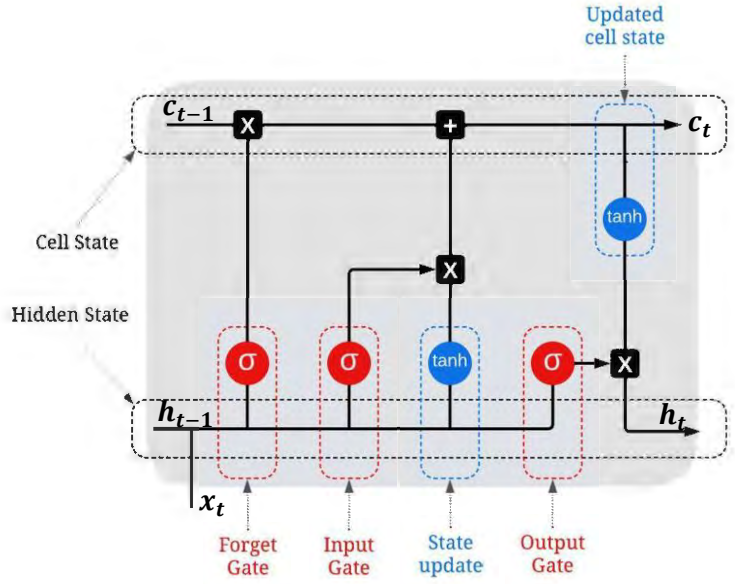

.Figure 7.1 The recurring cell of LSTM

Here, $\{W_i, R_i, b_i\}$ and $\{W_c, R_c, b_c\}$ are input weights, recurrent weights, and the bias of the input and cell states, respectively. The cell state is updated as:

$$C_t = f_t C_{t-1} + i_t \tilde{C}_t \tag{7.10}$$

The old state is multiplied with the forget gate output and the second term represents the new scaled candidate values. To determine the hidden state of the current time step, a hyperbolic tangent function is first applied to the updated cell state and the hidden states can be obtained as:

$$\begin{cases} o_t = \sigma(W_o z_t + R_o h_{t-1} + b_o) \\ h_t = o_t \cdot \tanh(C_t) \end{cases} \tag{7.11}$$

Here, $\{W_o, R_o, b_o\}$ are input weights, recurrent weights, and bias of the output gate, respectively. The hidden state h_t is then connected to a dense layer to predict the dynamic response at the current time step, expressed as:

$$y_t = W_h h_t + b_h \tag{7.12}$$

where $\{W_h, b_h\}$ represents the weight and bias, respectively.

The implementation was realised with dense, fully connected layer and thus enables learning from all combinational features of the previous layer. A repeating LSTM module is shown in Figure 7.1. Given time-series training data, optimisation algorithms can be used to train an LSTM. The Mean Squared Error (MSE) between the training set and the LSTM predictions is minimised to determine the weights and bias of the LSTM.

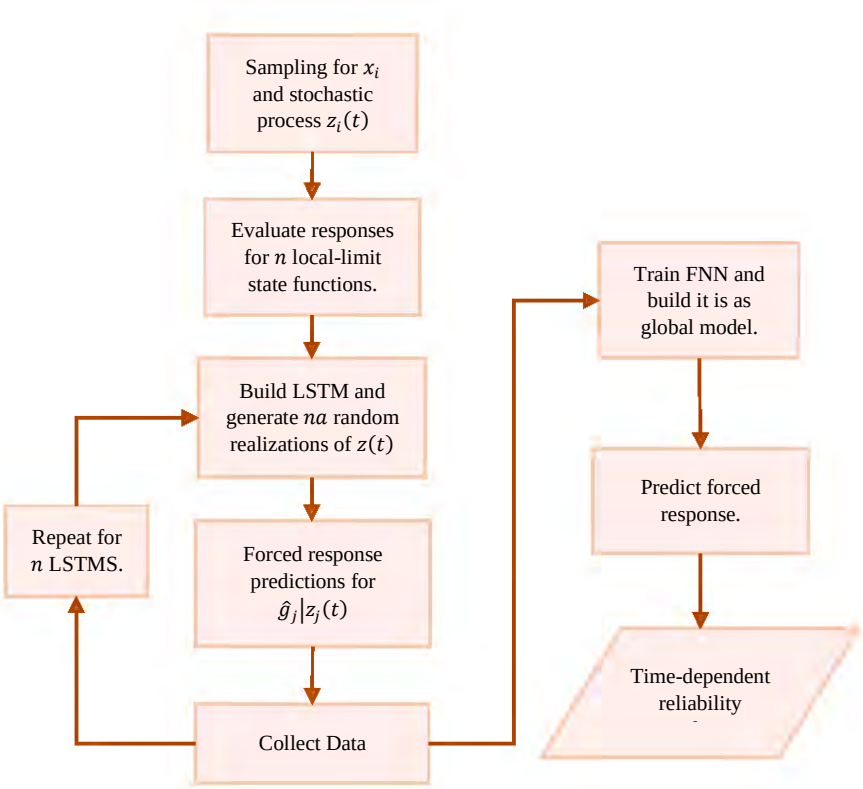

Figure 7.2. Flowchart of the proposed LTSM-augmented deep learning framework for time-dependent reliability analysis

During the training, the natural responses are not considered and, hence, LSTM lacks the ability to handle time-independent uncertainties. Thus, the natural responses are treated as tags for various LSTMs. As a result, multiple local-limit state functions are identified, and multiple LSTM models are constructed based on the collected time-series data corresponding to each local-limit function. The input data for the i^{th} LSTM model is:

$$\mathrm{X}_{train} = \begin{bmatrix} z_i(t_1) & t_1 \\ z_i(t_2) & t_2 \\ \vdots & \vdots \\ z_i(t_s) & t_s \end{bmatrix} \tag{7.13}$$

The evaluated responses $g_i = [z_i(t_1), z_i(t_2), \dots, z_i(t_s)]$ are the training labels for the LSTM.

7.1.4 LSTM-augmented Feedforward Neural Network

As aforementioned, the LSTM models can model the local-limit state functions with time-independent uncertainties. To make the algorithm more rigorous, a feedforward neural network is adopted to serve as the global surrogate model for the dynamic system. Hence, the outputs from multiple LSTM models are fed to a FNN with three layers, namely, input layer, hidden layer, and the output layer. Each hidden layer has a set of fully-connected-independent neurons. Assuming the neuron m' is connected to p neurons in the previous layer, the computation process for this neuron can be detailed as:

$$m' = f_{act}\left(\sum_{i=1}^{p}(w_i m_i + b_i)\right) \tag{7.14}$$

where $f_{act}(\cdot)$ stands for the activation function, which may vary from layer to layer, and $\{w_i, b_i\}$ represent the weights and bias of the i^{th} neuron. Such a fully connected layer is referred to as a dense layer and can capture complex patterns by allowing complete interaction between layers. Although the literature mentions various activation functions, the $ReLU$ function is used in this research due to its straightforward computation. More importantly, this function can avoid the vanishing gradient problem. The forced response predictions by the i^{th} LSTM model are obtained as follows:

$$\hat{G}^i = \left\{\hat{g}_j \middle| z_j(t), j = 1,2,\dots,na, t = 1,2,\dots,s\right\} \tag{7.15}$$

where na represents the random realisations of the stochastic process, generated for making the predictions of the time-dependent system responses for the local-limit state function. For the j^{th} sample $z_j(t)$, the response predictions are the forced response approximations of the local-limit state function described as:

$$\hat{g}_j \middle| z_j(t) \approx g\big(x_i, z_j(t), t\big), t = 1,2,\dots,s \tag{7.16}$$

Here, x_i represents the fixed time-independent random variables for the i^{th} local-limit state function. For training the FNN, one of the most important aspects is defining the architecture of the network, *i.e.*, selecting the number of hidden layers and the number of neurons in each layer. Conventionally, for a given data set, a network with a higher number of layers and neurons is expected to perform better. However, it raises the computational complexity and the probability of the model overfitting the training data. Therefore, the number of hidden layers was set to two and the number of neurons was heuristically determined method.

7.1.5 Sequential Time-Dependent Reliability

For a lower limb exoskeleton, the state of the joints is correlated. Hence, a sequential time-dependent system reliability analysis method is required. Therefore, three LSTM-augmented deep learning networks were trained to determine the limit state function of the hip, knee, and the ankle joint, respectively, with a reliability of $R_h(t)$, $R_k(t)$, and $R_a(t)$. These joints are shown in the conceptual model of the lower limb exoskeleton in Figure 3.7 of Chapter 3 of this thesis. Consequently, the reliability of the exoskeleton can then be defined as:

$$R = \Pr\{H \cap K \cap A\} \tag{7.17}$$

Where $H, K,$ and A are the safety for the hip, knee, and ankle, respectively. Equation (6.17) can also be written as:

$$R = \Pr\{H\} \cdot \Pr\{K\} \cdot \Pr\{A\}$$
$$= R_h \cdot R_k \cdot R_a \quad (7.18)$$

where R_h, R_k, and R_a are the time-dependent reliability for the hip, knee, and ankle, respectively. However, since the exoskeleton has a correlation of failure processes due to error propagation, the system is not typical. Hence, it is necessary to decouple the time sequence and consider error propagation, which can be done by defining different events, which form a serial configuration. The events can be defined as:

E_1: the motion accuracy of the hip joint is satisfied.

E_2: the motion accuracy of the knee joint including propagated error from the hip joint is satisfied, provided that the hip joint is safe.

E_3: the motion accuracy of the ankle joint including propagated error from the hip and the knee joint is satisfied, provided that the knee joint is safe.

In other words, the event can be mathematically represented as:

$$E_1: H \quad (7.19a)$$

$$E_2: K_a|H \quad (7.19b)$$

$$E_3: A_a|K_a \quad (7.19c)$$

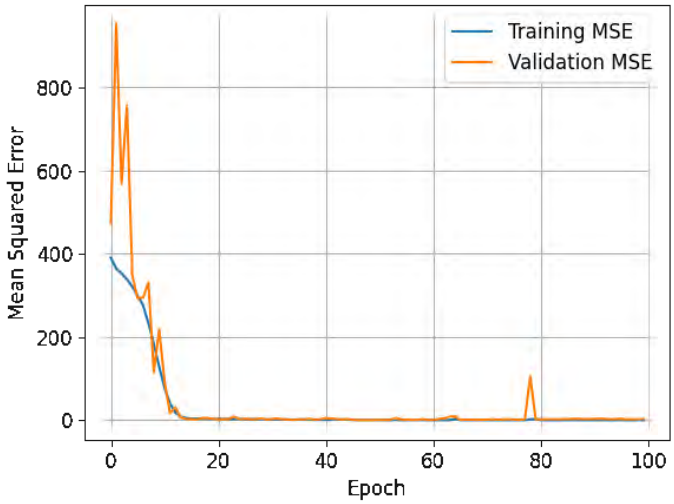

Figure 7.3 Training and validation losses for the LSTM-augmented FNN.

So, Equation (7.18) can be written as:

$$R = \Pr\{E_1\} \cdot \Pr\{E_2\} \cdot \Pr\{E_3\}$$
$$= R_1 \cdot R_2 \cdot R_3 \quad (7.20)$$

Equations (7.21a-c) describe the values of R_1, R_2, and R_3:

$$R_1 = \Pr\{E_1\} = R_h \quad (7.21a)$$

$$R_2 = \Pr\{E_2\} = \frac{R_k}{R_1} \quad (7.21b)$$

$$R_3 = \Pr\{E_3\} = \frac{R_a}{R_2} \quad (7.21c)$$

7.1.6 Experimental Procedure for the LSTM Framework

The complete procedure of employing the LSTM-augmented deep learning framework is summarised in Figure 7.2. First, n random realisations of the natural response and the stochastic process are generated. The corresponding forced responses are then evaluated based on the local-limit state functions and the i^{th} LSTM model can be realised based on the input $[z_i(t), t]$ and the output $g_i(t)$. For each local limit state function, na random realisations of the stochastic process are generated, and the LSTM model estimates the forced response $\hat{G}^i$ according to Equation (7.15). The FNN is utilised to make forced response predictions by specifying a time interval and classifying the sample based on the indicator function described in Equation 7.6. Subsequently, the time-dependent system reliability can be estimated using Equation 7.7.

This approach was implemented in Python 3.9 by utilising the popular libraries

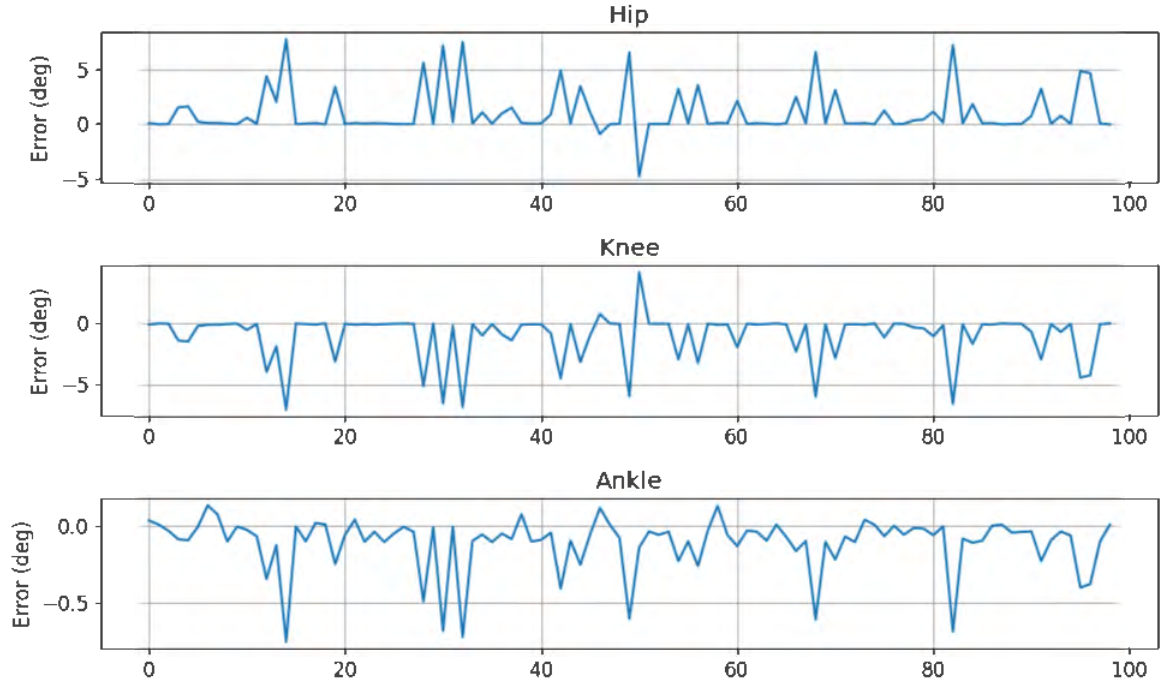

Figure 7.4 Error between the true and predicted values for the hip, knee, and ankle joints.

"Keras" and "TensorFlow" for constructing the LSTM and the FNN. The batch size was fixed to 32 and an Adam optimiser was adopted with the default learning rate of 0.001 to train the neural networks. The number of neurons were set as 64 and 32 for the first and second hidden layers, respectively. The link lengths $(L1, L2, \dots, L9)$, which were presented and discussed in detail in Figure 3.5 and Section 3.2.2 of this thesis, were considered as natural responses and the angular orientation of the link $L9$ with the vertical axis (θ) was considered as the stochastic process for each LSTM-augmented FNN.

7.1.7 Reliability Results

The training and validation loss of the LSTM-augmented FNN is shown in Figure 7.3. Since both losses are close to each other, we can be sure that the problem of over-fitting has been avoided. This figure shows the performance of the FNN dedicated to the hip angle. The knee and the ankle angle had similar performances. The error between the true and predicted values of the hip, knee, and ankle is shown in Figure 7.4. To calculate the reliability, the probability of failure was defined using Equation (7.6) where $\varepsilon = [5°, 5°, 0.5°]$ for hip, knee, and ankle joints, respectively, based on the range of motion of each joint. Figures 7.3 and 7.4 are for a single iteration of running the model.

Based on the results, the reliability values are determined as: $R_1 = 0.92, R_2 =$

Table 7.1 Mean, Standard Deviation, Minimum and Maximum of the reliability values.

Factor	Mean	Standard Deviation	Minimum	Maximum
R_1	0.85	0.03	0.75	0.94
R_2	0.68	0.04	0.56	0.83
R_3	0.55	0.05	0.40	0.69
R	0.56	0.05	0.41	0.70

$0.98, R_3 = 0.95$, and $R = 0.87$. For further analysis, the model was run for 200 iterations and the results are presented in Figure 7.5 for R_1 (Figure 7.5a), R_2 (Figure 7.5b), R_3 (Figure 7.5c), and R (Figure 7.5d). The mean and standard deviations of the reliability values are summarised in Table 7.1.

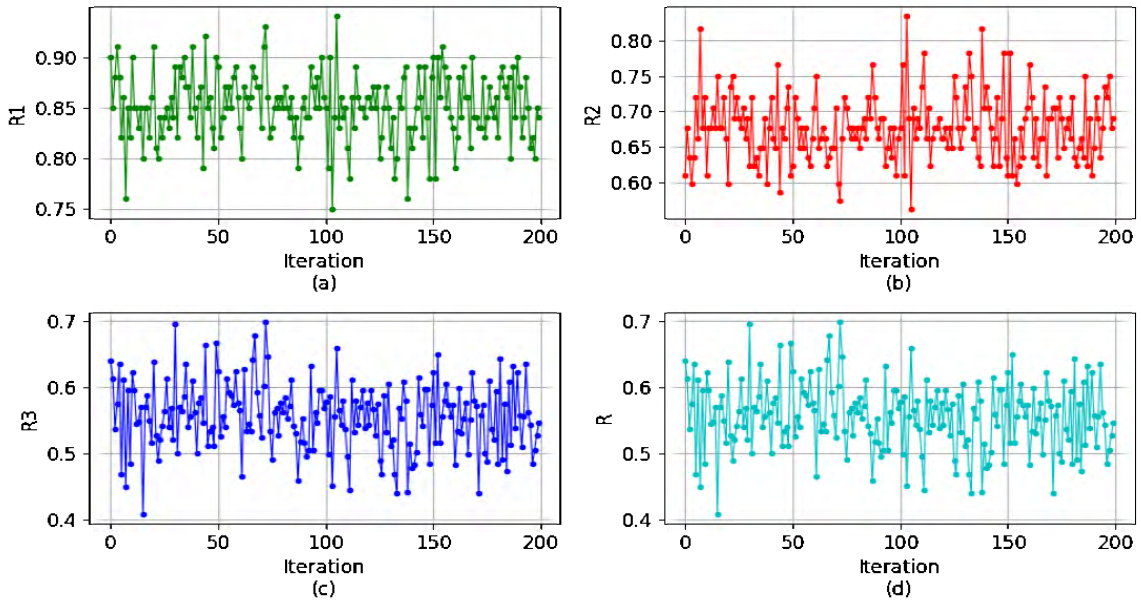

Figure 7.5 Reliability values for 200 iterations for the lower limb exoskeleton using LSTM-augmented FNN. (a) R_1 for hip, (b) R_2 for knee, (c) R_3 for ankle, and (d) R overall reliability.

To systematically handle time-independent random variables and stochastic processes, multiple LSTM models are first constructed to learn local-limit state functions. With the local surrogate LSTMs, a set of augmented data is collected by predicting forced responses for random realisations of the stochastic process. Based on the augmented data, a feedforward neural network can be trained as a surrogate model for the dynamic system. Based on the results the reliability values are determined as: $R_1 = 0.92, R_2 = 0.98, R_3 = 0.95$, and $R = 0.87$ have demonstrated the accuracy and efficiency of the proposed framework as reliability value of higher than 0.85 indicates the that the results are acceptable [218].

7.1.8 Limitations of Using an LSTM Framework

From Figure 7.5(c), it is evident that the lowest value of R_3 is 0.4, which is not desirable. There are certain factors that influence the reliability value in this case. Since R_3 denotes the reliability of the ankle joint, it is dependent on the permissible error for the ankle, which is a very small value $(0.5°)$. This implies that the margin of error for the ankle joint is set very low and, thus, the reliability of the joint decreases as well. Furthermore, since an LSTM network is being used, it improves its prediction over time. The worst-case values are noticed when the performance of the LSTM is not at its best. Another limitation associated with this work is the lack of literature and, hence, statistically validating the method against others. These values can be improved in future by attachment of sensors with the prototype and collecting data from these sensors before performing the reliability analysis Although, S. Yu *et. al.* [219] have analysed the reliability of an exoskeleton for lower limb rehabilitation, it is a properly actuated robot with hydraulic actuators. The reliability of an underactuated exoskeleton for gait rehabilitation has not been analysed in the literature according to the author's best knowledge.

7.2 Chapter Summary

This chapter tested the reliability of the lower limb robot exoskeleton system by using a machine learning based approach. As reliability analysis of the lower limb exoskeleton is a complex topic that involves many factors, a machine learning based approach was used. An LSTM-augmented deep learning framework was established for time-dependent reliability analysis by quantifying the uncertainties based on kinematic accuracy during the given time interval. A limit state function was defined as the failure criterion as a function of all variables with uncertainties. The probability density function of the LSF was determined using an LSTM network. To systematically handle time-independent random variables and stochastic processes, multiple LSTM models were first constructed to learn local-limit state functions. With the local surrogate LSTMs, a set of augmented data is collected by predicting forced responses for random realisations of the stochastic process. Based on the augmented data, a feedforward neural network was trained as a surrogate model for the dynamic system. The reliability values were determined as: $R_1 = 0.92, R_2 = 0.98, R_3 = 0.95$, and $R = 0.87$ and have demonstrated the accuracy and efficiency of the proposed framework. The next chapter presents the conclusions along with the major outcomes and a future perspective of this research work.

CHAPTER 8 CONCLUSIONS

The principal goal of this work was to investigate various research issues for the development of a lightweight and high strength lower limb robot exoskeleton for the gait rehabilitation of elderly and physically disabled people. The research was conducted to meet the growing demand for an automated rehabilitation solution for the benefit of physical therapists, patients, and the process of rehabilitation at large. This research proposed a lightweight underactuated mechanism design along with a lightweight and high strength material to provide the required motion and force trajectories for the rehabilitation treatments of the hip, knee, and ankle joints. Research objectives were drawn from the challenges posed by the wearable robot for its mechanism design, material characterisation and the reliability analysis. This chapter summarises the important conclusions drawn from this research work. Major research contributions to the body of knowledge in the field of gait rehabilitation robot exoskeletons are also highlighted in the following sections of this chapter.

8.1 Major Outcomes and Contributions

One of the major outcomes of this research was the conceptualisation and development of a lower limb robot exoskeleton model for the purpose of gait rehabilitation by using a lightweight and highly stiff material. A novel mechanism was developed by combining a lightweight manufacturing material and a single actuator to provide motion to hip, knee, and ankle joints. The previously used material for such a mechanism was approximately five times heavier and made that robot impractical for use with human subjects who were unable to perform the activities of daily living [56]. A finite element modelling based approach was employed to conduct a comparison of various manufacturing materials and the most suitable material with the highest strength-to-weight ratio was selected. Furthermore, the performance indices for the topology and material optimisation using a multi-mode single objective Genetic Algorithm (GA) were obtained from the finite element analysis. The material and topology optimisation used the material properties to optimise the weight of the designed lower limb exoskeleton model. To the best of the author's knowledge, the GA have never been used for this optimisation purpose before, in which the mechanism of lower limb robot exoskeleton design has been optimised from the material properties.

From the optimisation results, the carbon reinforced fibre composite material was found to be a suitable design material for the designed lower limb rehabilitation robot exoskeleton. Before moving towards the fabrication of the lower limb robot, the material

properties were experimentally determined keeping in mind the anisotropic behaviour of that material. Hence, in the present research work, two types of material characterisation were performed. In the first one, the comparison of different materials among the commonly used exoskeleton materials was performed. In the second one, the material characterisation as a function of fibre orientations for the carbon reinforced fibre polymer was conducted. From the later, the suitable orientation to fabricate the reliable robot prototype was obtained and used to fabricate the components of the lower limb exoskeleton, which were assembled to create a complete lower limb robot exoskeleton.

To conclude, a reliability analysis was carried out by using a machine learning based approach to account for the complexity of the reliability problem, which involves many parameters. An LSTM-augmented deep neural network algorithm was designed to estimate the time-dependent reliability of joint displacement and the positions of the end-effector first. After decoupling time sequence and failures correlation due to error propagation, the original reliability problem was then transferred to a series of time-dependent reliability models. The time-dependent system reliability analysis was finally realised by calculating the conditional probability. An underacted mechanism was initially developed and tested for time-dependent reliability, which has never been tested before using an LSTM based approach. Although, S. Yu *et. Al.* [219] have analysed the reliability of an exoskeleton for lower-limb rehabilitation, it is a properly actuated robot with hydraulic actuators. The reliability of an underactuated exoskeleton for gait rehabilitation, on the other hand, has not been analysed in the literature according to the author's best knowledge. Further details on the above research outcomes and contributions are being provided in the following subsections.

8.1.1 Development of a Lower Limb Robot Exoskeleton Design

A lightweight material for a lower limb rehabilitation robot exoskeleton employing an underactuated Stephenson III six-bar linkage mechanism was proposed for the first time as an outcome of the research presented in this thesis. The proposed design, which is compact, wearable, and lightweight, can provide the required hip, knee, and ankle motions and force trajectories in the sagittal plane, while maintaining kinematic compatibility, was conceptualised in the form of a 3D model. This model was then tested by using finite element analysis by applying the desired torque and the distributed mass at various parts of the lower limb to assess the mechanical strength of model for the various manufacturing materials. To keep the model lightweight, the mechanism design was based on single actuator that moves all the lower limb joints. The material parameters, which were used as performance indices for the

topology and material optimisation, were also extracted from the finite element modelling results and the optimisation was carried out at the next stage of this research work. Furthermore, from the results of finite element modelling a suitable lightweight and high strength material was selected for obtaining a physical prototype model of the lower limb robot exoskeleton and the weight of the exoskeleton was further reduced by topology and material optimisation.

8.1.2 Topology and Material Optimisation of the Lower Limb Exoskeleton

To minimise the overall weight of the robot, structural optimisation was carried out using a multi-mode single objective genetic algorithm. Functional and non-functional design requirements were formulated as constraints to be used during the optimisation experiments. The topology and material optimisation presented insights into the robot design requirements. As a result of this process, a significant reduction in the robot's weight was achieved without compromising the mechanical performance. In the optimisation scheme, a multi-mode single-objective GA was used for the weight minimisation by reducing the cross-sectional area of the 3D designed CAD model of exoskeleton links. From a weight comparison of the CAD and optimised lower limb robot exoskeleton model, a decrease of 30 % in overall weight was obtained for all three materials. The three materials – structural steel, aluminium, and carbon reinforced fibre – were compared both in finite element modelling and during optimisation to determine the most suitable material for the manufacturing of a lightweight robot exoskeleton. A mathematical model was formulated that can be used for any number of materials. To the best of the author's knowledge, no prior study has been reported in the literature regarding the topology and material optimisation of an underactuated lower limb robot exoskeleton.

A material characterisation was carried out during the modelling and optimisation stage of this research work. Carbon reinforced fibre was found to be the most suitable one for the lightweight rehabilitation robot application as this material has the highest strength-to-weight ratio as compared to other two materials. The research presented in this thesis also covered the fabrication and assembly process of the designed lower limb exoskeleton, so to deal with the anisotropic behaviour of carbon reinforced fibre, material testing was carried out for various fibre orientations to obtain the most suitable fibre orientation.

8.1.3 Material Characterisation and Robot Assembly

One of the major contributions of this thesis was the characterisation of a manufacturing material as a function of fibre orientations for lower limb exoskeleton, which can be used for other robotic rehabilitation devices as well. To begin with, Hashin's failure criteria was exploited to develop a comprehensive optimisation condition for fibre fabrication. The

minimization of failure probability through Genetic Algorithm (GA) led to an interesting result where the failure probabilities of two orientations were very close to each other. To analyse further, carbon reinforced fibre polymer material sheets were brought into the shape of a tensile testing specimen. The specimens were designed at various fibre orientations of $\theta = 0°$ and bidirectional laminates with fibre orientations of $\theta = 0\text{-}90°$ and $\theta = \pm 45°$. The monotonic tensile test results showed the totally different material behaviour for all three fibre orientations with the perfectly ductile behaviour shown by the specimen designed at a fibre orientation of $\theta = \pm 45°$. In fact, the material with a ductile behaviour was found to work better under various loading conditions, which is the mass of the human body in the case of rehabilitation robot applications. Furthermore, this way of material characterisation can be extended to use the carbon reinforced fibre polymer for other rehabilitation applications, for example, of the upper limb. To the best of the author's knowledge, there is no prior research study published on the application of Hashin's Failure Criteria and its experimental validation to find a most suitable fibre orientation in robotic applications. The various components of lower limb were fabricated by using the fibre orientation of $\theta = \pm 45°$ to obtain a reliable structure.

After the material characterisation, the robot protype was assembled by joining the various components, which were initially cut and machined by a CNC machine. The assembly process was carried out manually to ensure the quality of the assembled prototype and to reduce risks of assembly defects. A single DC motor actuator was used to keep the prototype lightweight and providing the necessary torque to all joints for a smooth motion. The reliability analysis of the developed lower limb robot model, which is the last major contribution of present research work, was carried out by using a machine learning based approach to ensure the designed model could perform well without failing for a certain period.

8.1.4 Reliability Analysis of the Lower Limb Exoskeleton

The final research contribution of the presented work is the time-dependent reliability analysis of the designed underactuated lower limb robot exoskeleton. Keeping in mind the complexity of the reliability analysis and the involvement of various factors, a machine learning based approach was used for a time-dependent reliability analysis. An LSTM-augmented deep neural network algorithm was designed to estimate the time-dependent reliability of the joint displacement and the positions of the end-effector. A limit state function was defined as the failure criterion as a function of all variables with uncertainties. The probability density function of the LSF was determined using an LSTM network.

To systematically handle time-independent random variables and stochastic processes, multiple LSTM models were first constructed to learn local-limit state functions. With the local surrogate LSTMs, a set of augmented data was collected by predicting forced responses for random realisations of the stochastic process. Based on the augmented data, a feedforward neural network was trained as a surrogate model for the dynamic system. Based on the results the reliability values were determined as: $R_1 = 0.92, R_2 = 0.98, R_3 = 0.95$, and $R = 0.87$, which demonstrated the accuracy and efficiency of the proposed framework. A statistical validation was not carried out in this work due to lack of literature published for underactuated robots. Although S. Yu *et al.* [219] have analysed the reliability of an exoskeleton for lower limb rehabilitation, it is a properly actuated robot with hydraulic actuators. The reliability of an underactuated exoskeleton for gait rehabilitation has not been analysed in the literature according to the author's best knowledge.

8.2 Future Work

This research has developed a lightweight and high strength lower limb robot exoskeleton for the purpose of gait rehabilitation. Although significant amount of work has been accomplished and the prototype developed has got the potential to be used for the rehabilitation treatments, a few additional milestones remain to be achieved due to the multi-disciplinary nature of this project. The proposed robot design requires improvements in terms of its conceptual design. One of the main issues compromising its performance is the friction of the linkage-based mechanism, so further research is needed to decrease friction and by doing so, the overall energy requirement of the robot can be reduced. For modelling and optimisation, the modelling of the stiffness and the analysis of the joints to avoid chattering is suggested, as chattering may cause degradation in the material stiffness.

Future research is strongly recommended to achieve further improvements in the strength-to-weight ratio of the designed lower limb exoskeleton. Three different fibre orientations were tested in the present work, which can be extended to other fibre orientations in future research. Prototype manufacturing can be done by using a combination of various orientations to obtain a hybrid orientation for the fabrication of a prototype that achieves more strength under external loading conditions. Moreover, some other materials can be developed by alteration of carbon reinforced fibres by the addition of certain resins, such as glass resins, to create an improved material. This work can also be extended for the development of rehabilitation robots for upper limbs. From a manufacturing point of view, an additive

manufacturing technique using 3D printing technologies for a better surface finish and a reduction in casting defects is strongly suggested for the future work.

Future research is strongly recommended on the reliability analysis of the carbon-reinforced lower limb exoskeleton in real-time over an extended period, by utilising the methodology developed in the present research work. The reliability results can be improved in future by attachment of sensors with the prototype and collecting data from these sensors before performing the reliability analysis. Further, the reliability analysis of the system should be conducted by including the human in the loop, as that would modify the system dynamics significantly. Furthermore, certain software tools need to be developed in order to achieve the desired reliability predictions, which will be helpful for the life estimations of the designed lower limb exoskeleton robot.

REFERENCES

[1] L.-Y. Gui, K. Zhang, Y.-X. Wang, X. Liang, J. M. Moura, and M. Veloso, "Teaching robots to predict human motion," in *2018 IEEE/RSJ International Conference on Intelligent Robots and Systems (IROS)*, 2018: IEEE, pp. 562-567.

[2] F. I. Khawaja, A. Kanazawa, J. Kinugawa, and K. Kosuge, "A human-following motion planning and control scheme for collaborative robots based on human motion prediction," *Sensors*, vol. 21, no. 24, p. 8229, 2021.

[3] T.-C. Lin, A. U. Krishnan, and Z. Li, "Shared autonomous interface for reducing physical effort in robot teleoperation via human motion mapping," in *2020 IEEE International Conference on Robotics and Automation (ICRA)*, 2020: IEEE, pp. 9157-9163.

[4] M. Javaid, A. Haleem, R. P. Singh, and R. Suman, "Substantial capabilities of robotics in enhancing industry 4.0 implementation," *Cognitive Robotics*, vol. 1, pp. 58-75, 2021.

[5] C. Wong, E. Yang, X.-T. Yan, and D. Gu, "An overview of robotics and autonomous systems for harsh environments," in *2017 23rd International Conference on Automation and Computing (ICAC)*, 2017: IEEE, pp. 1-6.

[6] A. H. Reddy, B. Kalyan, and C. S. Murthy, "Mine rescue robot system–a review," *Procedia Earth and Planetary Science*, vol. 11, pp. 457-462, 2015.

[7] B. S. Parsley, "Robotics in orthopedics: a brave new world," *The Journal of arthroplasty*, vol. 33, no. 8, pp. 2355-2357, 2018.

[8] A. Langer, R. Feingold-Polak, O. Mueller, P. Kellmeyer, and S. Levy-Tzedek, "Trust in socially assistive robots: Considerations for use in rehabilitation," *Neuroscience & Biobehavioral Reviews*, vol. 104, pp. 231-239, 2019.

[9] V. Klamroth-Marganska, "Stroke rehabilitation: therapy robots and assistive devices," *Sex-Specific Analysis of Cardiovascular Function*, pp. 579-587, 2018.

[10] P. Langhorne, J. Bernhardt, and G. Kwakkel, "Stroke rehabilitation," *The Lancet*, vol. 377, no. 9778, pp. 1693-1702, 2011.

[11] M. Shishehgar, D. Kerr, and J. Blake, "A systematic review of research into how robotic technology can help older people," *Smart Health*, vol. 7, pp. 1-18, 2018.

[12] J. Cao, S. Q. Xie, R. Das, and G. L. Zhu, "Control strategies for effective robot assisted gait rehabilitation: the state of art and future prospects," *Medical engineering & physics*, vol. 36, no. 12, pp. 1555-1566, 2014.

[13] M. Goffredo, C. Iacovelli, E. Russo, S. Pournajaf, C. Di Blasi, D. Galafate, L. Pellicciari, M. Agosti, S. Filoni, and I. Aprile, "Stroke gait rehabilitation: a comparison of end-effector, overground exoskeleton, and conventional gait training," *Applied Sciences,* vol. 9, no. 13, p. 2627, 2019.

[14] Z. Qian and Z. Bi, "Recent development of rehabilitation robots," *Advances in Mechanical Engineering,* vol. 7, no. 2, p. 563062, 2015.

[15] J. Laut, M. Porfiri, and P. Raghavan, "The present and future of robotic technology in rehabilitation," *Current physical medicine and rehabilitation reports,* vol. 4, pp. 312-319, 2016.

[16] M. Mekki, A. D. Delgado, A. Fry, D. Putrino, and V. Huang, "Robotic rehabilitation and spinal cord injury: a narrative review," *Neurotherapeutics,* vol. 15, pp. 604-617, 2018.

[17] N. Ouendi, R. Hubaut, S. Pelayo, F. Anceaux, and L. Wallard, "The rehabilitation robot: factors influencing its use, advantages and limitations in clinical rehabilitation," *Disability and Rehabilitation: Assistive Technology,* pp. 1-12, 2022.

[18] P. Poli, G. Morone, G. Rosati, and S. Masiero, "Robotic technologies and rehabilitation: new tools for stroke patients' therapy," *BioMed research international,* vol. 2013, 2013.

[19] J. Laut, M. Porfiri, and P. Raghavan, "The Present and Future of Robotic Technology in Rehabilitation," *Current Physical Medicine and Rehabilitation Reports,* vol. 4, no. 4, pp. 312-319, 2016/12/01 2016, doi: 10.1007/s40141-016-0139-0.

[20] A. Gonzalez, L. Garcia, J. Kilby, and P. McNair, "Robotic devices for paediatric rehabilitation: a review of design features," *BioMedical Engineering OnLine,* vol. 20, no. 1, pp. 1-33, 2021.

[21] B. S. Rupal, S. Rafique, A. Singla, E. Singla, M. Isaksson, and G. S. Virk, "Lower-limb exoskeletons: Research trends and regulatory guidelines in medical and non-medical applications," *International Journal of Advanced Robotic Systems,* vol. 14, no. 6, p. 1729881417743554, 2017.

[22] H. M. Qassim and W. Wan Hasan, "A review on upper limb rehabilitation robots," *Applied Sciences,* vol. 10, no. 19, p. 6976, 2020.

[23] Ü. Önen, F. M. Botsalı, M. Kalyoncu, M. Tınkır, N. Yılmaz, and Y. Şahin, "Design and actuator selection of a lower extremity exoskeleton," *IEEE/ASME Transactions on mechatronics,* vol. 19, no. 2, pp. 623-632, 2013.

[24] J. Minguella, P. R. Challa, M. De Los Santos, J. Lobo, P. Morey, and J. Font, "Re-design of a component of a lower-limb robotic exoskeleton for integrating sensing

capacity and enhancing multi-material direct additive manufacturing," in *IOP Conference Series: Materials Science and Engineering*, 2021, vol. 1193, no. 1: IOP Publishing, p. 012097.

[25] B. Chen, H. Ma, L.-Y. Qin, F. Gao, K.-M. Chan, S.-W. Law, L. Qin, and W.-H. Liao, "Recent developments and challenges of lower extremity exoskeletons," *Journal of Orthopaedic Translation,* vol. 5, pp. 26-37, 2016.

[26] R. Riener, "Technology of the robotic gait orthosis Lokomat," *Neurorehabilitation technology,* pp. 395-407, 2016.

[27] J. F. Veneman, R. Kruidhof, E. E. Hekman, R. Ekkelenkamp, E. H. Van Asseldonk, and H. Van Der Kooij, "Design and evaluation of the LOPES exoskeleton robot for interactive gait rehabilitation," *IEEE Transactions on neural systems and rehabilitation engineering,* vol. 15, no. 3, pp. 379-386, 2007.

[28] K. N. Winfree, P. Stegall, and S. K. Agrawal, "Design of a minimally constraining, passively supported gait training exoskeleton: ALEX II," in *2011 IEEE international conference on rehabilitation robotics*, 2011: IEEE, pp. 1-6.

[29] K. Tan, S. Koyama, H. Sakurai, T. Teranishi, Y. Kanada, and S. Tanabe, "Wearable robotic exoskeleton for gait reconstruction in patients with spinal cord injury: A literature review," *Journal of orthopaedic translation,* vol. 28, pp. 55-64, 2021.

[30] P. K. Jamwal, S. Hussain, and M. H. Ghayesh, "Robotic orthoses for gait rehabilitation: An overview of mechanical design and control strategies," *Proceedings of the Institution of Mechanical Engineers, Part H: Journal of Engineering in Medicine,* vol. 234, no. 5, pp. 444-457, 2020.

[31] H. Parmar, T. Khan, F. Tucci, R. Umer, and P. Carlone, "Advanced robotics and additive manufacturing of composites: towards a new era in Industry 4.0," *Materials and manufacturing processes,* vol. 37, no. 5, pp. 483-517, 2022.

[32] P. A. Vikhar, "Evolutionary algorithms: A critical review and its future prospects," in *2016 International conference on global trends in signal processing, information computing and communication (ICGTSPICC)*, 2016: IEEE, pp. 261-265.

[33] Z. Yanjun, Z. Wanqing, G. Wenqing, and L. Shuguang, "Finite Element Simulation of Soldier Lower Extremity Exoskeleton," *Journal of Multimedia,* vol. 8, no. 6, 2013.

[34] W. Cao, C. Chen, D. Wang, X. Wu, L. Chen, T. Xu, and J. Liu, "A lower limb exoskeleton with rigid and soft structure for loaded walking assistance," *IEEE Robotics and Automation Letters,* vol. 7, no. 1, pp. 454-461, 2021.

[35] D. Shi, W. Zhang, W. Zhang, and X. Ding, "A review on lower limb rehabilitation exoskeleton robots," *Chinese Journal of Mechanical Engineering,* vol. 32, no. 1, pp. 1-11, 2019.

[36] P. Urhal, A. Weightman, C. Diver, and P. Bartolo, "Robot assisted additive manufacturing: A review," *Robotics and Computer-Integrated Manufacturing,* vol. 59, pp. 335-345, 2019.

[37] M. Leman, J. Annisa, M. Jamaludin, S. Mohamddan, and H. Hazmi, "Kinematic and dynamic model analysis for an improved design of home-based wearable lower limb rehabilitation robot," in *AIP Conference Proceedings*, 2023, vol. 2643, no. 1: AIP Publishing LLC, p. 050035.

[38] K. Kong and D. Jeon, "Design and control of an exoskeleton for the elderly and patients," *IEEE/ASME Transactions on mechatronics,* vol. 11, no. 4, pp. 428-432, 2006.

[39] J. Meuleman, E. Van Asseldonk, G. Van Oort, H. Rietman, and H. Van Der Kooij, "LOPES II—design and evaluation of an admittance controlled gait training robot with shadow-leg approach," *IEEE transactions on neural systems and rehabilitation engineering,* vol. 24, no. 3, pp. 352-363, 2015.

[40] M. R. Tucker, C. Shirota, O. Lambercy, J. S. Sulzer, and R. Gassert, "Design and characterization of an exoskeleton for perturbing the knee during gait," *IEEE Transactions on Biomedical Engineering,* vol. 64, no. 10, pp. 2331-2343, 2017.

[41] T. Wallin, J. Pikul, and R. F. Shepherd, "3D printing of soft robotic systems," *Nature Reviews Materials,* vol. 3, no. 6, pp. 84-100, 2018.

[42] K. E. Gordon, G. S. Sawicki, and D. P. Ferris, "Mechanical performance of artificial pneumatic muscles to power an ankle–foot orthosis," *Journal of biomechanics,* vol. 39, no. 10, pp. 1832-1841, 2006.

[43] M. Vukobratovic, D. Hristic, and Z. Stojiljkovic, "Development of active anthropomorphic exoskeletons," *Medical and biological engineering,* vol. 12, pp. 66-80, 1974.

[44] A. Seireg and J. Grundmann, "Design of a multitask exoskeletal walking device for paraplegics," *Biomechanics of medical devices,* vol. 7, pp. 569-644, 1981.

[45] Y. Saito, K. Kikuchi, H. Negoto, T. Oshima, and T. Haneyoshi, "Development of externally powered lower limb orthosis with bilateral-servo actuator," in *9th International Conference on Rehabilitation Robotics, 2005. ICORR 2005.*, 2005: IEEE, pp. 394-399.

[46] H. I. Krebs, J. J. Palazzolo, L. Dipietro, M. Ferraro, J. Krol, K. Rannekleiv, B. T. Volpe, and N. Hogan, "Rehabilitation robotics: Performance-based progressive robot-assisted therapy," *Autonomous robots,* vol. 15, pp. 7-20, 2003.

[47] T. Gurriet, S. Finet, G. Boeris, A. Duburcq, A. Hereid, O. Harib, M. Masselin, J. Grizzle, and A. D. Ames, "Towards restoring locomotion for paraplegics: Realizing dynamically stable walking on exoskeletons," in *2018 IEEE International Conference on Robotics and Automation (ICRA)*, 2018: IEEE, pp. 2804-2811.

[48] J. M. Font-Llagunes, U. Lugrís, D. Clos, F. J. Alonso, and J. Cuadrado, "Design, control, and pilot study of a lightweight and modular robotic exoskeleton for walking assistance after spinal cord injury," *journal of Mechanisms and Robotics,* vol. 12, no. 3, p. 031008, 2020.

[49] M. Juszczak, E. Gallo, and T. Bushnik, "Examining the effects of a powered exoskeleton on quality of life and secondary impairments in people living with spinal cord injury," *Topics in spinal cord injury rehabilitation,* vol. 24, no. 4, pp. 336-342, 2018.

[50] R. Riener, L. Lünenburger, I. C. Maier, G. Colombo, and V. Dietz, "Locomotor training in subjects with sensori-motor deficits: an overview of the robotic gait orthosis lokomat," *Journal of Healthcare Engineering,* vol. 1, no. 2, pp. 197-216, 2010.

[51] B. Chen, C.-H. Zhong, X. Zhao, H. Ma, X. Guan, X. Li, F.-Y. Liang, J. C. Y. Cheng, L. Qin, and S.-W. Law, "A wearable exoskeleton suit for motion assistance to paralysed patients," *Journal of orthopaedic translation,* vol. 11, pp. 7-18, 2017.

[52] D. S. Pina, A. A. Fernandes, R. N. Jorge, and J. Gabriel, "Designing the mechanical frame of an active exoskeleton for gait assistance," *Advances in Mechanical Engineering*, vol. 10, no. 2, p. 1687814017743664, 2018.

[53] S. Wang, L. Wang, C. Meijneke, E. Van Asseldonk, T. Hoellinger, G. Cheron, Y. Ivanenko, V. La Scaleia, F. Sylos-Labini, and M. Molinari, "Design and control of the MINDWALKER exoskeleton," *IEEE transactions on neural systems and rehabilitation engineering,* vol. 23, no. 2, pp. 277-286, 2014.

[54] G. S. Sawicki and D. P. Ferris, "A pneumatically powered knee-ankle-foot orthosis (KAFO) with myoelectric activation and inhibition," *Journal of neuroengineering and rehabilitation,* vol. 6, no. 1, p. 23, 2009.

[55] A. Ekelem, G. Bastas, C. M. Durrough, and M. Goldfarb, "Variable geometry stair ascent and descent controller for a powered lower limb exoskeleton," *Journal of Medical Devices,* vol. 12, no. 3, 2018.

[56] S. Ghosh, N. Robson, and J. McCarthy, "Design of wearable lower leg orthotic based on six-bar linkage," in *International Design Engineering Technical Conferences and Computers and Information in Engineering Conference*, 2017, vol. 58172: American Society of Mechanical Engineers, p. V05AT08A064.

[57] L. Zhou, W. Chen, W. Chen, S. Bai, J. Zhang, and J. Wang, "Design of a passive lower limb exoskeleton for walking assistance with gravity compensation," *Mechanism and Machine Theory*, vol. 150, p. 103840, 2020.

[58] E. Shahabpoor, A. Pavic, and V. Racic, "Interaction between walking humans and structures in vertical direction: A literature review," *Shock and vibration*, vol. 2016, 2016.

[59] A. M. Dollar and H. Herr, "Active orthoses for the lower-limbs: challenges and state of the art," in *2007 IEEE 10th International Conference on Rehabilitation Robotics*, 2007: IEEE, pp. 968-977.

[60] M. Vukobratovic and D. Juricic, "Contribution to the synthesis of biped gait," *IEEE Transactions on Biomedical Engineering*, no. 1, pp. 1-6, 1969.

[61] K. H. Sonawale, A. Arredondo, and J. M. McCarthy, "Computer aided design of useful spherical watt I six-bar linkages," in *International Design Engineering Technical Conferences and Computers and Information in Engineering Conference*, 2013, vol. 55935: American Society of Mechanical Engineers, p. V06AT07A064.

[62] J. Wu, A. Purwar, and Q. Ge, "Interactive Dimensional Synthesis and Motion Design of Planar 6 R Single-Loop Closed Chains via Constraint Manifold Modification," 2010.

[63] G. S. Soh, "Rigid Body Guidance of Human Gait as Constrained TRS Serial Chain," in *International Design Engineering Technical Conferences and Computers and Information in Engineering Conference*, 2014, vol. 46360: American Society of Mechanical Engineers, p. V05AT08A063.

[64] M. M. Plecnik and J. Michael McCarthy, "Computational design of Stephenson II six-bar function generators for 11 accuracy points," *Journal of Mechanisms and Robotics*, vol. 8, no. 1, 2016.

[65] B. Y. Tsuge, M. M. Plecnik, and J. Michael McCarthy, "Homotopy directed optimization to design a six-bar linkage for a lower limb with a natural ankle trajectory," *Journal of Mechanisms and Robotics*, vol. 8, no. 6, p. 061009, 2016.

[66] J. Wang, Y. Pang, X. Chang, W. Chen, and J. Zhang, "Mechanical design and optimization on lower limb exoskeleton for rehabilitation," in *2019 14th IEEE*

Conference on Industrial Electronics and Applications (ICIEA), 2019: IEEE, pp. 137-142.

[67] A. Darwich, H. Nazha, A. Sliman, and W. Abbas, "Ankle–foot orthosis design between the tradition and the computerized perspectives," *The International Journal of Artificial Organs,* vol. 43, no. 5, pp. 354-361, 2020.

[68] R. Atmaja, M. Munadi, and M. Tauviqirrahman, "Stress analysis of lower limb exoskeleton for walking assistance using finite element method," 2017.

[69] F. Liu, W. M. Cheng, and L. He, "Finite element analysis of portable exoskeleton based on ergonomics parameters model," in *Applied Mechanics and Materials*, 2012, vol. 215: Trans Tech Publ, pp. 168-173.

[70] S. A. A. Moosavian, M. R. Mohamadi, and F. Absalan, "Augmented modeling of a lower limb assistant robot and human body," in *2018 6th RSI International Conference on Robotics and Mechatronics (IcRoM)*, 2018: IEEE, pp. 337-342.

[71] R. A. Wicaksono, S. D. Hariyanto, P. Prihandoko, G. S. Prihandana, and T. Sriani, "Design and analysis of exoskeleton as a rehabilitation device," in *Applied Mechanics and Materials*, 2016, vol. 842: Trans Tech Publ, pp. 423-429.

[72] H. Koch and K. Mombaur, "Exoopt-a framework for patient centered design optimization of lower limb exoskeletons," in *2015 IEEE International Conference on Rehabilitation Robotics (ICORR)*, 2015: IEEE, pp. 113-118.

[73] F. Duddeck, S. Hunkeler, P. Lozano, E. Wehrle, and D. Zeng, "Topology optimization for crashworthiness of thin-walled structures under axial impact using hybrid cellular automata," *Structural and Multidisciplinary Optimization,* vol. 54, pp. 415-428, 2016.

[74] F. Pierrot, V. Nabat, O. Company, S. Krut, and P. Poignet, "Optimal design of a 4-DOF parallel manipulator: From academia to industry," *IEEE Transactions on Robotics,* vol. 25, no. 2, pp. 213-224, 2009.

[75] M. Stock and K. Miller, "Optimal kinematic design of spatial parallel manipulators: application to linear delta robot," *J. Mech. Des.*, vol. 125, no. 2, pp. 292-301, 2003.

[76] S. Khatami and F. Sassani, "Isotropic design optimization of robotic manipulators using a genetic algorithm method," in *Proceedings of the IEEE Internatinal Symposium on Intelligent Control*, 2002: IEEE, pp. 562-567.

[77] Y. Yang and Y. Yang, "Optimal design of a 2-DOF planar parallel manipulator," in *2010 International Conference on Mechanic Automation and Control Engineering*, 2010: IEEE, pp. 2259-2264.

[78] L. Sha, A. Lin, X. Zhao, and S. Kuang, "A topology optimization method of robot lightweight design based on the finite element model of assembly and its applications," *Science Progress*, vol. 103, no. 3, p. 0036850420936482, 2020.

[79] S. Jatsun, S. Savin, and A. Yatsun, "Improvement of energy consumption for a lower limb exoskeleton through verticalization time optimization," in *2016 24th Mediterranean Conference on Control and Automation (MED)*, 2016: IEEE, pp. 322-326.

[80] S. JATSUN, S. SAVIN, A. YATSUN, and A. POSTOLNYI, "Control system parameter optimization for lower limb exoskeleton with integrated elastic elements," in *Advances in Cooperative Robotics*: World Scientific, 2017, pp. 797-805.

[81] R. Gätzi, M. Uebersax, and O. König, "Structural optimization tool using genetic algorithms and ansys," in *Proc. 18. CAD-FEM User's Meeting, Internationale FEM-Technologietage, Graf-Zeppelin-Haus, Friedrichshafen, June*, 2000.

[82] B. Ren, J. Liu, and J. Chen, "Simulating human–machine coupled model for gait trajectory optimization of the lower limb exoskeleton system based on genetic algorithm," *International Journal of Advanced Robotic Systems*, vol. 17, no. 1, p. 1729881419893493, 2020.

[83] P. K. Jamwal, S. Hussain, and S. Q. Xie, "Three-stage design analysis and multicriteria optimization of a parallel ankle rehabilitation robot using genetic algorithm," *IEEE Transactions on Automation Science and Engineering*, vol. 12, no. 4, pp. 1433-1446, 2014.

[84] B. Ding, J. Qian, L. Shen, and Y. Zhang, "Finite element analysis and optimized design of exoskeleton for lower extremity rehabilitation training," in *2012 IEEE International Conference on Robotics and Biomimetics (ROBIO)*, 2012: IEEE, pp. 1397-1402.

[85] J. H. Hernández, S. S. Cruz, R. López-Gutiérrez, A. González-Mendoza, and R. Lozano, "Robust nonsingular fast terminal sliding-mode control for sit-to-stand task using a mobile lower limb exoskeleton," *Control Engineering Practice*, vol. 101, p. 104496, 2020.

[86] N. K. Al-Hayali, J. S. Chiad, S. M. Nacy, and O. Hussein, "A review of passive and quasi-passive lower limb exoskeletons for gait rehabilitation, *Journal of Mechanical Engineering Research and Developments* " *vol*, vol. 44, pp. 428-439, 2021.

[87] V. G. Gokhare, D. Raut, and D. Shinde, "A review paper on 3D-printing aspects and various processes used in the 3D-printing," *Int. J. Eng. Res. Technol*, vol. 6, no. 06, pp. 953-958, 2017.

[88] S. A. Kolakowsky-Hayner, J. Crew, S. Moran, and A. Shah, "Safety and feasibility of using the EksoTM bionic exoskeleton to aid ambulation after spinal cord injury," *J Spine*, vol. 4, no. 3, 2013.

[89] G. Zeilig, H. Weingarden, M. Zwecker, I. Dudkiewicz, A. Bloch, and A. Esquenazi, "Safety and tolerance of the ReWalk™ exoskeleton suit for ambulation by people with complete spinal cord injury: a pilot study," *The journal of spinal cord medicine*, vol. 35, no. 2, pp. 96-101, 2012.

[90] Y. Sankai, "HAL: Hybrid assistive limb based on cybernics," in *Robotics research*: Springer, 2010, pp. 25-34.

[91] H. Yu, S. Huang, G. Chen, Y. Pan, and Z. Guo, "Human–robot interaction control of rehabilitation robots with series elastic actuators," *IEEE Transactions on Robotics*, vol. 31, no. 5, pp. 1089-1100, 2015.

[92] G. Colombo, M. Joerg, R. Schreier, and V. Dietz, "Treadmill training of paraplegic patients using a robotic orthosis," *Journal of rehabilitation research and development*, vol. 37, no. 6, pp. 693-700, 2000.

[93] D. Zanotto, P. Stegall, and S. K. Agrawal, "ALEX III: A novel robotic platform with 12 DOFs for human gait training," in *2013 IEEE International Conference on Robotics and Automation*, 2013: IEEE, pp. 3914-3919.

[94] R. Lu, Z. Li, C.-Y. Su, and A. Xue, "Development and learning control of a human limb with a rehabilitation exoskeleton," *IEEE Transactions on Industrial Electronics*, vol. 61, no. 7, pp. 3776-3785, 2013.

[95] F. Chen, Y. Yu, Y. Ge, and Y. Fang, "WPAL for human power assist during walking using dynamic equation," in *2009 International Conference on Mechatronics and Automation*, 2009: IEEE, pp. 1039-1043.

[96] D. Aoyagi, W. E. Ichinose, S. J. Harkema, D. J. Reinkensmeyer, and J. E. Bobrow, "A robot and control algorithm that can synchronously assist in naturalistic motion during body-weight-supported gait training following neurologic injury," *IEEE Transactions on Neural Systems and Rehabilitation Engineering*, vol. 15, no. 3, pp. 387-400, 2007.

[97] S. Hussain, S. Q. Xie, and P. K. Jamwal, "Robust nonlinear control of an intrinsically compliant robotic gait training orthosis," *IEEE Transactions on Systems, Man, and Cybernetics: Systems*, vol. 43, no. 3, pp. 655-665, 2012.

[98] C. M. Thalman, T. Hertzell, and H. Lee, "Toward a soft robotic ankle-foot orthosis (sr-afo) exosuit for human locomotion: Preliminary results in late stance plantarflexion

assistance," in *2020 3rd IEEE International Conference on Soft Robotics (RoboSoft)*, 2020: IEEE, pp. 801-807.

[99] E. Wojciechowski, A. Y. Chang, D. Balassone, J. Ford, T. L. Cheng, D. Little, M. P. Menezes, S. Hogan, and J. Burns, "Feasibility of designing, manufacturing and delivering 3D printed ankle-foot orthoses: a systematic review," *Journal of foot and ankle research*, vol. 12, no. 1, p. 11, 2019.

[100] R. Churchwell, K. W. Hollander, and C. Theisen, "The use of additive manufacturing to fabricate structural components for wearable robotic devices," in *International Design Engineering Technical Conferences and Computers and Information in Engineering Conference*, 2015, vol. 57120: American Society of Mechanical Engineers, p. V05AT08A044.

[101] S. Sharma, "3D-printed prosthetics roll off the presses," *Chemical Engineering*, 2014.

[102] M. del Carmen Sanchez-Villamañan, J. Gonzalez-Vargas, D. Torricelli, J. C. Moreno, and J. L. Pons, "Compliant lower limb exoskeletons: a comprehensive review on mechanical design principles," *Journal of neuroengineering and rehabilitation*, vol. 16, no. 1, p. 55, 2019.

[103] M. Vukobratovic, B. Borovac, D. Surla, and D. Stokic, *Biped locomotion: dynamics, stability, control and application*. Springer Science & Business Media, 2012.

[104] A. B. Zoss, H. Kazerooni, and A. Chu, "Biomechanical design of the Berkeley lower extremity exoskeleton (BLEEX)," *IEEE/ASME Transactions on mechatronics*, vol. 11, no. 2, pp. 128-138, 2006.

[105] R. Riener, L. Lunenburger, S. Jezernik, M. Anderschitz, G. Colombo, and V. Dietz, "Patient-cooperative strategies for robot-aided treadmill training: first experimental results," *IEEE transactions on neural systems and rehabilitation engineering*, vol. 13, no. 3, pp. 380-394, 2005.

[106] F. Hussain, R. Goecke, and M. Mohammadian, "Exoskeleton robots for lower limb assistance: A review of materials, actuation, and manufacturing methods," *Proceedings of the Institution of Mechanical Engineers, Part H: Journal of Engineering in Medicine*, vol. 235, no. 12, pp. 1375-1385, 2021.

[107] J. L. Contreras-Vidal and R. G. Grossman, "NeuroRex: A clinical neural interface roadmap for EEG-based brain machine interfaces to a lower body robotic exoskeleton," in *2013 35th Annual International Conference of the IEEE Engineering in Medicine and Biology Society (EMBC)*, 2013: IEEE, pp. 1579-1582.

[108] C. Pais-Vieira, M. Khazraei, J. Neves-Amado, A. Perrotta, E. Morya, R. Moioli, E. Shapkova, and M. Pais-Vieira, "Method for positioning and rehabilitation training with the ExoAtlet® powered exoskeleton," *MethodsX*, p. 100849, 2020.

[109] R. J. Farris, H. A. Quintero, S. A. Murray, K. H. Ha, C. Hartigan, and M. Goldfarb, "A preliminary assessment of legged mobility provided by a lower limb exoskeleton for persons with paraplegia," *IEEE Transactions on neural systems and rehabilitation engineering*, vol. 22, no. 3, pp. 482-490, 2013.

[110] D. W. Haldane, C. S. Casarez, J. T. Karras, J. Lee, C. Li, A. O. Pullin, E. W. Schaler, D. Yun, H. Ota, and A. Javey, "Integrated manufacture of exoskeletons and sensing structures for folded millirobots," *Journal of Mechanisms and Robotics*, vol. 7, no. 2, 2015.

[111] P. Cherelle, V. Grosu, P. Beyl, A. Mathys, R. Van Ham, M. Van Damme, B. Vanderborght, and D. Lefeber, "The MACCEPA actuation system as torque actuator in the gait rehabilitation robot ALTACRO," in *2010 3rd IEEE RAS & EMBS International Conference on Biomedical Robotics and Biomechatronics*, 2010: IEEE, pp. 27-32.

[112] A. Tsukahara, Y. Hasegawa, K. Eguchi, and Y. Sankai, "Restoration of gait for spinal cord injury patients using HAL with intention estimator for preferable swing speed," *IEEE Transactions on neural systems and rehabilitation engineering*, vol. 23, no. 2, pp. 308-318, 2014.

[113] S. K. Banala, S. H. Kim, S. K. Agrawal, and J. P. Scholz, "Robot assisted gait training with active leg exoskeleton (ALEX)," *IEEE transactions on neural systems and rehabilitation engineering*, vol. 17, no. 1, pp. 2-8, 2008.

[114] S. Tanabe, S. Hirano, and E. Saitoh, "Wearable Power-Assist Locomotor (WPAL) for supporting upright walking in persons with paraplegia," *NeuroRehabilitation*, vol. 33, no. 1, pp. 99-106, 2013.

[115] A. Martinez, B. Lawson, and M. Goldfarb, "A controller for guiding leg movement during overground walking with a lower limb exoskeleton," *IEEE Transactions on Robotics*, vol. 34, no. 1, pp. 183-193, 2017.

[116] G. Chen, C. K. Chan, Z. Guo, and H. Yu, "A review of lower extremity assistive robotic exoskeletons in rehabilitation therapy," *Critical Reviews™ in Biomedical Engineering*, vol. 41, no. 4-5, 2013.

[117] C.-P. Chou and B. Hannaford, "Measurement and modeling of McKibben pneumatic artificial muscles," *IEEE Transactions on robotics and automation*, vol. 12, no. 1, pp. 90-102, 1996.

[118] T.-Y. Choi, B.-S. Choi, and K.-H. Seo, "Position and compliance control of a pneumatic muscle actuated manipulator for enhanced safety," *IEEE Transactions on Control Systems Technology*, vol. 19, no. 4, pp. 832-842, 2010.

[119] J. R. Koller, C. D. Remy, and D. P. Ferris, "Biomechanics and energetics of walking in powered ankle exoskeletons using myoelectric control versus mechanically intrinsic control," *Journal of neuroengineering and rehabilitation*, vol. 15, no. 1, pp. 1-14, 2018.

[120] P. Beyl, M. Van Damme, R. Van Ham, B. Vanderborght, and D. Lefeber, "Pleated pneumatic artificial muscle-based actuator system as a torque source for compliant lower limb exoskeletons," *IEEE/ASME Transactions on Mechatronics*, vol. 19, no. 3, pp. 1046-1056, 2013.

[121] H. Vallery, J. Veneman, E. Van Asseldonk, R. Ekkelenkamp, M. Buss, and H. Van Der Kooij, "Compliant actuation of rehabilitation robots," *IEEE Robotics & Automation Magazine*, vol. 15, no. 3, pp. 60-69, 2008.

[122] A. J. Young and D. P. Ferris, "State of the art and future directions for lower limb robotic exoskeletons," *IEEE Transactions on Neural Systems and Rehabilitation Engineering*, vol. 25, no. 2, pp. 171-182, 2016.

[123] K. Kong, J. Bae, and M. Tomizuka, "Control of rotary series elastic actuator for ideal force-mode actuation in human–robot interaction applications," *IEEE/ASME transactions on mechatronics*, vol. 14, no. 1, pp. 105-118, 2009.

[124] J. F. Veneman, R. Ekkelenkamp, R. Kruidhof, F. C. van der Helm, and H. van der Kooij, "A series elastic-and bowden-cable-based actuation system for use as torque actuator in exoskeleton-type robots," *The international journal of robotics research*, vol. 25, no. 3, pp. 261-281, 2006.

[125] M. B. Yandell, B. T. Quinlivan, D. Popov, C. Walsh, and K. E. Zelik, "Physical interface dynamics alter how robotic exosuits augment human movement: implications for optimizing wearable assistive devices," *Journal of neuroengineering and rehabilitation*, vol. 14, no. 1, pp. 1-11, 2017.

[126] A. T. Asbeck, S. M. De Rossi, K. G. Holt, and C. J. Walsh, "A biologically inspired soft exosuit for walking assistance," *The International Journal of Robotics Research*, vol. 34, no. 6, pp. 744-762, 2015.

[127] J. Kim, G. Lee, R. Heimgartner, D. Arumukhom Revi, N. Karavas, D. Nathanson, I. Galiana, A. Eckert-Erdheim, P. Murphy, and D. Perry, "Reducing the metabolic rate of walking and running with a versatile, portable exosuit," *Science*, vol. 365, no. 6454, pp. 668-672, 2019.

[128] G. A. Pratt and M. M. Williamson, "Series elastic actuators," in *Proceedings 1995 IEEE/RSJ International Conference on Intelligent Robots and Systems. Human Robot Interaction and Cooperative Robots*, 1995, vol. 1: IEEE, pp. 399-406.

[129] B. Keshtegar and Z. Meng, "A hybrid relaxed first-order reliability method for efficient structural reliability analysis," *Structural Safety,* vol. 66, pp. 84-93, 2017.

[130] Y. Wang, P. Hao, H. Yang, B. Wang, and Q. Gao, "A confidence-based reliability optimization with single loop strategy and second-order reliability method," *Computer Methods in Applied Mechanics and Engineering,* vol. 372, p. 113436, 2020.

[131] C. Jiang, H. Qiu, Z. Yang, L. Chen, L. Gao, and P. Li, "A general failure-pursuing sampling framework for surrogate-based reliability analysis," *Reliability Engineering & System Safety,* vol. 183, pp. 47-59, 2019.

[132] M. Li and Z. Wang, "Active resource allocation for reliability analysis with model bias correction," *Journal of Mechanical Design,* vol. 141, no. 5, p. 051403, 2019.

[133] N.-C. Xiao, M. J. Zuo, and C. Zhou, "A new adaptive sequential sampling method to construct surrogate models for efficient reliability analysis," *Reliability Engineering & System Safety,* vol. 169, pp. 330-338, 2018.

[134] Z. Zhu and X. Du, "Reliability analysis with Monte Carlo simulation and dependent Kriging predictions," *Journal of Mechanical Design,* vol. 138, no. 12, p. 121403, 2016.

[135] T. Zhou and Y. Peng, "Structural reliability analysis via dimension reduction, adaptive sampling, and Monte Carlo simulation," *Structural and Multidisciplinary Optimization,* vol. 62, no. 5, pp. 2629-2651, 2020.

[136] W. Yun, Z. Lu, and X. Jiang, "A modified importance sampling method for structural reliability and its global reliability sensitivity analysis," *Structural and Multidisciplinary Optimization,* vol. 57, pp. 1625-1641, 2018.

[137] S. Xiao, S. Oladyshkin, and W. Nowak, "Reliability analysis with stratified importance sampling based on adaptive Kriging," *Reliability Engineering & System Safety,* vol. 197, p. 106852, 2020.

[138] G. Li, B. Li, and H. Hu, "A novel first–order reliability method based on performance measure approach for highly nonlinear problems," *Structural and Multidisciplinary Optimization,* vol. 57, pp. 1593-1610, 2018.

[139] Y. Dong, A. Teixeira, and C. G. Soares, "Application of adaptive surrogate models in time-variant fatigue reliability assessment of welded joints with surface cracks," *Reliability Engineering & System Safety,* vol. 195, p. 106730, 2020.

[140] J. Feng, L. Liu, D. Wu, G. Li, M. Beer, and W. Gao, "Dynamic reliability analysis using the extended support vector regression (X-SVR)," *Mechanical Systems and Signal Processing*, vol. 126, pp. 368-391, 2019.

[141] D. Wang, C. Jiang, H. Qiu, J. Zhang, and L. Gao, "Time-dependent reliability analysis through projection outline-based adaptive Kriging," *Structural and Multidisciplinary Optimization*, vol. 61, pp. 1453-1472, 2020.

[142] Z. Wang and P. Wang, "A nested extreme response surface approach for time-dependent reliability-based design optimization," *Journal of Mechanical Design*, vol. 134, no. 12, p. 121007, 2012.

[143] C. Jiang, X. Wei, Z. Huang, and J. Liu, "An outcrossing rate model and its efficient calculation for time-dependent system reliability analysis," *Journal of Mechanical Design*, vol. 139, no. 4, p. 041402, 2017.

[144] S. Yu, Y. Zhang, Y. Li, and Z. Wang, "Time-variant reliability analysis via approximation of the first-crossing PDF," *Structural and Multidisciplinary optimization*, vol. 62, pp. 2653-2667, 2020.

[145] T. Zafar, Y. Zhang, and Z. Wang, "An efficient Kriging based method for time-dependent reliability based robust design optimization via evolutionary algorithm," *Computer Methods in Applied Mechanics and Engineering*, vol. 372, p. 113386, 2020.

[146] L. Hawchar, C. El Soueidy, and F. Schoefs, "An Adaptive Kriging Method for Solving Time-Variant Reliability-Based Design Optimization," in *12th International Conference on Structural Safety & Reliability ICOSSAR2017*, 2017.

[147] L. Xing and S. V. Amari, *Binary decision diagrams and extensions for system reliability analysis*. John Wiley & Sons, 2015.

[148] W.-S. Lee, D. L. Grosh, F. A. Tillman, and C. H. Lie, "Fault tree analysis, methods, and applications ඏ a review," *IEEE transactions on reliability*, vol. 34, no. 3, pp. 194-203, 1985.

[149] A. Lisnianski, "Extended block diagram method for a multi-state system reliability assessment," *Reliability Engineering & System Safety*, vol. 92, no. 12, pp. 1601-1607, 2007.

[150] A. Shrestha and L. Xing, "A logarithmic binary decision diagram-based method for multistate system analysis," *IEEE Transactions on Reliability*, vol. 57, no. 4, pp. 595-606, 2008.

[151] J. Devooght and B. Tombuyses, "The use of the component influence graph to reduce the size of Markovian availability problems," *Reliability Engineering & System Safety,* vol. 46, no. 3, pp. 237-244, 1994.

[152] F. Grabski, *Semi-Markov processes: applications in system reliability and maintenance*. Elsevier, 2014.

[153] A. Charki, P.-O. Logerais, D. Bigaud, C. M. Kébé, and A. Ndiaye, "Lifetime assessment of a photovoltaic system using stochastic Petri nets," *International Journal of Modelling and Simulation,* vol. 37, no. 3, pp. 149-155, 2017.

[154] L. Lei, Y. Zhang, X. S. Shen, C. Lin, and Z. Zhong, "Performance analysis of device-to-device communications with dynamic interference using stochastic Petri nets," *IEEE transactions on wireless communications,* vol. 12, no. 12, pp. 6121-6141, 2013.

[155] D. Ge, M. Lin, Y. Yang, R. Zhang, and Q. Chou, "Quantitative analysis of dynamic fault trees using improved sequential binary decision diagrams," *Reliability Engineering & System Safety,* vol. 142, pp. 289-299, 2015.

[156] J. B. Dugan, S. J. Bavuso, and M. A. Boyd, "Dynamic fault-tree models for fault-tolerant computer systems," *IEEE Transactions on reliability,* vol. 41, no. 3, pp. 363-377, 1992.

[157] S. Zupei, W. Yao, and H. Xiangrui, "A quantification algorithm for a repairable system in the GO methodology," *Reliability Engineering & System Safety,* vol. 80, no. 3, pp. 293-298, 2003.

[158] H. Muhammad, Y. Hidekazu, M. Takeshi, and Y. Ming, "Common cause failure analysis of PWR containment spray system by GO-FLOW methodology," *Nuclear Engineering and Design,* vol. 262, pp. 350-357, 2013.

[159] N. Khakzad, "Application of dynamic Bayesian network to risk analysis of domino effects in chemical infrastructures," *Reliability Engineering & System Safety,* vol. 138, pp. 263-272, 2015.

[160] X. Wu, H. Liu, L. Zhang, M. J. Skibniewski, Q. Deng, and J. Teng, "A dynamic Bayesian network based approach to safety decision support in tunnel construction," *Reliability Engineering & System Safety,* vol. 134, pp. 157-168, 2015.

[161] P.-E. Labeau, C. Smidts, and S. Swaminathan, "Dynamic reliability: towards an integrated platform for probabilistic risk assessment," *Reliability engineering & system safety,* vol. 68, no. 3, pp. 219-254, 2000.

[162] H.-H. Wang, Y.-H. Wang, C.-W. Liang, and Y.-C. Li, "Assessment of deep learning using nonimaging information and sequential medical records to develop a prediction

model for nonmelanoma skin cancer," *JAMA dermatology*, vol. 155, no. 11, pp. 1277-1283, 2019.

[163] S. Yu, Z. Wang, and K. Zhang, "Sequential time-dependent reliability analysis for the lower extremity exoskeleton under uncertainty," *Reliability Engineering & System Safety*, vol. 170, pp. 45-52, 2018/02/01/ 2018, doi: https://doi.org/10.1016/j.ress.2017.10.006.

[164] A. W. Gebisa and H. G. Lemu, "A case study on topology optimized design for additive manufacturing," in *IOP conference series: materials science and engineering*, 2017, vol. 276, no. 1: IOP Publishing, p. 012026.

[165] D. A. Snelling, C. B. Williams, and A. P. Druschitz, "Mechanical and material properties of castings produced via 3D printed molds," *Additive Manufacturing*, vol. 27, pp. 199-207, 2019.

[166] Y. Shao, Z. Xiang, H. Liu, and L. Li, "Conceptual design and dimensional synthesis of cam-linkage mechanisms for gait rehabilitation," *Mechanism and Machine Theory*, vol. 104, pp. 31-42, 2016.

[167] S. R. Naghibi, A. A. Pirmohamadi, and S. A. A. Moosavian, "Control of flexible-joint underactuated manipulators in task space," in *2016 4th International Conference on Robotics and Mechatronics (ICROM)*, 2016: IEEE, pp. 1-6.

[168] Y. Zhu, X. Cai, H. Jin, and J. Zhao, "On the design of lower extremity exoskeleton with single drive (LEESD)," in *2014 IEEE International Conference on Robotics and Biomimetics (ROBIO 2014)*, 2014: IEEE, pp. 993-998.

[169] Y.-H. Kang, J.-W. Lin, and W.-C. You, "Comparative study on the synthesis of path-generating four-bar linkages using metaheuristic optimization algorithms," *Applied Sciences*, vol. 12, no. 15, p. 7368, 2022.

[170] D. J. Hyun, H. Park, T. Ha, S. Park, and K. Jung, "Biomechanical design of an agile, electricity-powered lower-limb exoskeleton for weight-bearing assistance," *Robotics and Autonomous Systems*, vol. 95, pp. 181-195, 2017.

[171] A. Ortlieb, M. Bouri, R. Baud, and H. Bleuler, "An assistive lower limb exoskeleton for people with neurological gait disorders," in *2017 International Conference on Rehabilitation Robotics (ICORR)*, 2017: IEEE, pp. 441-446.

[172] M. Silva, B. Freitas, R. Andrade, O. Carvalho, D. Renjewski, P. Flores, and J. Espregueira-Mendes, "Current perspectives on the biomechanical modelling of the human lower limb: a systematic review," *Archives of Computational Methods in Engineering*, vol. 28, pp. 601-636, 2021.

[173] Y. Endo, M. Miura, and M. Sakamoto, "The relationship between the deep squat movement and the hip, knee and ankle range of motion and muscle strength," *Journal of Physical Therapy Science,* vol. 32, no. 6, pp. 391-394, 2020.

[174] P. K. Jamwal, S. Q. Xie, S. Hussain, and J. G. Parsons, "An adaptive wearable parallel robot for the treatment of ankle injuries," *IEEE/ASME Transactions on mechatronics,* vol. 19, no. 1, pp. 64-75, 2012.

[175] M. Silva, B. Freitas, R. Andrade, Ó. Carvalho, D. Renjewski, P. Flores, and J. Espregueira-Mendes, "Current perspectives on the biomechanical modelling of the human lower limb: a systematic review," *Archives of Computational Methods in Engineering,* vol. 28, pp. 601-636, 2021.

[176] C. Prakash, R. Kumar, and N. Mittal, "Recent developments in human gait research: parameters, approaches, applications, machine learning techniques, datasets and challenges," *Artificial Intelligence Review,* vol. 49, pp. 1-40, 2018.

[177] S. K. Au, P. Dilworth, and H. Herr, "An ankle-foot emulation system for the study of human walking biomechanics," in *Proceedings 2006 IEEE International Conference on Robotics and Automation, 2006. ICRA 2006.*, 2006: IEEE, pp. 2939-2945.

[178] C. Xu, Y. Makihara, X. Li, Y. Yagi, and J. Lu, "Gait recognition from a single image using a phase-aware gait cycle reconstruction network," in *Computer Vision–ECCV 2020: 16th European Conference, Glasgow, UK, August 23–28, 2020, Proceedings, Part XIX 16*, 2020: Springer, pp. 386-403.

[179] D.A.Winter, *Biomechanics and motor Control of Human Movement*, Fourth ed. Waterloo, Ontario, Canada: JohnWiley & Sons., , 1979.

[180] D. Chakraborty, A. Rathi, R. Singh, V. K. Pathak, K. Chaudhary, and H. Chaudhary, "Design of a Stephenson III six-bar path generating mechanism for index finger rehabilitation device using nature-inspired algorithms," *Neural Computing and Applications,* vol. 33, pp. 17315-17329, 2021.

[181] E. Macho, M. Urízar, V. Petuya, and A. Hernández, "Improving Skills in Mechanism and Machine Science Using GIM Software," *Applied Sciences,* vol. 11, no. 17, p. 7850, 2021.

[182] V. M. Petuya, E.; Altuzarra, O.; Pinto, C. and Hernández, A., "Educational Software Tools for the Kinematic Analysis of Mechanisms. Computer Applications in Engineering Education," vol. 22, pp. 72-86, 2014.

[183] F. Hussain, M. Mohammadian, and R. Goecke, "Topology and material optimization of an underactuated robot for gait rehabilitation," *Mechanics Based Design of Structures and Machines*, pp. 1-18, 2023, doi: 10.1080/15397734.2023.2252492.

[184] M. d. C. Sanchez-Villamañan, J. Gonzalez-Vargas, D. Torricelli, J. C. Moreno, and J. L. Pons, "Compliant lower limb exoskeletons: a comprehensive review on mechanical design principles," *Journal of neuroengineering and rehabilitation,* vol. 16, no. 1, pp. 1-16, 2019.

[185] S. Bhavikatti, *Finite element analysis*. New Age International, 2005.

[186] D. Roylance, "Finite element analysis," *Department of Materials Science and Engineering, Massachusetts Institute of Technology, Cambridge,* 2001.

[187] S. K. Parashar and J. K. Sharma, "A review on application of finite element modelling in bone biomechanics," *Perspectives in Science,* vol. 8, pp. 696-698, 2016.

[188] R. M. Pidaparti, *Engineering finite element analysis*. Springer Nature, 2022.

[189] M. A. Wahab, *The mechanics of adhesives in composite and metal joints: finite element analysis with ANSYS*. DEStech Publications, Inc, 2014.

[190] N.-H. Kim, B. V. Sankar, and A. V. Kumar, *Introduction to finite element analysis and design*. John Wiley & Sons, 2018.

[191] M. F. bin Abdul Hamid, M. H. bin Mohd Ramli, N. A. Che Zakaria, and Z. Mohamed, "Conceptual design and FEM analysis of an exoskeleton suit for post-stroke patient: a lower limbs Exo suit," in *11th Asian-Pacific Conference on Medical and Biological Engineering: Proceedings of the Online Conference APCMBE 2020, May 25-27, 2020,* 2021: Springer, pp. 126-134.

[192] S. AM and E. Balaji, "Structural Analysis of Lower Limb Exoskeleton During Walking."

[193] F. Hussain, M. Mohammadian, and R. Goecke, "Topology and material optimization of an underactuated robot for gait rehabilitation," *Mechanics Based Design of Structures and Machines,* Article 2023, doi: 10.1080/15397734.2023.2252492.

[194] J.-Y. Kim and B.-K. Cho, "Development of a lower limb exoskeleton worn on the front of a human," *Journal of Intelligent & Robotic Systems,* vol. 96, no. 1, pp. 49-64, 2019.

[195] J. P. Saers, Y. Cazorla-Bak, C. N. Shaw, J. T. Stock, and T. M. Ryan, "Trabecular bone structural variation throughout the human lower limb," *Journal of human evolution,* vol. 97, pp. 97-108, 2016.

[196] S. Arunkumar, S. Mahesh, M. Rahul, N. Ganesh, and K. Maheshwaran, "Design and analysis of lower limb exoskeleton with external payload," *International Journal on Interactive Design and Manufacturing (IJIDeM)*, pp. 1-18, 2023.

[197] B. Liu, L. Sha, K. Huang, W. Zhang, and H. Yang, "A topology optimization method for collaborative robot lightweight design based on orthogonal experiment and its applications," *International Journal of Advanced Robotic Systems*, vol. 19, no. 1, p. 17298814211056143, 2022.

[198] M. Spoerk, C. Savandaiah, F. Arbeiter, G. Traxler, L. Cardon, C. Holzer, and J. Sapkota, "Anisotropic properties of oriented short carbon fibre filled polypropylene parts fabricated by extrusion-based additive manufacturing," *Composites Part A: Applied Science and Manufacturing*, vol. 113, pp. 95-104, 2018.

[199] A. McDaid, K. Kora, S. Xie, J. Lutz, and M. Battley, "Human-inspired robotic exoskeleton (HuREx) for lower limb rehabilitation," in *2013 IEEE International Conference on Mechatronics and Automation*, 2013: IEEE, pp. 19-24.

[200] E. J. Barbero, *Introduction to composite materials design*. CRC press, 2017.

[201] R. T. Ferreira and I. A. Ashcroft, "Optimal orientation of fibre composites for strength based on Hashin's criteria optimality conditions," *Structural and Multidisciplinary Optimization*, vol. 61, no. 5, pp. 2155-2176, 2020.

[202] I. Daniel, B. Werner, and J. Fenner, "Strain-rate-dependent failure criteria for composites," *Composites Science and Technology*, vol. 71, no. 3, pp. 357-364, 2011.

[203] S. Tsai, "Strength characteristics of composite materials annual report, jan. 1964-jan. 1965," 1965.

[204] S. W. Tsai and E. M. Wu, "A General Theory of Strength for Anisotropic Materials," *Journal of Composite Materials*, vol. 5, no. 1, pp. 58-80, 1971, doi: 10.1177/002199837100500106.

[205] J. Majak and S. Hannus, "Orientational Design of Anisotropic Materials Using the Hill and Tsai–Wu Strength Criteria," *Mechanics of Composite Materials*, vol. 39, no. 6, pp. 509-520, 2003/11/01 2003, doi: 10.1023/B:MOCM.0000010623.38596.3e.

[206] R. T. L. Ferreira and I. A. Ashcroft, "Optimal orientation of fibre composites for strength based on Hashin's criteria optimality conditions," *Structural and Multidisciplinary Optimization*, vol. 61, no. 5, pp. 2155-2176, 2020/05/01 2020, doi: 10.1007/s00158-019-02462-w.

[207] C. W. Ziemian, R. D. Ziemian, and K. V. Haile, "Characterization of stiffness degradation caused by fatigue damage of additive manufactured parts," *Materials & Design*, vol. 109, pp. 209-218, 2016.

[208] P. Kelly, "Solid mechanics part I: An introduction to solid mechanics," *A Creative Commons Attributions, Mountain View, CA*, vol. 94042, 2013.

[209] R. C. Sharma, P. Kumar, A. Rawat, H. P. Singh, A. Rawat, and M. R. Taluja, "Modal Analysis Of Macpherson Strut Suspension System Using Ansys," *Ilkogretim Online*, vol. 20, no. 3, pp. 3476-3486, 2021.

[210] H. Sun, Z. Ning, G. Wang, W. Liang, S. Pauly, Y. Huang, S. Guo, X. Xue, and J. Sun, "In-situ tensile testing of ZrCu-based metallic glass composites," *Scientific reports*, vol. 8, no. 1, p. 4651, 2018.

[211] *ASTM Standard D638–10, Standard Test Method for Tensile Properties of Plastics*, (Available from: www.astm.org). West Conshohocken, Pennsylvania, 2010

[212] A. Bhowmik, D. Dey, and A. Biswas, "Characteristics study of physical, mechanical and tribological behaviour of SiC/TiB 2 dispersed aluminium matrix composite," *Silicon*, pp. 1-14, 2021.

[213] W. Zhang, P. K. Liaw, and Y. Zhang, "A novel low-activation VCrFeTa x W x (x= 0.1, 0.2, 0.3, 0.4, and 1) high-entropy alloys with excellent heat-softening resistance," *Entropy*, vol. 20, no. 12, p. 951, 2018.

[214] C. Ziemian, D. Cipoletti, S. Ziemian, M. Okwara, and K. Haile, "Monotonic and cyclic tensile properties of ABS components fabricated by additive manufacturing," in *2014 International Solid Freeform Fabrication Symposium*, 2014.

[215] S. Sarkar, C. S. Kumar, and A. K. Nath, "Effects of heat treatment and build orientations on the fatigue life of selective laser melted 15-5 PH stainless steel," *Materials Science and Engineering: A*, vol. 755, pp. 235-245, 2019.

[216] B. Y. Ekren, S. S. Heragu, A. Krishnamurthy, and C. J. Malmborg, "Simulation based experimental design to identify factors affecting performance of AVS/RS," *Computers & Industrial Engineering*, vol. 58, no. 1, pp. 175-185, 2010.

[217] M. Li and Z. Wang, "LSTM-augmented deep networks for time-variant reliability assessment of dynamic systems," *Reliability Engineering & System Safety*, vol. 217, p. 108014, 2022.

[218] M. M. Konor, S. Morton, J. M. Eckerson, and T. L. Grindstaff, "Reliability of three measures of ankle dorsiflexion range of motion," *International journal of sports physical therapy*, vol. 7, no. 3, p. 279, 2012.

[219] J. Wang, X. Li, T.-H. Huang, S. Yu, Y. Li, T. Chen, A. Carriero, M. Oh-Park, and H. Su, "Comfort-centered design of a lightweight and backdrivable knee exoskeleton," *IEEE Robotics and Automation Letters*, vol. 3, no. 4, pp. 4265-4272, 2018.